

# **Synthesis and Characterization of Ethylene-Acrylic Acid Copolymers Produced under High Pressure**

Dissertation

zur Erlangung des Doktorgrades

der Mathematisch-Naturwissenschaftlichen Fakultäten

der Georg-August-Universität zu Göttingen

vorgelegt von

**Undrakh Nergui**

aus Ulaanbaatar, Mongolei

Göttingen 2009

D 7

Referent: Prof. Dr. M. Buback

Koreferent: Prof. Dr. H-U. Krebs

Tag der mündlichen Prüfung: 08.07.09

## Zusammenfassung

Es wurden freie radikalische Polymerisationen von Ethylen (E) zusammen mit Acrylsäure (AA) in einem kontinuierlich betriebenen Rührkessel bei Synthesedrücken von bis zu 2300 bar und Temperaturen von bis zu 300 °C durchgeführt. Die Copolymerproben wurden mit Hilfe verschiedener physikalischer Methoden analysiert. Die Synthese bei Drücken und Temperaturen weit oberhalb der Trübungspunktkurve, welche das Ein- und Zweiphasengebiet trennt, resultiert in statistischen Copolymeren. Nicht-statistische Copolymere können wiederum bei der Synthese nahe der Phasengrenze entstehen. Der Aspekt der Verteilung ist vor allem bei Copolymeren von Bedeutung, bei denen eine Monomereinheit nicht polar und die andere polar ist und außerdem Wasserstoffbrückenbindungen bilden kann.

Das Molekulargewicht der Copolymere nimmt mit steigendem Synthesedruck zu. E-AA-Copolymere, welche bei höheren Drücken produziert wurden, zeigen eine Schulter in der Molmassenverteilung, die ebenfalls im Fall der bei hohen Temperaturen hergestellten Proben auftritt und somit backbiting-Reaktionen zugeordnet wird.

Die Ergebnisse der DSC-Messungen zeigen deutliche Unterschiede zwischen den nahe an der und weit weg von der Phasengrenze synthetisierten Proben. Eine zusätzliche  $\beta$ -Relaxation unterhalb der Glasatemperatur kann im Falle der Niederdruckproben beobachtet werden, welche auf einen nicht-statistischen Charakter der Copolymere deutet. Die Intensität dieser  $\beta$ -Relaxation nimmt mit steigendem Acrylsäuregehalt zu, was der verstärkten Bildung von dimeren Acrylsäuresegmenten zugeschrieben wird, welche die Segmentbewegung herabsetzen. Solche Unterschiede können in den DSC-Thermogrammen der E-MA- und E-MMA-Copolymere, welche sowohl bei niedrigen und hohen Drücken hergestellt wurden, nicht beobachtet werden. Da das DSC-Thermogramm des E-Methacrylsäure-Copolymers, welches nahe der Phasengrenze synthetisiert wurden, ebenfalls diese zusätzliche  $\beta$ -Relaxation aufweist, kann dieser Effekt auf die Bildung von Wasserstoffbrücken der Säurereste im Copolymer zurückgeführt werden.

Die Röntgenmessungen zeigen unterschiedliche Strukturen für die statistischen und nicht-statistischen Copolymere. Da nicht-statistische Copolymere mehr dimere Acrylsäuresegmente

enthalten als statistische Copolymere, ist in diesem Fall die Ordnung herabgesetzt. Statistische Copolymere zeigen eine Mischung aus kristalliner und amorpher Struktur, wohingegen die nicht-statistischen Copolymere eine ausschließlich amorphe Struktur aufweisen. Für die Referenzsysteme bestehend aus E-MMA- und E-MA-Copolymeren kann gefolgert werden, dass unabhängig vom Synthesedruck Copolymere mit statistischer Verteilung der Acrylatreste entstehen. Die Fraktionen der vernetzten dimeren Acrylsäure- und Methacrylsäuresegmente in den E-AA- und E-MAA-Copolymeren sind hingegen im Falle der Synthese bei niedrigeren Drücken ausgeprägter. In PLD- und SAXS-Messungen können keine signifikanten Unterschiede zwischen den Niederdruck- und Hochdruck-E-AA-Copolymerproben festgestellt werden.

# Table of contents

<b>Zusammenfassung</b>	i
<b>Table of contents</b>	iii
<b>1 Introduction</b>	1
<b>2 Theoretical background</b>	3
2.1 Ideal polymerization kinetics .....	3
2.1.1 Initiation .....	4
2.1.2 Propagation .....	4
2.1.3 Termination .....	5
2.2 Transfer reactions .....	6
<b>3 Materials and experimental set-up</b>	9
3.1 Chemicals .....	9
3.2 Experimental set-up of high pressure copolymerisation .....	9
3.3 High-pressure Continuously Stirred Tank Reactor .....	12
3.4 Selection of the measurement conditions .....	15
3.5 Experiment .....	15
3.5.1 Preparation of Synthesis .....	15
3.5.2 Start of the experiment .....	16
3.5.3 End of the experiment .....	16
3.5.4 Cleaning the reactor after each experiment .....	17
3.5.5 Dosage of comonomer (acrylic acid) .....	17
3.5.6 Dosage of an initiator solution .....	18
3.6 Copolymerization experiment .....	18
3.6.1 High pressure samples .....	19
3.6.2 Low pressure samples .....	19
3.6.3 Initiator solution .....	21
3.6.4 Samples produced under adiabatic conditions .....	21
3.6.5 Produced polymer samples .....	22

<b>4</b>	<b>Experimental methods used for characterization of copolymers</b>	<b>23</b>
4.1	Measurement of Cloud-Point Pressures .....	23
4.2	Determination of the molecular weight distribution .....	26
4.3	FT-IR and ATR-FT-IR spectroscopy .....	27
4.4	Differential Scanning Calorimetry .....	30
4.5	Dynamic Mechanical Analysis .....	32
4.6	Pulsed laser deposition technique .....	32
4.7	Powder X-ray diffraction method .....	34
4.8	Small angle X-ray scattering .....	35
4.8.1	Scattering from the particles .....	36
4.9	Scanning electron microscopy .....	37
4.10	Solid State NMR-Spectroscopy .....	38
<b>5</b>	<b>Results and discussion</b>	<b>41</b>
5.1	Cloud Point Pressure of the E/poly(E-co-AA) system .....	41
5.2	Determination of acrylic acid content in the copolymer .....	43
5.3	Determination of molecular weight distribution of copolymer sample	50
5.4	ATR-FT-IR spectroscopy investigations.....	55
5.4.1	Comparision of ATR-FT-IR spectra of high-pressure and low-pressure samples.....	56
5.4.2	Effect of AA content on the ratio of the integrated absorbance of low-/high pressure samples .....	58
5.5	Density calculation of the reaction mixture in the reactor .....	59
5.5.1	Comparison of density in the reactor for high-pressure and low-pressure samples .....	60
5.6	Calorimetric studies via Differential Scanning Calorimetry.....	60
5.6.1	DSC analyses of PE and PMAA homopolymer systems .....	61
5.6.2	DSC analyses of E-AA copolymers produced at different pressures ...	61
5.6.3	DSC measurement of E-AA copolymers with different content of AA in the copolymer .....	63
5.6.4	Variation of the synthesis temperature .....	64
5.6.5	DSC measurement of copolymer samples produced under adiabatic conditions .....	67

5.6.6	DSC measurement of analogous systems .....	66
5.7	Results of powder X-ray diffraction .....	71
5.7.1	X-ray diffraction of PE and E-AA copolymers.....	71
5.7.2	Calculation of Full Width at the half maximum (FWHM) .....	74
5.7.3	Powder X-ray measurement of reference system .....	74
5.8	Result of Small Angle X-ray scattering (SAXS) .....	77
5.9	Structure analysis of solid state NMR-spectroscopy .....	79
5.10	Result of the Pulsed Laser Deposition .....	83
5.10.1	PLD of polymers produced from polar monomer .....	83
5.10.2	Surface structure of polyethylene .....	84
5.10.3	Surface structure analysis of PE prepared by PLD .....	87
5.10.4	Surface structure of produced E-AA copolymer layers using by PLD	88
5.11	Results of measuring the hardness of random and non-random E-AA copolymers	89
<b>6</b>	<b>Summary</b>	93
	<b>List of abbreviations</b>	95
	<b>References</b>	97
	<b>Acknowledgements</b>	103

# Chapter 1

## Introduction

Nowadays it is difficult to imagine our life without synthetic polymeric materials, as such products are largely used in nearly any field of life ranging from simple packing material over clothing to specialized high-tech devices, e.g. for aerospace engineering and life sciences. The outstanding position of synthetic materials over natural materials arises from their unique versatility, reliability, workability and durability.

The synthetic generation of polymer was first observed in 1839 by Simon during the distillation of styrene from natural styrax. He obtained a solid, transparent reaction product of which the chemical nature remained unknown until the pioneering work of Staudinger<sup>1</sup> in the 1920s who first proposed a macromolecular chain-structure consisting of chemically bonded monomeric units. Since that early work, the polymer industry has rapidly evolved. Polymers are synthesized via polycondensation and by catalytic, ionic or free-radical polymerization (FRP) with a steadily increasing worldwide production exceeding 200 millions of tons per year and an annual turnover (in 2004) of over 70 billion euro in Germany alone (with a worldwide market share of about 8%).<sup>2</sup>

Polymers may be synthesized via polycondensation, catalytic, ionic or free-radical polymerization. Especially radical polymerization allows for the generation of a large variety of versatile materials. Typical high-volume commodity free-radical polymerization products are polyethylene, polystyrene, poly(meth-)acrylates and halogenated polymers.<sup>4-9</sup> With the combination of two or more different monomers via copolymerization, free radical polymerization gives access to an even larger number of materials with very different physical properties.<sup>10-12</sup>

The aim of this work is to produce *poly* (ethene-*co*-acrylic acid) random and non-random copolymers and to determine chemical, mechanical and optical properties via different analytical methods. The difference between random and non-random ethene-acrylic acid (E-AA) copolymer is the distribution of the acid moieties in the polymer chain as shown in



Figure 1.1. Non-random copolymers may contain more dimer species compared to random copolymers.<sup>13,14</sup>

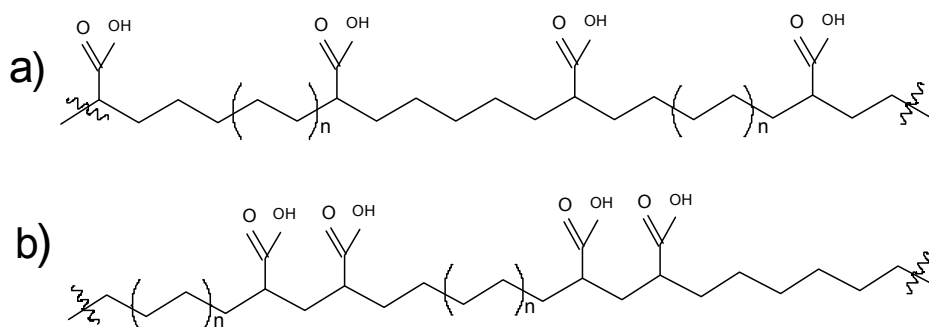


*Figure 1.1: Systematic scheme of random (a) and non-random (b) E-AA copolymers at same ethylene chain*

Ethylene /  $\alpha,\beta$ -ethylenically unsaturated carboxylic acid (e.g., (meth)acrylic acid) random copolymers are known and widely used in both the acid form and as the partially neutralized derivatives (ionomers) because of their desirable properties and ease of fabrication<sup>15,16</sup>. However, the copolymers and ionomers of commerce have limited stiffness, hardness, creep resistance and high temperature resistance because the acid comonomer in a widely dispersed, substantially random sequence distribution effectively destroys the crystallinity without adding a compensating rigid structure.<sup>17-20</sup>

High-pressure copolymerizations of ethene (E) with acrylic acid (AA) and of ethene with methacrylic acid (MAA) are carried out at conditions similar to those of the high-pressure ethene homopolymerization and of ethene-acrylic ester copolymerizations. The E-(M)AA copolymers and ionomers derived from these materials are widely used because of their unique properties for packaging and coating applications. The E-AA and E-MAA systems, in addition, are of considerable fundamental interest which is directed toward the understanding of copolymerization behaviour of monomers that differ significantly in polarity and in reactivity.

## Chapter 2

### Theoretical background

Free-radical polymerization is still commercially the most important and scientifically the most thoroughly investigated polymerization. Among the reasons for this is the fact that useful high molecular weight polymers and copolymers can be prepared from a wide variety of monomers. The intensive systematic study of these reactions dates back to the chain reaction nature of some polymerizations was identified, and it became apparent that free radicals could be the active intermediates. Free-radical polymerization is a type of polymerization, in which the propagating species is a long chain radical, usually initiated by the attack of free radicals derived by thermal or photo-chemical decomposition of initiators.<sup>22</sup> Polymerization proceeds by the chain addition of monomer molecules to the free-radical ends of growing chain molecules. Finally two propagating species (growing free-radicals) combine or disproportionate to terminate the chain growth and form one or two polymer molecules.<sup>23,24</sup>

#### 2.1 Ideal polymerization kinetics

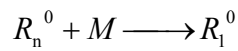
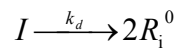
Ideal polymerization kinetics is based on four assumptions:

- all reactions are irreversible
- monomeric species are only consumed in propagation steps
- all macroradicals show the same reactivity, irrespective of their chain length
- termination takes place only by disproportionation or bimolecular radical combination

With these assumptions, the kinetic scheme of a free-radical polymerization can be characterized by three fundamental steps: the formation of radicals, chain growth of these radicals by propagation and termination of the radical chains.<sup>25</sup>

### 2.1.1 Initiation

In the initiation reaction an initiator decomposes into two primary radicals which can start the reaction. The formation of radicals can take place by thermal, chemical or photochemical activation of an initiator. This process involves two reactions.<sup>31-33</sup>



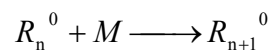
The initiator decomposition is a unimolecular reaction resulting in two initiator radicals with a rate coefficient  $k_d$ .

$$\frac{dc_{R,I}}{dt} = 2 \cdot k_d \cdot f \cdot c_I \quad (2.1)$$

Where  $c_{R,I}$  is the radical concentration of initiator-derived radicals,  $k_d$  the initiator decomposition coefficient,  $f$ , the initiator efficiency and  $c_I$  the initiator concentration.

### 2.1.2 Propagation

During the propagation step macroradicals are formed by addition of monomer molecules<sup>26</sup>.



This leads to the following expression for the rate of propagation:

$$-\frac{dc_M}{dt} = k_p \cdot c_M \cdot c_R \quad (2.2)$$

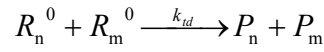
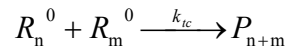
$k_p$  - propagation rate coefficient

$c_R$  - radical concentration

$c_M$  - monomer concentration

### 2.1.3 Termination

Chain termination proceeds either via combination of two macroradicals  $R_n^\circ$  and  $R_m^\circ$  forming a polymer molecule with the chain length  $n+m$ ,  $P_{n+m}$ , or by disproportionation of two macroradicals.<sup>25</sup>



Generally, the individual rate coefficients  $k_{tc}$  and  $k_{td}$  yield the overall termination rate<sup>26</sup> coefficient,  $k_t$ :

$$k_t = k_{tc} + k_{td}$$

The termination rate is given by:

$$-\frac{dc_R}{dt} = 2 \cdot k_t \cdot c_R^2 \quad (2.3)$$

Assuming steady state conditions, the number of formed radicals is equal to the number of consumed radicals:

$$2 \cdot k_t \cdot c_R^2 = 2 \cdot k_d \cdot f \cdot c_I \quad (2.4)$$

$$c_R = \left( \frac{k_d \cdot f \cdot c_I}{k_t} \right)^{0.5} \quad (2.5)$$

Introducing this equation (2.5) into the equation 2.2, the overall rate of polymerization,  $r_p$  is derived according to:

$$r_p = -\frac{dc_M}{dt} = \frac{k_p \cdot c_M}{\sqrt{k_t}} \cdot \sqrt{k_d \cdot f \cdot c_I} \quad (2.6)$$

$$k = k_p \cdot \sqrt{k_d \cdot f \cdot c_I} \quad (2.7)$$

The overall rate of polymerization ( $r_p$ ) is of first order with respect to the monomer concentration ( $c_M$ ) and of half order with respect to the initiator concentration ( $c_I$ ). The overall rate coefficient  $k$  does not only depend on the rate coefficients of the chain propagation, initiator decomposition and chain termination, but also on the radical efficiency “ $f$ ”, which is a probability factor for a primary radical to react with monomer rather than to react with other radicals and to become inactive. To express the conversion of monomer as a function of time, the differential rate equation has to be integrated. With  $c_{M,0}$  and  $c_I$  representing the initial monomer and initiator concentrations and assuming  $c_I$  to be constant with time, the result is:

$$\ln \frac{c_M}{c_{M,0}} = -k \cdot c_I^{0.5} \cdot t \quad (2.8)$$

For total monomer conversion ( $x$ ) the following equation applies:<sup>27</sup>

$$\frac{dx}{dt} = -k \cdot c_I^{0.5} \cdot (1 - x) \quad (2.9)$$

$$x = 1 - \exp(-k \cdot c_I^{0.5} \cdot t) \quad (2.10)$$

If the initiator concentration is not constant during polymerization and the initiator decomposition is of first order, the following equation can be used to calculate the maximum monomer conversion:

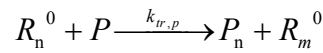
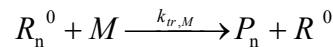
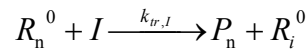
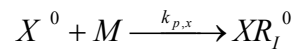
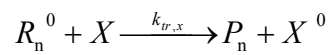
$$x_{\max} = 1 - \exp\left(-\frac{2k \cdot c_I^{0.5}}{k_d}\right) \quad (2.11)$$

## 2.2 Transfer reactions

According to the classical mechanism for free-radical polymerizations, as shown in the following reaction scheme, a propagating radical  $R^\circ$ , once generated, has three options to

react. It may propagate, terminate in a radical-radical reaction or undergo a chain-transfer reaction.

Chain transfer involves the reaction of a propagating chain  $R_n^\circ$  with a transfer agent to terminate one polymer chain and produce a new radical  $X^\circ$ , which initiates another chain  $XR_i^\circ$ . The substrate for the chain transfer may be a chain-transfer agent (X), initiator (I), monomer (M), polymer (P) or some other component of the polymerization mixture.<sup>30</sup>



$k_{tr,X}$ ,  $k_{tr,M}$ ,  $k_{tr,I}$  and  $k_{tr,P}$  are the rate coefficients for the chain transfer to CTA, monomer, initiator, and polymer, respectively.

$$C_T = \frac{k_{tr,x}}{k_p} \quad (2.12)$$

The chain-transfer constant  $C_T$  is defined as the ratio of  $k_{tr,X}$  to  $k_p$ . The higher  $C_T$ , the lower is the concentration of chain-transfer agent that is required for a particular molecular weight reduction<sup>34</sup>.

$$\frac{1}{DP_n} = \frac{1}{DP_{n,0}} + C_T \frac{[CTA]}{[M]} \quad (2.13)$$

This effect on polymer molecular weight is quantitatively given by the Mayo<sup>35</sup> equation in (2.13) which expresses the reciprocal of the number average degree of polymerization,  $DP_n$ , as a function of the rates of chain growth and chain transfer.



## Chapter 3

### Materials and experimental set-up

#### 3.1 Chemicals

The list of chemicals used in this work is shown in Table 3.1 with indicating purity and manufacturer. (Meth)acrylic acid and initiator solution were degassed by an on-line degasser (ERC 3415 degasser, ERC, Altegolfsheim (Regensburg, Germany)). The other chemicals were used without further purification.

Chemicals	Purity	Manufacturer
ethene	99.9 %	Linde
acrylic acid	99.5%	Acros organics
methacrylic acid	$\geq 99$ %	Merck-Schuchardt
methyl acrylate	$\geq 99$ %	Fluka AG
methyl methacrylate	$\geq 99$ %	Fluka AG
cyclohexane	$\geq 99$ %	Fluka AG
di- <i>tert</i> -butylperoxide	$\geq 98$ %	Merck-Schuchardt
<i>tert</i> -butylperoxyacetate	50 % in <i>iso</i> -dodecane	Akzo Nobel
nitrogen	4.6	Linde

*Table 3.1: Chemicals used in this work*

#### 3.2 Experimental set-up of high-pressure copolymerisation

The Mini-Technical experimental setup of high-pressure free-radical polymerizations in the continuously stirred tank reactor (CSTR) has been described by Buback et al.,<sup>36,38-40</sup> Busch<sup>37</sup>, Dröge<sup>40</sup> and Wittkowski<sup>41</sup> in detail. Thus only, an overview of the experimental set-up will be given in the present chapter. The flow sheet of this setup is presented in Figure 3.1.



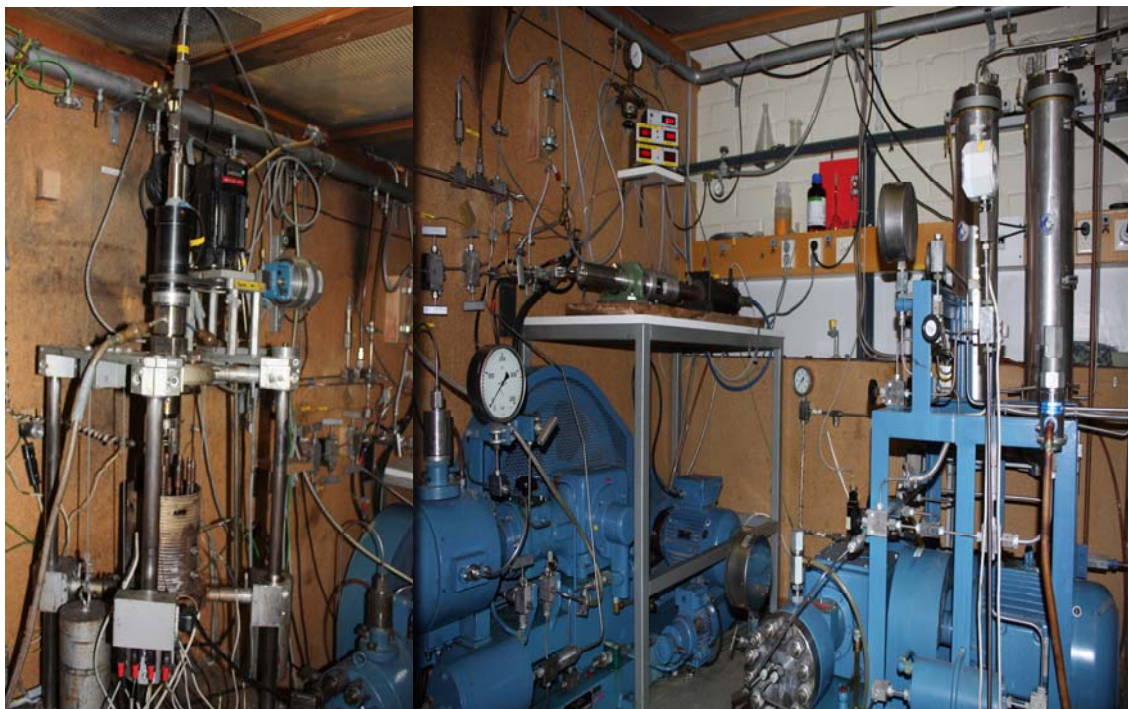
The core part of the setup is a continuously stirred tank reactor for operation up to 300 °C and 3000 bar. The CSTR has an internal volume of about 50 mL. In order to guarantee a continuous high purity of the ethene, the gas is cleaned up within the plant. For this, two cylindrical receivers with a volume of 11.7 l each are directly inserted into the flow system before the first compression stage. These autoclaves, consisting of a high-grade steel pipe of 1000 mm length, are used up to a pressure of 50 bar.<sup>42-44</sup>

Ethene of 99.9 % purity (Linde) is freed from oxygen by passing the monomer flux through a catalyst tower equipped with the BASF copper/copper oxide catalysts (BASF, R3-15). Purification of ethene within the polymerization setup prior to compression and initiator dosage ensures that the monomer has the same extremely low oxygen content for the entire set of experiments. After passing the catalyst tower and drying unit, ethene is depressurized to about 10 bar prior to penetrating the mass flow meter (5851E, Brooks-Instrument, Mannheim), which monitors the ethene flux with an accuracy of  $\pm 1$  % up to a maximum flow of  $2 \text{ kg}\cdot\text{h}^{-1}$ , and heated up to 28 °C. Via a two-stage membrane compressor unit (Hofer, Mühlheim / Ruhr), for operation up to 800 bar, and a third compression stage (Hofer, Mühlheim / Ruhr), for operation up to 3000 bar, ethene is brought to the reaction pressure. A dosage unit is equipped with a degasser (ERC 3215 degasser, Altegolfsheim) HPLC pump (Type Maxi-Star 1000, Knauer), and membrane pump (Type K3, Lewa). The membrane pump is used for acrylic and methacrylic acid in order to keep these monomers away from corrosive parts whereas the HPLC pump is used for introducing a peroxide solution (initiator in cyclohexane) into the monomer flux prior to passing the third compression stage.

The homogeneity of the reaction is controlled by a video camera which is positioned in front of a sapphire window at the bottom of the CSTR. On the other hand, homogeneity can be checked via an optical high-pressure cell which is positioned just behind the CSTR and is inserted into the optical compartment of a Fourier transform IR/NIR spectrometer (Bruker IFS 88).<sup>46</sup>

The mean residence time for the continuously operated stirred tank reactor was selected to be around 150 seconds. The agitator is magnetically driven from outside and operated at 1500 rpm. Polymer is quantitatively collected over a pre-selected time interval. Depending on the degree of monomer conversion, at each stationary operation condition three samples of typically a few grams of polymer were taken.

a)



b)



Figure 3.1: Picture of the experimental setup: a) CSTR and compressors b) HPLC pump for CTA or initiator and K3 pump for comonomer

Temperature was measured by means of sheathed thermocouples (CIA 250, CGE Alsthom) at two positions within the CSTR. One is located in the bottom part of the reactor (at the reaction chamber), the other one is in the top part of the reactor. In addition, temperature  $T$  was measured in the capillaries, and in the pressure release valve. Also,  $T$  was measured in the heating jacket of the CSTR. Via this latter thermocouple, PID control (Eurotherm 2208) of the CSTR temperature was performed. Heating the CSTR, and the pressure release valve was carried out electrically (Pyrolon-M,  $16\Omega\cdot\text{m}^{-1}$ , Les Cables de Lyon) with sheathed heating wire being embedded into a brass matrix that is tightly fitted around each of these high-pressure components. The pressure was measured with transducers (HBM-Messtechnik class 2).<sup>47</sup>

The safety pressure valves (Maxfactor) were installed in order to avoid possible danger of high pressure. When the system reaches a pressure of more than 3000 bar, then the cap of the valves are opened over electro-pneumatically steered valves the ethene supply is interrupted at the same time and the reactor content can be released into the exhaust air. The electrical monitoring (IFM electronics, SN 0150) has been installed in order to guarantee a sufficient exhaust air stream at any time. This monitoring keeps exhaust air at least 4 m/s with a delivered flow of  $1\text{ kg}\cdot\text{h}^{-1}$  Ethene.

### 3.3 High-pressure Continuously Stirred Tank Reactor

The high-pressure Continuously Stirred Tank Reactor (CSTR) is one of the main parts of the mini-technique plant. Detailed information about constructions and development are described in the works of Busch<sup>48</sup>, Buback et al.<sup>49,50</sup> and Lovis<sup>43</sup>. A schematic view of the high-temperature high-pressure CSTR is shown in Figure 3.2. The CSTR consists of a cylindrical tube of 170 mm length which has an inner diameter of 42 mm and an outer diameter of 150 mm. The internal volume of the CSTR is about 50 ml.

The reactor body is made of high-temperature-resistant nickel alloy flanges (RGT 601, material NR. 2.4668, Arbed Saarlust) in the top as well in the bottom part. For safety reasons the relation of outer to inner diameter of the reactor should be above 2.5 and the material must be resistant against 3000 bar and 300 °C.

The bottom of the reactor is sealed with a steel ram (RGT 12, Werkstoff-Nr. 2.4969, Arbed-Saarlust) which facilitates the connection of flange and main cell body via twelve

bolts with 90 Nm force each. The steel ram contains a sapphire window (UV-Grade, Roditi, Union Carbide) with a diameter of 38.1 mm and a height of 22.4 mm for optical control of the reaction system.

The top of the reactor is locked by a cone ring sealed lens (material RGT 12). The lens has an inner diameter of 11 mm, and is used in order to connect the agitating cage with the agitating drive. The bottom part of the lens contains a high-grade steel ball bearing (SS-6000-2 ZJ), which facilitates a gentle passage of the educts.

The main part of the stirrer consists of a high-pressure magnetic drive (Type 0,75-4-50 KMP 35N Spec., Autoclave Engineers). A water cooling system is installed in the stirrer to minimize the heat flow from reactor to magnetic drive. The stirrer is connected to a Pulley Synchro-Servo-Motor (Seidel) with an electronic speed controller. The maximum number of revolutions per minute of this motor is 2000.

The CSTR has six borings perpendicular to the cylindrical axis with a diameter of 1.8 mm each. These borings are located in three different heights. One boring is connected with an outlet capillary and is used for discharge of the reaction mixture, another one contains a monitoring thermocouple for the heating of the reactor, and the others are used for thermocouples for controlling the temperature of the reaction chamber, jacket and upper part of the reactor.

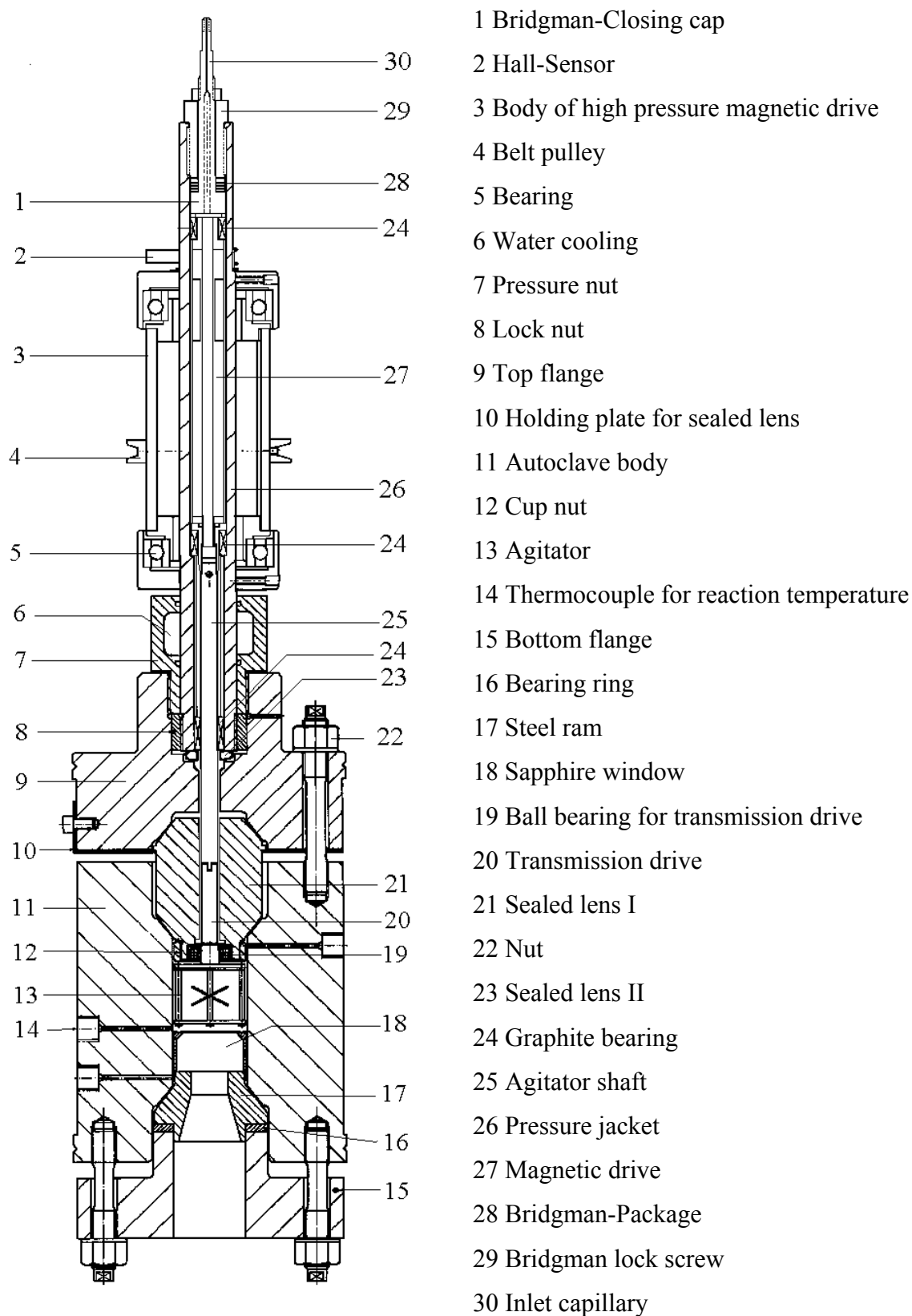


Figure 3.2: High-pressure CSTR

### 3.4 Selection of the measurement conditions

The selection of experimental pressure and temperature of the copolymerization of ethene and acrylic acid is based on the following aspects:

*(1) Pressure and temperature limit of the apparatus:*

The experimental setup for copolymerization reaction is operated at pressures up to 3000 bar and temperatures up to 300 °C.

*(2) Phase boundary:*

Temperature and pressure of the reaction is limited to lower values by the inhomogeneity of the reaction mixture. The phase behaviour of the monomer/polymer system needs to be known to ensure that polymerization takes place in a homogeneous fluid phase and to optimize separation processes after reaction. Copolymer samples should be chemically homogeneous which means that the composition of each individual macromolecule is more or less the same and thus is close to the one of the entire set of copolymer samples. If copolymerization reaction takes place in heterogeneous phase, it can lead to a fouling process in the reactor and could increase the risk of thermal decomposition. Despite chemical homogeneity, the copolymer samples may be random or non-random with respect to the distribution of the polar groups. Random copolymers are expected to be produced well above the phase boundary, on the other hand non-random copolymers may occur in syntheses close to this phase boundary. Homogeneity of the reacting system is monitored by visual inspection through a sapphire window. The phase behaviour of the ethene /poly (ethene-co-(meth)acrylic acid) system is available from literature.<sup>41</sup>

### 3.5 Experiment

#### 3.5.1 Preparation of synthesis

Prior to every experiment, reactor, fine-tuning valve and capillaries were cleaned. First, the remainder of polymer from the previous experiment in the reactor was removed by filling in heated isododecane for 3-4 hours and mechanical cleaning. Finally the remains were rinsed with acetone. Capillaries and other parts of the high-pressure cell were heated and flushed with compressed ethene. The reactor was kept under compressed ethene at 2500 bar for at

least 12 hours in order to check for any leak in the reactor. All the safety devices and experimental setup were checked visually.

### 3.5.2 Start of the experiment

To start the experiment, the pressure inside the system had to be released. Then water cooling for both compressor and reactor was turned on. All the outlet valves were kept closed and the third step compressor was started. Simultaneously, the heating of reactor and fine-tuning valve were turned on. When the system reaches the selected temperature, the compressor one and two were turned on. Afterwards, the ethene flux was started and the bypasses were closed. Stirrer and comonomer pump were turned on to start pumping. The mass flow of ethene flux was  $1.8 \text{ kg}\cdot\text{h}^{-1}$ .

Pressure is regulated by the fine-tuning valve. There is one valve which is connected directly to the outlet channel for security reasons. When pressure of the system gets out of control, then one can adjust the pressure by this valve.

When the desired pressure and temperature were reached (after about 10 minutes), the initiator solution was applied to the system via the HPLC pump. After the system reached stationary conditions, where pressure, temperature and monomer conversion were stable (at least 15 minutes after initiator entered into the reaction chamber), polymer samples were collected. At least three samples were taken within every 10 minutes for each stationary polymerization condition.

### 3.5.3 End of the experiment

At the end of the polymer synthesis, first the initiator dosage (HPLC pump) was stopped and it had to be waited until the reaction temperature dropped down and the jacket temperature got stable. After that, the valve for acid comonomer flow was closed and the K3 pump was switched off. The ethene flow had to pass through the system for at least 15 more minutes in order to clean acid and initiator solution from the compressor and reactor. Finally, stirrer, compressors and heating of the system were turned off.

### 3.5.4 Cleaning the reactor after each experiment

HPLC and comonomer pumps (K3) were rinsed with a mixture of isododecane and acetone for 8-10 hours at a high flow rate. Copolymer with a high content of acrylic acid units can be easily removed by the acetone whereas low acid content of copolymer is not. Therefore, the reactor was filled with hot isododecane solution for several hours, then cleaned mechanically with a metal brush and finally rinsed with acetone.

### 3.5.5 Dosage of comonomer (acrylic acid)

The pressure of the acrylic acid dosage is normally up to 300 bar. However, it can be varied depending on the pressure in the reactor. When the comonomer pump (K3) reaches its maximum pressure of 480 bar then it turns off automatically and stops pumping acid into the system. If the pump flow is not constant during the copolymerization of ethene and acrylic acid, it can lead to thermal decomposition of the polymer. If the reaction pressure reaches 2500 bar, also the pressure after the second stage of compressor will increase. Simultaneously the pressure of the K3 pump goes up to more than 400 bar which makes reaction risky. For that reason the maximum reaction pressure has been chosen to be 2300 bar, which reduces the risk of decomposition as well as provides significantly more stable conditions of the reaction.

It is possible to pump acid directly into the reactor via the syringe pump at pressures well above 1000 bar. For the low pressure samples this is not possible since acrylic acid becomes solid at room temperature and at pressure 700 bar. The findings of Wittkowski show that the HPLC pump does not work for the acrylic acid.<sup>41</sup> Even the special pump (K3) which is produced for pumping the acid makes some problem while pumping acrylic acid. Often the K3 pump stops completely and shows “error” at the display. If the K3 pump stops only once during the experiment and then restarts to work, there will be a loss of continuous flow of monomer into the reaction mixture. Repeated cleaning and replacement of insert and exhaust valves of the K3 pump did not show significant improvement. According to Wittkowski's<sup>41</sup> suggestion compressed air was used for cooling and heating was carried out up to 70 °C, but this also didn't work. The alternative way was to dilute the acrylic acid solution. Therefore cyclohexane was chosen as a solvent since the initiator solution was also dissolved in



cyclohexane. A 50:50 (weight ratio) cyclohexane and acrylic acid solution was introduced via the K3 pump which gave a stable flow and solved the pumping problem.

### 3.5.6 Dosage of an initiator solution

For homopolymer synthesis a syringe pump was placed between the third compression step and the reactor to inject peroxide solution. In case of ethene and acrylic acid copolymerization the HPLC pump was used instead of the syringe pump to inject the initiator solution. There are some advantages using the HPLC pump:

- a) The syringe pump has a limited volume of only 12 ml therefore a stable flow is not achievable over long time periods. On the contrary the HPLC pump provides a continuous flow and it can produce a high flow rate for a long time.
- b) When the syringe pump is used, it is difficult to determine the precise flow rate of the initiator solution but in case of the HPLC pump the flow rate of the initiator solution is easily adjustable.
- c) By using the HPLC pump, monomer (via the K3 pump) and initiator solution can be introduced into the system at the same pressure.

## 3.6 Copolymerisation experiment

In chapter 3.2, the general aspects of the high-pressure polymerization were described. In this section the selection of the reaction conditions which have been optimized during the copolymerization experiment will be discussed.

The aim of a one day measurement is to produce at least 2 groups of samples at the same reaction temperature, where the pressure has to be as different as possible. Despite chemical homogeneity, the copolymer samples may be random or non-random with respect to the distribution of the polar groups. The aspect of randomness should play a particular role in the case of copolymers where one type of monomer units is non-polar and the other one being highly polar and being even capable to form hydrogen bonds. *Poly(ethene-co-acrylic acid)* should be a perfect example for a copolymer that may exhibit non-random distributions of the polar moieties. Information about phase boundaries of the ethene based copolymers is available from literature<sup>53</sup>. A phase diagram is obtained based on measurements of

ethene/copolymer system, whereas a phase boundary can shift a little bit due to solvation of polymer in supercritical ethene.

### 3.6.1 High-pressure samples

High-pressure samples are copolymers which are produced far off the phase boundary. Under high-pressure conditions, even at the maximum pressure of the system, the experiment could run without any problem. High-pressure copolymers must be synthesized at a pressure well above the phase boundary and in this work it was 2300 bar. High reaction temperatures insure homogeneity of the reaction even if there is a pressure jump. Low reaction temperatures, however, can cause the reaction to run in heterogeneous phase. In the beginning of the reaction, the mixture inside the reactor is very clear (transparent) that one can see the movement of the stirrer through the sapphire window. When initiator is fed into the reaction mixture, the reaction temperature increases very fast (reaching even a temperature of 30 °C through 40 °C above the jacket temperature) and the mixture takes on a grey colour even though homogeneity of the system was seen.

### 3.6.2 Low-pressure samples

Low-pressure copolymer samples are synthesized at pressures close to the phase boundary. The pressure difference between high- and low-pressure samples must be as big as possible, therefore 1300 bar was chosen as a synthesis pressure for most low-pressure samples. For the syntheses, where the reaction temperature is below 240 °C, it is necessary to choose a reaction pressure above 1300 bar due to the phase boundary of the copolymer. Therefore, all experiments at low pressure were carried out in homogeneous phase. Homogeneity of the samples can be visually controlled via the video camera which delivers images from the inside of the reactor during polymerization. When acrylic acid is used as the comonomer, as soon as the initiator enters into the reactor, the reaction mixture turns to grey colour which indicates that polymerization is taking place in homogenous phase. Whenever reactions take place in heterogeneous phase, a small white phase appears because the produced copolymer is not soluble in supercritical ethene. When reactions proceed further in heterogeneous phase, the size of the white phase is getting bigger eventually the entire

reaction mixture becomes white. However, when pressure increases step by step the colour of the reaction mixture turns from grey to white which indicates the reaction now proceeds in homogeneous phase. When the reaction mixture is kept in heterogeneous phase it may lead to fouling. The fouling process starts when bulk polymer is deposited at the reactor wall and the stirrer. Thereby the volume of the reactor is reduced significantly. Therefore, in order to keep conversion constant, more initiator needs to be injected into the reaction mixture. But a large amount of initiator will change the microstructure of the produced copolymer. For the high reaction temperature (higher than 260 °C) it is possible to work at pressures below 1300 bar, i. e. to work under low-pressure sample conditions.

According to the phase boundary diagram (see Figure 3.3) obtained by Buback et al<sup>51,52</sup>, it is possible to synthesize non-random copolymer at the high-pressure (2300 bar) and low reaction temperature conditions. For this purpose samples at 2300 bar were produced in the temperature range of 200 to 210 °C. To get samples at 200 °C the reaction temperature and the jacket temperature should be around 160 °C. To start the experiment at this low temperature, the system needs a huge amount of initiator (TxF). Feeding such a big amount of initiator causes the reaction to start abruptly and the reaction temperature increases very fast up to 230 °C. Even when the flow rate of the initiator is decreased very gently, the reaction stops immediately. Other initiator which is suitable for low temperature could be used but in that case produced polymer does not have the same properties as a copolymer produced at high temperature (above 230 °C).

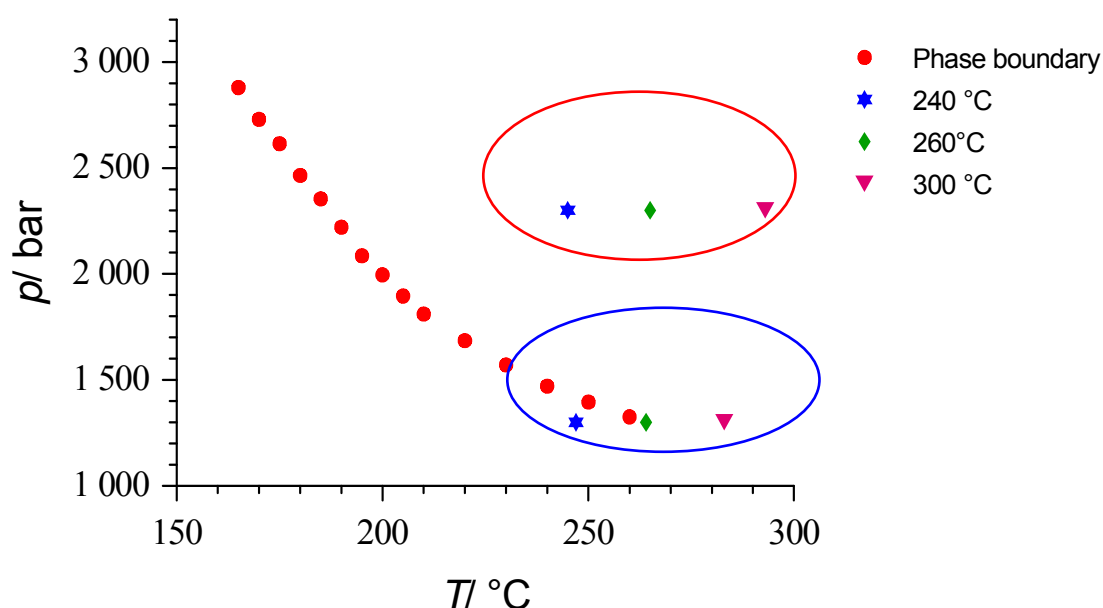


Figure 3.3: Strategy to synthesize random and non-random E-AA copolymers

### 3.6.3 Initiator solution

For the first series of measurements an initiator cocktail which consists of *tert*-butylperoxyacetate (TxF) and di-*tert*-butylperoxide (TxB) was used. Those two initiators differ in their optimal temperature ( $T_{\text{opt}}$ ), where  $T_{\text{opt}}$  for TxF is around 220 °C and for TxB is 260 °C. Above the optimal temperature the initiator efficiency decreases. The initiator cocktail was used for the experiments where the jacket temperature is chosen to be 220 °C. Unfortunately for those experiments it was not possible to handle the reaction due to the reaction temperature was unstable. The second candidate could be TxB which has been used for several copolymerizations as an initiator. Syntheses where the jacket temperature needs to be 220 °C requires a relatively high amount of initiator (TxB) in order to start the reaction. Such a large amount of initiator starts more chains and the rate coefficient of initiator decomposition increases due to reaction enthalpy. Those chains lead to a high temperature in the reaction system and increase the speed of the thermal self reaction. When a thermal reaction takes place spontaneously in the reaction system, it increases the risk of uncontrollability. This loss of control in most cases will end in a decomposition of monomer (ethene) to carbon. Decomposition of monomer happens when the system reaches very high pressures and temperatures within short time. The safety valve opens in the range 3009 to 3289 bar according to the manufacturer. Once decomposition of initiator occurs it is necessary to control the length of the screws and if the change of the screw length is greater than 1 % compared to original length then it must be replaced. After decomposition the reactor must be completely dismantled and cleaned and carbon must be removed from all part by rinsing with acetone.

### 3.6.4 Samples produced under adiabatic conditions

Some samples were produced under adiabatic conditions, which mean that the reaction temperature and the jacket temperature were identical. The advantage of this condition is that fouling of the polymer is decreased. The overall conversion is only temperature dependent. Reactions under adiabatic conditions were done at temperatures of 240 and 260 °C respectively. Samples which have produced at 240 °C showed no pressure dependence of conversion whereas for samples made at a temperature of 260°C conversion was dependent

on pressure. This finding could be explained by an increased solubility of TxF in the monomer by applying pressure at higher temperature. This pressure dependence was not observed in case TxB was used as the initiator for reactions at 260 °C.

### **3.6.5 Produced polymer samples**

Samples synthesized in this work can be divided into the following groups:

1. Copolymers which have different content of acid units
2. Copolymers produced under variation of temperature
3. Copolymers produced under variation of pressure
4. Copolymers produced under adiabatic conditions
5. Ethene copolymers with different comonomers

## Chapter 4

### Experimental methods used for characterization of copolymers

#### 4.1 Measurement of Cloud-Point Pressures (CPP)

In order to secure that reaction occurs in homogeneous phase, the cloud-point pressure of the poly(ethene-*co*-acrylic acid)/ethene mixture were determined. CPP curves were measured in an autoclave (figure 4.1) with variable internal volume. The design of the cell closely follows the construction principles used in optical transmission-type cells. The cylindrical cell body of 171 mm length and of 22 and 80 mm inner and outer diameter, respectively, is made from stainless steel (RGT 601, German Werkstoff-No. 2.4969, Arbed-Saarstahl).<sup>53</sup> The cell is sealed conically with a steel plug on either side. Each plug is pressed against the cell body via a flange that is held with six bolts on either side. The internal volume is separated from the pressurizing medium (heptane) with a movable piston sealed with a Karlez O-ring. The flat piston surface which faces the sapphire window (of 18 mm outer diameter and 10 mm length) is polished to assist the observation of phase separation in the internal volume. This volume is monitored by an endoscope camera (Optikon). The pictures are permanently displayed on a screen and are taped together with the associated pressure and temperature conditions for a more detailed analysis after the experiment. The pressure is recorded with a transducer (DMS 3 kbar, HBM-Messtechnik) in the cold part of the pressure-transmitting (heptane) system to  $\pm 6$  bar. The cell is heated from the outside with a resistance wire-heating (Pyrolon-M16,  $16\Omega\cdot\text{m}^{-1}$ , Les Cables de Lyon) embedded into a brass matrix that is fitted onto the autoclave. The temperature is measured within  $\pm 0.3$  K via a sheathed thermocouple that sits in the fluid mixture under investigation. The ethene/copolymer mixture is stirred by a Teflon<sup>®</sup>-coated small magnet that is driven (through the non-magnetic cell wall) by a larger outside magnet.

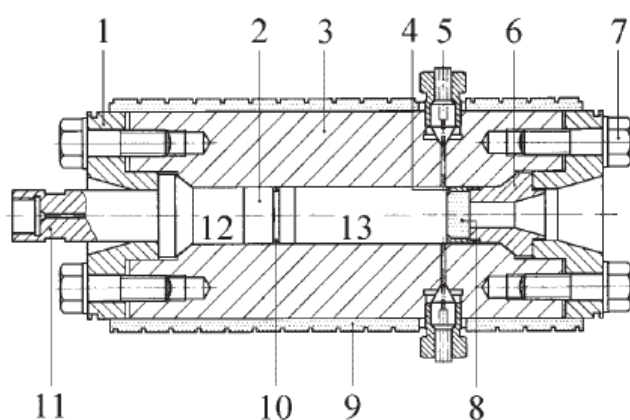


*Figure 4.1: High-pressure optical cell for measurements of the cloud-point pressure:*

1 flange; 2 movable piston; 3 cell body; 4 steel cap; 5 sheathed thermocouple; 6 plug; 7 bolt; 8 sapphire window; 9 heating mounted onto a brass jacket; 10 O-ring; 11 plug with connecting bore to the pressurizing system; 12 pressurizing fluid (heptane); 13 internal volume.

The procedure of measuring the CPPs is as follows: About 250 mg copolymer plus 30 mg of the inhibitor (2,6-di-tert-butyl-4-methylphenol, for synthesis, Merck-Schuchardt) were introduced into the autoclave before sealing. The air inside the autoclave was removed by flushing the internal volume at least eight times with ethene at a pressure of 10 bar. Ethene, to be used for preparing the E/copolymer mixture, is fed into the high-pressure cell by means of an auxiliary autoclave which contains about 8 g ethene which has been introduced at  $-10^{\circ}\text{C}$  and 80 bar. The amount of ethene fed into the internal volume of the high-pressure cell is accurately measured by weighing the auxiliary autoclave before and after feeding. The E mass is chosen such that the copolymer weight fraction within all CPP experiments is  $3 \pm 0.2$  wt.-%. After heating the high-pressure cell to the desired temperature, the pressure is increased, by means of the pressure generator in the heptane branch, until the E/copolymer mixture becomes homogeneous. The pressure is then slowly reduced to reach the cloud-point situation of the mixture at the selected temperature. Following the suggestion made in the literature<sup>54-56</sup>, the CPP is defined as the pressure at which the homogeneous monomer/polymer mixture turns opaque to such an extent that the magnetic stir bar can no longer be seen. Each CPP is measured at least three times. The reproducibility was better than  $\pm 10$  bar in most cases and always better than  $\pm 20$  bar. After recording the CPP at one temperature,  $T$  was increased and, after reaching constant  $T$  again, the CPP at the new temperature was measured.

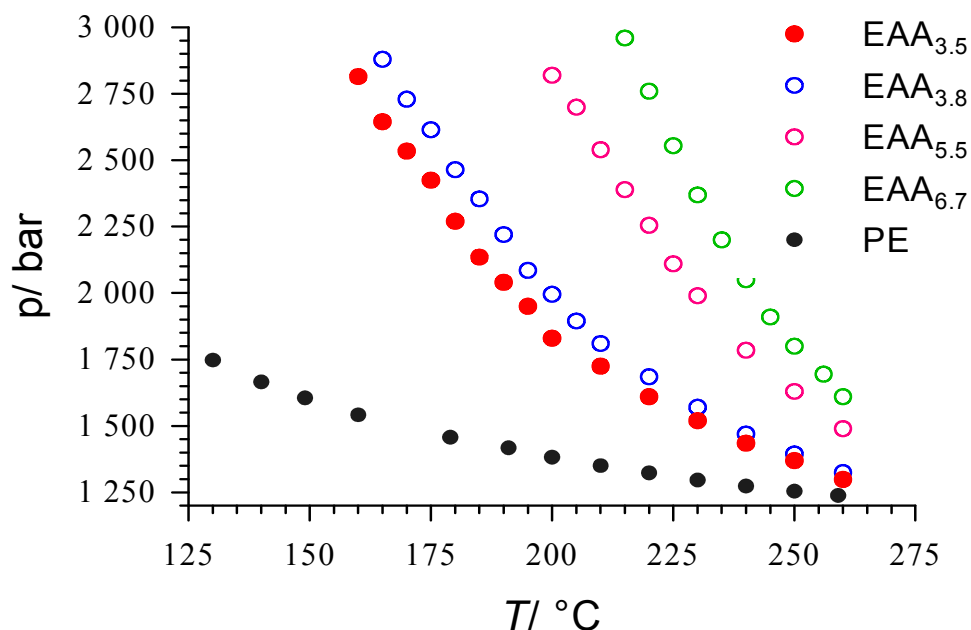


Figure 4.2: The CPP curve of E/Poly(ethene-co-acrylic acid)

An important aspect to be considered within phase behaviour studies into E-containing mixture at high pressures and temperatures relates to the fact that the system is potentially reactive and polymerization as well as polymer degradation may occur. By adding inhibitor, polymerization may be prevented unless the temperature is too high and/or the system is maintained under extreme conditions for a too extended period. On the other hand, the amount of inhibitor should not be too large, as this might affect phase behaviour. Indications for some reaction during CPP experiments on E/poly(E-co-acrylate) systems have been reported by Müller and Oellrich<sup>57</sup>. In his CPP experiments on E/poly(E-co-AA), Wind<sup>58</sup> observed gradual appearance of color and a decrease in pressure over a 48 h interval at 200 °C. To circumvent or at least reduce problems associated with reaction, CPPs were measured from low to high temperature. Moreover, for at least three temperatures, the CPP was re-measured upon cooling the system after measuring CPP at the highest temperature of the experimental series. Within these duplicate experiments, the CPPs determined during stepwise increase of temperature, were reproduced within the above-mentioned accuracy of  $\pm 20$  bar. Moreover, none of the polymer samples showed even minor indications of any colour developed during the thermodynamic measurement. Considering the evidence from these additional studies, it appears justified to consider the CPP curves measured within the



present study as thermodynamic data without interference from any kind of reaction during CPP determination.

## 4.2 Determination of the Molecular weight distribution

Size-Exclusion-Chromatography (SEC) was used to determine the molecular weight distribution of the ethene-*co*-acrylic acid polymer. The SEC system consists of a Waters inline degasser, a Waters 515 double pump, a JASCO AS-2055 auto sampler and a Waters 2410 differential refractometry. The system includes one pre-column and three separation columns:<sup>59</sup>

- (1) PSS SDV, 8x50 mm, 5  $\mu$
- (2) PSS SDV, 8x300 mm, 5  $\mu$ ,  $10^5$  Å
- (3) PSS SDV, 8x300 mm, 5  $\mu$ ,  $10^3$  Å
- (4) PSS SDV, 8x300 mm, 5  $\mu$ ,  $10^2$  Å

The SEC measurement operates at 35 °C and tetrahydrofuran (THF) used as an eluent with a flow rate of  $1.0 \text{ ml} \cdot \text{min}^{-1}$ . Calibration of the setup is carried out with polystyrene (PS) standards ( $M = 410$  through  $2 \cdot 10^6 \text{ g} \cdot \text{mol}^{-1}$ ). The primary SEC was processed with the software "PSS WinSEC" for Windows. Due to the high nonpolar ethene part in the copolymer, some samples were insoluble in THF under setup conditions.

The molecular weight distribution of THF-insoluble copolymer samples was determined by a high-temperature SEC setup at the Institute for Technical and Macromolecular Chemistry at the University of Darmstadt in cooperation with the group of Prof. M. Busch. The high-temperature SEC setup operates at 140 °C, and consists of one pre-column and three main separation columns:

- (1) PSS Polefin, 8x50 mm, 10  $\mu$
- (2) PSS Polefin, 8x300 mm,  $10^6$  Å
- (3) PSS Polefin, 8x300 mm,  $10^4$  Å
- (4) PSS Polefin, 8x300 mm,  $10^3$  Å

1,2,4-Trichlorobenzene (TCB) is used as an eluent with a flow rate of  $0.95 \text{ ml}\cdot\text{min}^{-1}$ , the injection volume was 200  $\mu\text{l}$ . o-xylene was used as an internal standard in order to correct the flow rate. Polyethylene standards from PSS (Polymer Standards Service) and polystyrene standards from Polymer Laboratories Company Ltd were used for calibration. The samples were etherified before the measurement in order to reduce the polarity of the polymer. For the etherification, a few milligram of the copolymer were put into a 25 ml standard glass with screw cap and 20 ml of TCB were added. The mixture is kept for two hours at  $140^\circ\text{C}$  in the oven. Subsequently, Silazan is added and the mixtures kept at least one more hour at  $140^\circ\text{C}$ . During this period, samples must be turned top to bottom and bottom to top twice, but without shaking. After that the samples are filtered through a  $1 \mu\text{m}$  Teflon membrane filter.

### 4.3 FT-IR and ATR-FT-IR spectroscopy

Infrared spectroscopy has been intensively used for polymer analysis to study branching, crosslinking, crystallinity, and residual monomer content.<sup>60-64</sup> From characteristic vibrational modes in the infrared (IR) or near infrared (NIR) composition can also be measured, which is of particular importance for copolymerization. In this work IR and NIR spectroscopy were used in order to determine composition of the E-AA copolymer.

The IR spectra were taken on a Fourier transform instrument (Bruker IFS 88) equipped with a globar light source, a Si-coated  $\text{CaF}_2$  beamsplitter and a DTGS detector and rinsed by carbon dioxide in order to remove compressed air. The spectra were processed using the software package OPUS (Spectrometry-Software, Bruker). A wavenumber range from 1300 to  $8000 \text{ cm}^{-1}$  was recorded and one hundred interferograms were co-added to increase the S/N ratio of each spectrum. The optical path length for the spectroscopy of the polymer samples ranged from 0.1 to 0.5 mm.

The spectra were measured for copolymer films produced on a Specac 15510 instrument at a temperature of  $140^\circ\text{C}$  and a pressure of  $3\cdot 10^6 \text{ N}$  forces. From 20 to 100 mg of copolymer, samples were prepared between two teflon films and pressed with two pressure plates which have a thickness of 0.1mm and are heated up to  $150^\circ\text{C}$  with  $3\cdot 10^6 \text{ N}$  force for 2 minutes, and cooled down to room temperature via water cooling. The polymer film is separated very carefully from teflon films and fixed on the cardboard.

At a later stage of this work, another measurement method, the Attenuated Total Reflectance Fourier Transform Infra-Red (ATR-FT-IR) was available. In case of ATR, reflexion by the sample surface is measured instead of transmission. The thickness of the polymer sample is not relevant within this technique. A diamond crystal was used as a carrier for the substances in the ATR unit (MVP 2 Star<sup>TM</sup> Harrick). The polymer sample is fixed at the diamond crystal with a screw driver, and there is no need for sample preparation since the polymer sample is solid.<sup>65</sup>

The IR absorbance spectrum of an E/AA (4.4 mol%) copolymer film is given in Figure 4.3. The cross-hatched area around 1700 cm<sup>-1</sup> is due to the IR absorbance of the C=O fundamental mode of AA units. The cross-hatched area under the absorbance band between 1440 and 1500 cm<sup>-1</sup> primarily originates from bending modes of CH<sub>2</sub> groups. The range between 1440 and 1500 cm<sup>-1</sup> was chosen for the analysis rather than the entire band extending to 1400 cm<sup>-1</sup> (and even smaller wavenumbers) as the intense CH<sub>2</sub> absorption of polyethylene also occurs in this region. The absorption around 1400 cm<sup>-1</sup> is partly assigned to the OH group of the COOH moiety. It should be noted that the ranges for band integration may be freely selected to some extent. Once the limiting wavenumbers and type of baseline (horizontal or connecting line through the absorbance values on either side of band) however are fixed, this information must clearly be stated to make the results useful for general application. The correlation of the data from IR spectroscopy and from elemental analysis is determined by Equation 4.1.<sup>49,66,67</sup>

$$\frac{\int(\text{CO})}{\int(\text{CH} + \text{OH})} = \frac{F_{\text{AA}}}{a + F_{\text{AA}} \cdot b} + c \quad (4.1)$$

The limits for integration of the C=O and for CH<sub>2</sub> absorbance of the E/(M)AA copolymers are given in Table 4.1.

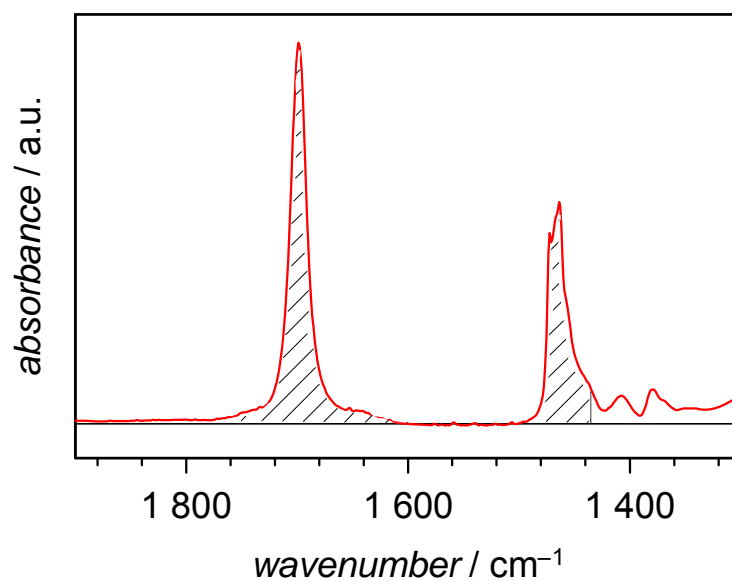


Figure 4.3: IR/NIR absorbance of poly (ethene-co-acrylic acid )

Copolymer	Integration limits	
	C=O band / $\text{cm}^{-1}$	CH, OH band / $\text{cm}^{-1}$
E-MAA	1950, 1550	1530, 1435
E-AA	1850, 1550	1530, 1435

Copolymer	Baseline for integration	
	C=O band / $\text{cm}^{-1}$	CH, OH band / $\text{cm}^{-1}$
E-MAA	1970, 1950, 1550, 1520	1550, 1545, 1535, 1530
E-AA	1850, 1820, 1550, 1520	1550, 1545, 1535, 1530

Copolymer	Coefficients			
	a	b	c	$F_{(M)AA}$ range
E-MAA	0.0272	0.0474	0.4117	0 - 0.15
E-AA	0.0089	0.1665	-0.574	0.025 - 0.08

Table 4.1: Wavenumber data referring to the IR analysis of the copolymer films and parameters which describe the correlation of E/ (M)AA copolymer compositions determined by elemental analysis and by FT/IR spectroscopy.<sup>66</sup>

#### 4.4 Differential Scanning Calorimetry

Differential Scanning Calorimetry is a thermal analysis method. DSC measures temperatures and heat flows associated with thermal transitions in a material.<sup>68</sup> Common usage includes investigation, selection, comparison and end-use performance evaluation of materials in research, quality control and production applications.<sup>69</sup> Material properties measured by DSC techniques include glass transitions, "cold" crystallization, phase transition, melting, crystallization, product stability, cure kinetics, and oxidative stability.<sup>70</sup> The principle scheme of a DSC setup consists of an oven and two parallel pans, one for sample and one for the reference (See figure 4.4).

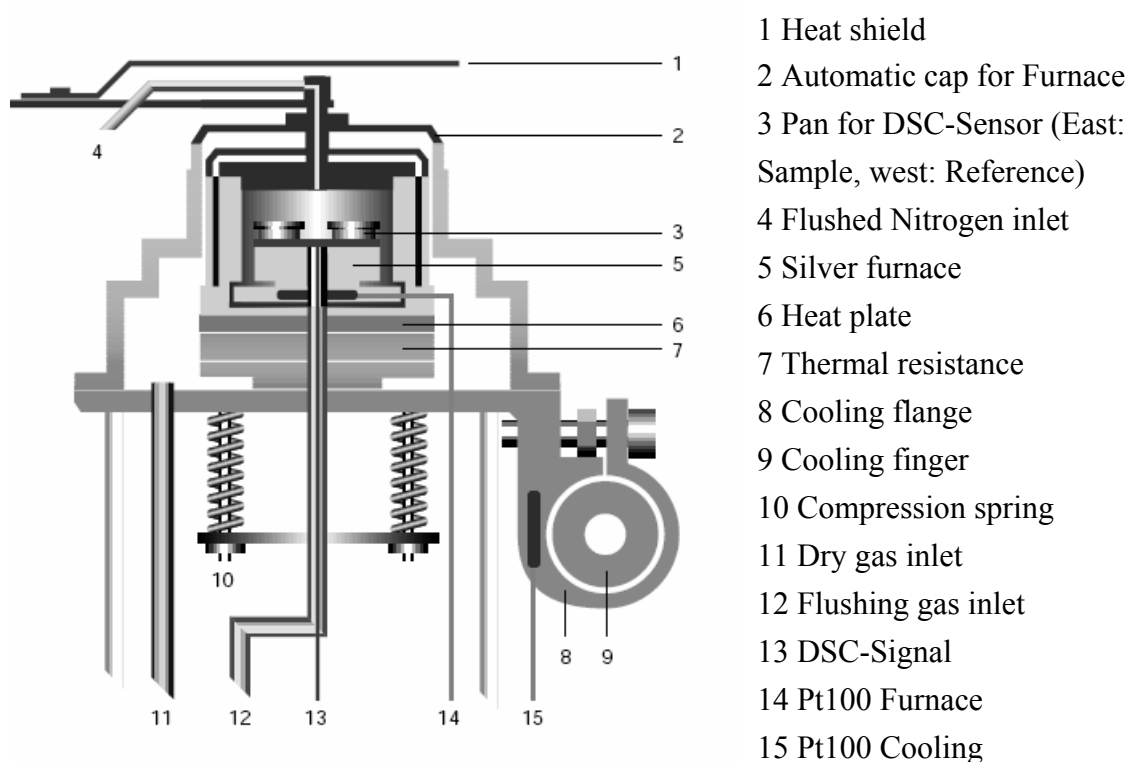
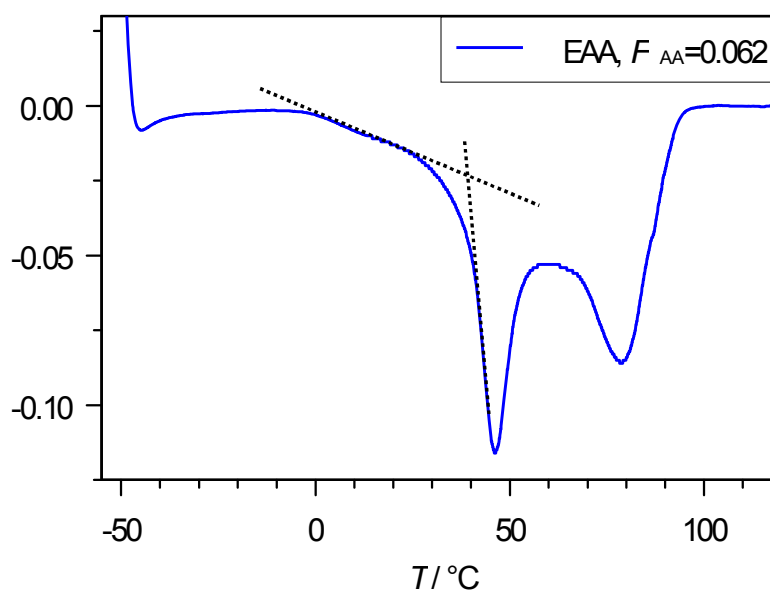


Figure 4.4: Scheme of DSC apparatus.<sup>71</sup>

The pairs of pans are separately heated electrically and cooled off. Measured is the differential heat flux as a function of time, it determined from the difference of the resistance

heating. The experimental data is depicted in a thermogram, provides information on the modification of the specific heat capacity of the investigated sample. In contrast to metals, semi-crystalline polymers have no sharp thermodynamic first order phase transitions.<sup>72</sup> However, they have relatively broad phase transition areas. The reason is that semi-crystalline polymers have different thicknesses of lamellar structure from crystallites. At the start of the melting area, such as initial temperature of the melting peaks, first the less perfect crystallites melt. Most crystals melt at the temperature associated with the peak maximum in the thermogram (see Figure 4.5). Also for the determination of the glass transition temperature peak maximum chose as a glass transition. In this work the glass transition and melting temperature was determined by the method shown in figure 4.5 (dashed lines).



*Figure 4.5: Calculation method of the glass and melting transitions temperature in the DSC-Thermogram of E-AA copolymer*

Differential scanning calorimetry (DSC) is performed by a Mettler Toledo DSC 820 equipped with a circulatory cryostat filled with ethanol. The minimum temperature which could reach by DSC setup was  $-55^\circ\text{C}$  and heating rate was chosen  $5^\circ\text{C}\cdot\text{min}^{-1}$ . An empty pan is used as a reference for the sample material. The furnace is flushed with nitrogen during the experiment to avoid moisture. A linear fit of the data for temperatures below melting

transition is used as baseline and subtracted from the data (see Figure 4.5). The data was further normalized to the sample weight of typically 15 mg.

#### 4.5 Dynamic Mechanical Analysis

The dynamic mechanical analysis (DMA) was used to determine the viscoelastic properties of the polymer samples.<sup>73</sup> The investigation of polymer samples was done in the group of Prof. Samwer at the Institute of Physics in Goettingen University.

A Perkin-Elmer DMA 7 was used for the dynamic mechanical analysis in the compression mode. To achieve reproducible conditions, the initially porous reaction product is filled into a PTFE mold.<sup>74</sup> Via a PTFE piston, the sample material is getting squeezed into a cylindrical shape at temperature slightly above the melting transition under high-vacuum conditions. The applied pressure equals initially 1 MPa but decreases during the heating period (2 h) via a drilled degassing hole shortly below the final piston level. The resulting sample cylinders of 5 mm in diameter and 5 – 10 mm in height are mounted in the DMA.<sup>75</sup> A parallel quartz plate setup is used exerting a static uniaxial pressure of typically 10 kPa superimposed by a half as high dynamic pressure at constant frequency of 5 Hz. All measurements have been executed in nitrogen atmosphere under continuous purification removing H<sub>2</sub>O and O<sub>2</sub>. Liquid N<sub>2</sub> cooling provides a vast temperature range with a stable heating rate at 5 K/min from 135 K onwards, limited by the onset of viscous flow.<sup>76</sup>

#### 4.6 Pulsed Laser Deposition Technique

Pulsed laser deposition (PLD) is a versatile technique for many reasons. Since with this method the energy source is located outside the chamber, the use of ultrahigh vacuum (UHV) as well as ambient gas is possible. Combined with a stoichiometry transfer between target and substrate this allows depositing all kinds of different materials, e.g., high-temperature superconductors, oxides, nitrides, semiconductors, metals and even polymers or fullerenes can be grown with high deposition rates.<sup>77-79</sup> The pulsed nature of the PLD process even allows for preparing complex polymer-metal compounds and multilayers.

PLD of polyethylene, poly(methylmethacrylate) and ethene-co-acrylic acid copolymer films have been carried out in cooperation with the group of Prof. H.-U. Krebs at the Institute for Material Physics in Goettingen University.

A typical set-up for PLD is schematically shown in Figure 4.6. In an ultrahigh vacuum chamber, elementary or alloy targets are struck at an angle of  $45^\circ$  by a pulsed and focused laser beam. The atoms and ions ablated from the target(s) are deposited on substrates. Mostly, the substrates are attached with the surface parallel to the target surface at a target-to-substrate distance of typically 2 to 10 cm.<sup>80</sup>

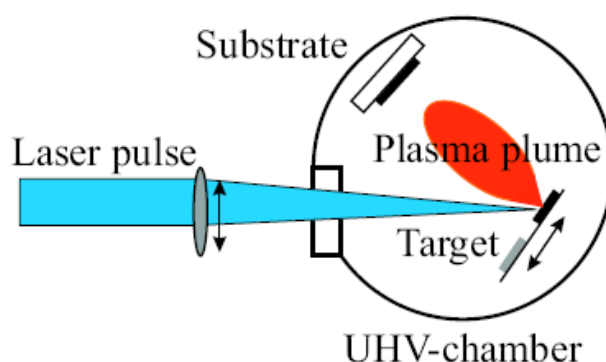


*Figure.4.6: Schematic diagram of a typical laser deposition set-up*

In our case, an excimer laser LPX 110i (Lambda Physik) with KrF radiation (wavelength 248 nm, pulse duration 30 ns) is focused onto targets consisting of dense, hot-pressed copolymers and polyethylene. The background pressure inside the deposition chamber was below  $5 \cdot 10^{-8}$  mbar. The copolymer and polyethylene films were deposited at room temperature using laser fluences between 30 and 9000 mJ/cm<sup>2</sup>. The average laser energy was measured by a Soliton joulemeter ED-500. Due to focusing geometry, the energy distribution on the target is Gaussian-like. The laser fluence was calculated by dividing the measured integral laser energy by the blackened area on a photosensitive paper. To reach the lower laser fluences, the focal laser spot was widened by moving the lens position and thus the target out of the focal position. Additionally, if necessary, a partially reflecting quartz mirror was used to weaken the laser intensity. Films with thicknesses up to about 1  $\mu$ m were deposited on Si substrates (size of 1 cm<sup>2</sup>) at a target-to-substrate distance of about 7 cm. Targets were



prepared by using a heated press. The polymer samples were pressed with the pressure of  $3 \cdot 10^{-7} \text{ N} \cdot \text{cm}^{-2}$ .

## 4.7 Powder X-ray diffraction method

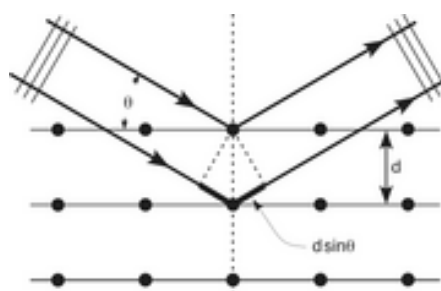


Figure 4.7: Diffraction angle for the x-ray method

The incoming beam (coming from upper left) causes each scatterer to re-radiate a small portion of its energy as a spherical wave. If scatterers are arranged symmetrically with a lattice distance  $d$ , these spherical waves will interfere constructively only in directions where their path-length difference ( $2d \sin \theta$  equals) is an integer multiple of the wavelength  $\lambda$ . In that case, part of the incoming beam is deflected by an angle  $2\theta$ , producing a reflection spot in the diffraction pattern (see Figure 4.7).<sup>81</sup> Crystals are regular arrays of atoms, and X-rays can be considered waves of electromagnetic radiation. The X-ray waves are primarily scattered through the electrons. Just as an ocean wave striking a lighthouse produces secondary circular waves emanating from the lighthouse, so an X-ray striking an electron produces secondary spherical waves emanating from the electron. This phenomenon is known as scattering, and the electron (or lighthouse) is known as the scatterer. A regular array of scatterers produces a regular array of spherical waves. Although these waves cancel one another out in most directions (destructive interference), they add constructively in a few specific directions, determined by Bragg's law:<sup>82</sup>

$$n\lambda = 2d \sin \theta \quad n=1,2,3,\dots$$

where  $n$  is any integer. These specific directions appear as spots on the diffraction pattern, often called *reflections*. Thus, X-ray diffraction results from an electromagnetic wave (the X-

ray) impinging on a regular array of scatterers (the repeating arrangement of atoms within the crystal). X-rays are used to produce the diffraction pattern because their wavelength  $\lambda$  is typically of the same order of magnitude (1-100 Ångströms) as the spacing  $d$  between planes in the crystal. In principle, any wave impinging on a regular array of scatterers produces diffraction. To produce significant diffraction, the spacing between the scatterers and the wavelength of the impinging wave should be roughly similar in size. In this work all powder X-ray measurements have been measured at the Institute of Physics in Goettingen University with cooperation of Andreas Meschede.

#### 4.8 Small-angle X-ray scattering (SAXS)

Small-angle X-ray scattering (SAXS) is a technique where the elastic scattering of X-rays (wavelength 0.1 ... 0.2 nm) by a sample which has inhomogeneities in the nm-range, is recorded at very low angles (typically 0.1 - 10°). This angular range contains information about the shape and size of macromolecules, characteristic distances of partially ordered materials, pore sizes, and other data. SAXS is capable of delivering structural information of macromolecules between 5 and 25 nm, of repeat distances in partially ordered systems of up to 150 nm.<sup>83</sup> USAXS (ultra-small angle X-ray scattering) can resolve even larger dimensions.

SAXS and USAXS belong to a family of X-ray scattering techniques that are used in the characterization of materials. In the case of biological macromolecules such as proteins, the advantage of SAXS over crystallography is that a crystalline sample is not needed. NMR methods encounter problems with macromolecules of higher molecular mass (> 30000-40000). However, owing to the random orientation of dissolved or partially ordered molecules, the spatial averaging leads to a loss of information in SAXS compared to crystallography.

In a SAXS instrument a monochromatic beam of X-rays is brought to a sample from which some of the X-rays scatter, while most of them simply go through the sample without interacting with it. The scattered X-rays form a scattering pattern which is then detected at a detector which is typically a 2-dimensional flat X-ray detector situated behind the sample perpendicular to the direction of the primary beam that initially hit the sample. The scattering pattern contains the information on the structure of the sample.

The major problem that must be overcome in SAXS instrumentation is the separation of the weak scattered intensity from the strong main beam. The smaller the desired angle, the more difficult this becomes. The problem is comparable to one encountered when trying to observe a weakly radiant object close to the sun, like the sun's corona. Only if the moon blocks out the main light source does the corona become visible. Likewise, in SAXS the non-scattered beam that merely travels through the sample must be blocked, without blocking the closely adjacent scattered radiation. Most available X-ray sources produce divergent beams and this compounds the problem. In principle the problem could be overcome by focusing the beam, but this is not easy when dealing with X-rays and was previously not done except on synchrotrons where large bent mirrors can be used. This is why most laboratory small angle devices rely on collimation instead. All SAXS measurement in this work is measured at the Max-Planck Institute of Biophysical Chemistry in Goettingen cooperation with Dr. J.Davaasambuu.

#### 4.8.1 Scattering from particles

Small-angle scattering from particles can be used to determine the particle shape or their size distribution. A small-angle scattering pattern can be fitted with intensities calculated from different model shapes when the size distribution is known. If the shape is known, a size distribution may be fitted to the intensity. Typically one assumes the particles to be spherical in the latter case. If the particles are dispersed in a solution and they are known to be monodisperse, and all of the same size, then a typical strategy is to measure different concentrations of particles in the solution. From the obtained SAXS patterns the intensity pattern for a single particle can be extrapolated. This is a necessary procedure that eliminates the concentration effect, which is a small shoulder that appears in the intensity patterns due to the proximity of neighboring particles. The average distance between particles is then roughly the distance  $2\pi/q^*$ , where  $q^*$  is the position of the shoulder on the scattering vector range  $q$ . The shoulder thus comes from the structure of the solution and this contribution is called the structure factor. For the small-angle X-ray scattering intensity can be written:

$$I(q) = P(q)S(q)$$

where

- $I(q)$  is the intensity as a function of the magnitude  $q$  of the scattering vector
- $P(q)$  is the form factor
- and  $S(q)$  is the structure factor.

When the intensities from low concentrations of particles are extrapolated to infinite dilution, the structure factor is equal to 1 and no longer disturbs the determination of the particle shape from the form factor  $P(q)$ . One can then easily apply the Guinier approximation (also called Guinier law), which applies only at the very beginning of the scattering curve, at small  $q$ -values. According to the Guinier approximation the intensity at small  $q$  depends on the radius of gyration of the particle.<sup>84</sup>

An important part of the particle shape determination is usually the distance distribution function  $p(r)$ , which may be calculated from the intensity using a Fourier transformation.<sup>85</sup>

$$p(r) = \frac{r^2}{2\pi} \int_0^\infty I(q) \frac{\sin qr}{qr} q^2 dq$$

The distance distribution function  $p(r)$  starts from zero at  $r = 0$  due to the multiplication by  $r^2$ . The shape of the  $p(r)$ -function tells something about the shape of the particle. If the function is very symmetric, the particle is also highly symmetric, like a sphere.<sup>[2]</sup> The distance distribution function should not be confused with the size distribution.

The particle shape analysis is especially popular in biological small-angle X-ray scattering, where the shapes of proteins and other natural colloidal polymers are determined.

## 4.9 Scanning electron microscopy

The film morphology was studied by scanning electron microscopy (Cambridge S360) in cooperation with group of Prof. Krebs at the Institute of Material Science of Goettingen University. To avoid charge effects, the films were covered by a thin gold layer of about 20 nm.

## 4.10 Solid State NMR spectroscopy

NMR spectroscopy has been used to determine the chemical composition of the copolymers. Quantitative  $^{13}\text{C}$ -NMR gives information about the micro-structure of copolymers and multidimensional NMR helps to understand the linkage patterns in the copolymers. All NMR spectroscopy measurements have been performed in cooperation with the group of Dr. M. Baldus, at the Max Planck Institute for Biophysical Chemistry in Goettingen.

Copolymers which are synthesized in this work are not soluble in the standard solvent (such as trichloromethane  $\text{d}_1$  ( $\text{CDCl}_3$ ) and tetrachlorethane  $\text{d}_2$  ( $\text{C}_2\text{D}_2\text{Cl}_4$ ) which are used for liquid state NMR) at room temperature. For this reason, high temperature ( $120^\circ\text{C}$ ) liquid state NMR spectroscopy must be used for the characterization of the synthesized copolymers.

A promising and well applied method for the structural characterization of the low soluble polymers is solid state NMR (ss-NMR). Polymer samples do not need an additional or special requirements for the measurement of ss-NMR.<sup>88,89</sup>

In solids, the couplings of nuclear spins with their local surroundings are anisotropic, leading to inhomogeneously broadened NMR spectra. In particular, ss  $^2\text{H}$ -NMR exploits the anisotropic coupling of the quadrupole moment of the  $^2\text{H}$  nucleus with an electric field gradient (EFG) tensor at the nuclear site. For aliphatic moieties, the EFG tensor is approximated to be axially symmetric with the unique axis along the C- $^2\text{H}$  bond; in this case, the angular dependence of the NMR frequency  $\omega(\vartheta)$  of a molecular site is given by:

$$\omega(\vartheta) = \omega_0 \pm 0.5\delta(3\cos^2\vartheta - 1)$$

where the polar angle  $\vartheta$  describes the orientation of the C- $^2\text{H}$  bond with the respect to the external magnetic field  $B_0$ . Here,  $\omega_0$  denotes the Larmor frequency and the anisotropy parameter  $\delta$  specifies the strength of the quadrupolar interaction. Thus, the orientation of a molecular segment is directly related to the position of a line in the resulting one-dimensional spectrum; and, for an isotropic distribution of sites, a powder pattern (Pake spectrum) is observed.<sup>89</sup>

Reorientations render  $\mathcal{Q}$  and thus  $\omega(\mathcal{Q})$  time dependent, with motions on a time scale of microseconds or faster resulting in characteristic changes of the one-dimensional  $^2\text{H}$ -NMR line shape. For example, the fast rotation of a methyl group about its  $C_3$  symmetry axis gives rise to a motionally averaged Pake spectrum, scaled by an averaged anisotropy parameter  $\bar{\delta} = -1/3\delta$ , with the unique axis of the EFG tensor pointing along the  $C_3$  axis.

Unique geometric information about microscopic molecular motions on a time scale of milliseconds to seconds is accessible by 2D exchange ss-NMR spectroscopy, which probes the orientation of a particular site at two subsequent times.<sup>90</sup>



## Chapter 5

### Results and discussions

#### 5.1 Cloud Point Pressure of the E/poly(E-co-AA) system

The phase behavior of the monomer/polymer system needs to be known to ensure that polymerization takes place in a homogeneous fluid phase and in order to optimize the separation process after reaction. “Chemically homogeneous” means that the composition of each individual macromolecule is more or less the same and thus is close to the one of the entire copolymer sample. Figure 5.1 shows the experimental observation of a cloud point. Depending on pressure, there could be 4 different situation associated with determination of cloudness of system.

1. Homogeneous solution (well above the phase boundary)
2. Beginning of cloudiness (above phase boundary)
3. Cloud point (exactly at the phase boundary)
4. Opaque solution (below phase boundary)

Plotted in Figure 5.2 are cloud point pressures, CPPs of E/poly(E-co-AA) systems with acrylic acid copolymer content varying from 3.5 mol % AA units, E<sub>96.5</sub>AA<sub>3.5</sub>, to 6.7 mol-% AA units, E<sub>6.7</sub>AA<sub>93.3</sub>. The subscripts refer to the mole percentage of comonomer units. For comparison, a CPP curve for E/PE is included in Figure 5.2. As is to be expected, the CPP increases with the content of AA in the copolymer. This effect is particularly pronounced at lower temperature.<sup>66</sup>



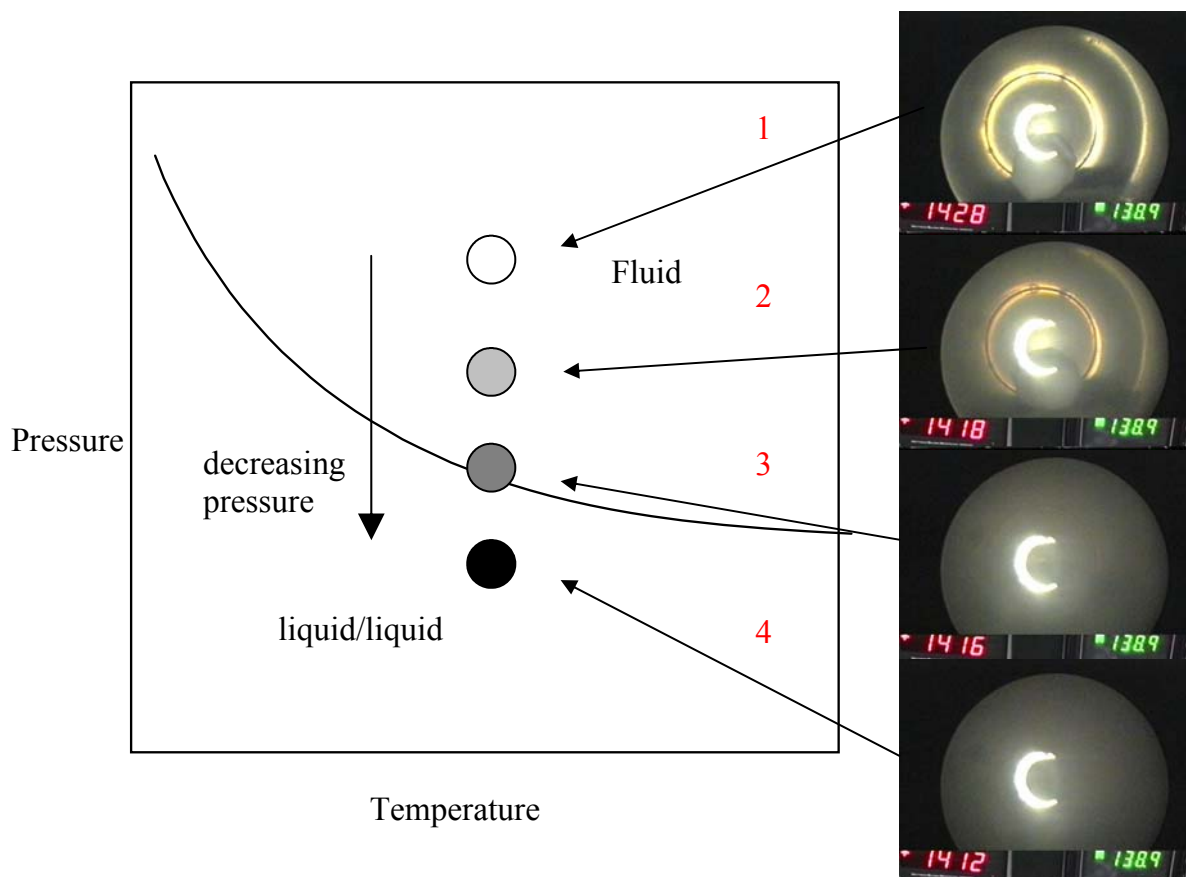


Figure 5.1: Picture of cloud point determination<sup>92</sup>

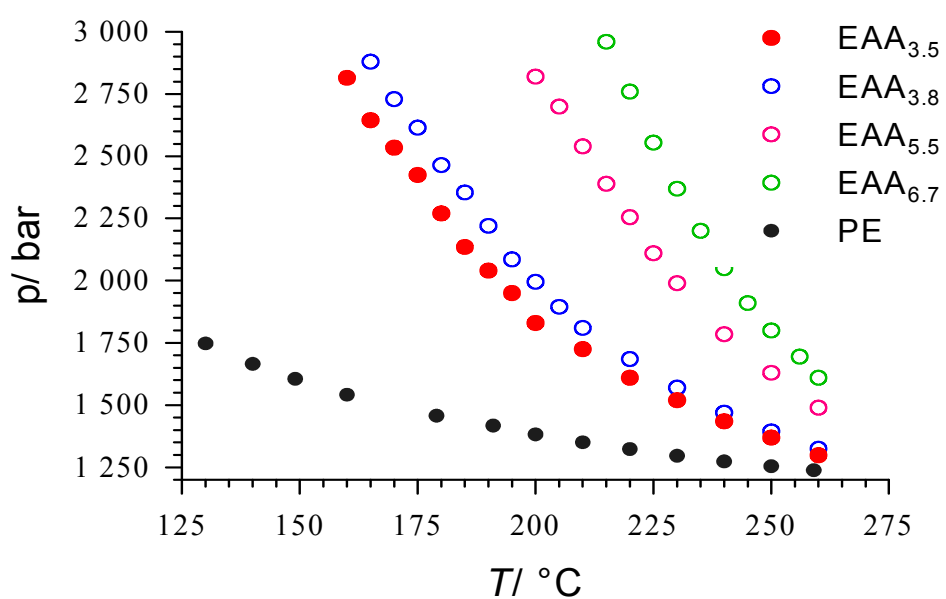


Figure 5.2: CPP vs temperature curves for several E/poly (E-co-AA) systems (with different content of acrylic acid)

Despite chemical homogeneity, the copolymer samples may be random or non-random with respect to the distribution of the polar groups. Random copolymers are expected to be produced in syntheses carried out at pressure and temperature conditions which are well above the cloud-point curve, which separates single-phase and two-phase regions. Non-random copolymer, on the other hand, may occur in syntheses close to this phase boundary. E-AA copolymers were produced under reaction conditions which were either relatively close or clearly apart from the cloud point pressure curve (see Figure 5.3)

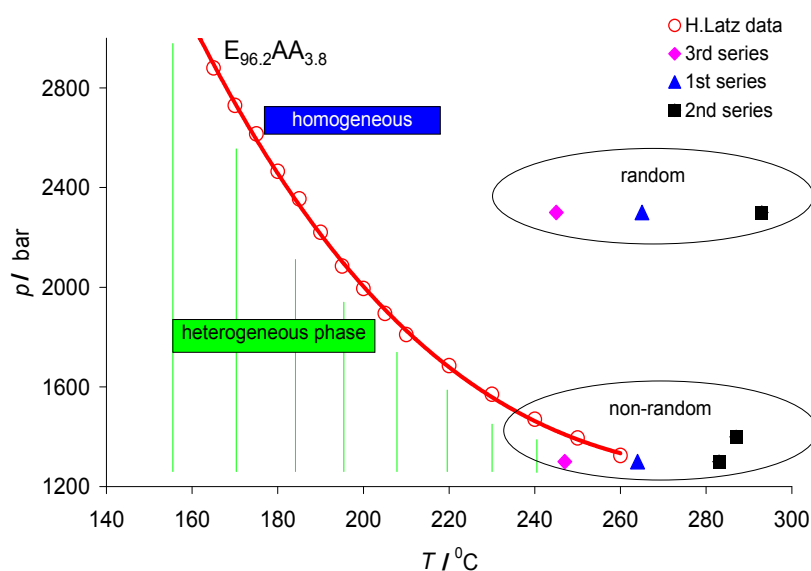


Figure 5.3: Strategy of producing E-AA copolymers

## 5.2 Determination of acrylic acid content in the copolymer

The composition of E-AA copolymer samples, synthesized in this work has been determined. In order to find an easy and exact method for the calculation of copolymer content, different methods have been applied e.g., FT-IR spectroscopy of thin films, ATR-FT-IR spectroscopy  $^{13}\text{C}$ -NMR-Spectroscopy and calculation from reactivity ratios. Figures 5.4 to 5.6 show the spectra obtained for EAA copolymers.

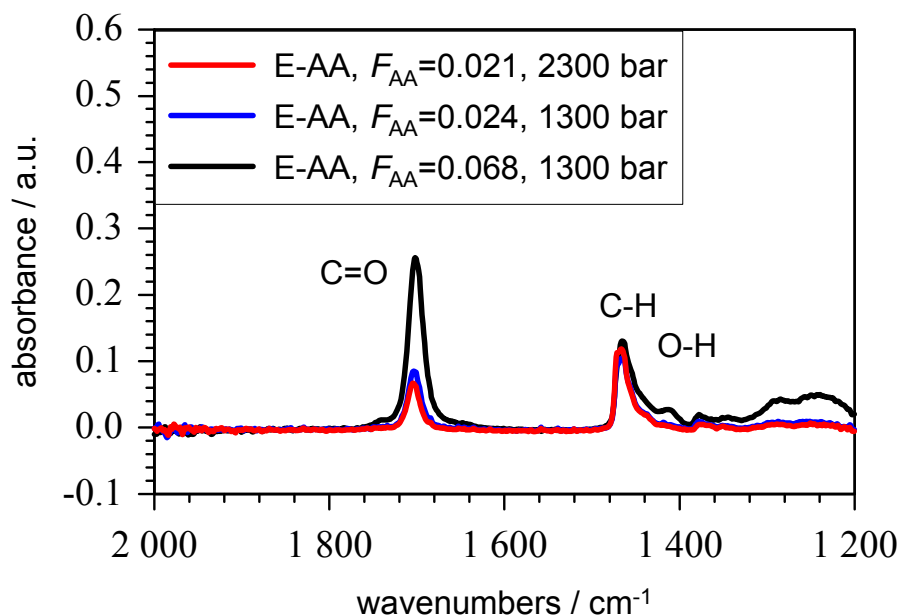


Figure 5.4: FT-IR-Absorption spectra of EAA films produced at different pressure and different content of AA.

One of the analytical methods for determination of the acrylic acid content in the produced copolymers is FT-IR spectroscopy. This method determines the content of acrylic acid by integration of the absorbance spectra of pressed films. A requirement for this method is to produce thin polymer films, which should be free from air and must be sufficiently thin for transmission measurement. In order to get adequate mechanical strength, a certain thickness of samples must be applied for the thin copolymer film. Unfortunately it was not possible to prepare thin films with the same thickness from all produced copolymers because of their different physical properties.

Figure 5.4 shows FT-IR spectra of copolymers produced at high (red) and low (blue) pressure with nearly the same content of acrylic acid and, on the other hand, a copolymer produced at low pressure with a high content of acrylic acid (6.8 mol%). There is no difference for the copolymers produced at different pressure with nearly the same content of acrylic acid but the FT-IR spectra of copolymer with relatively higher content of acrylic acid ( $F_{AA}=0.068$ ) shows significantly higher absorbance in the region of 1700 wavenumbers, which is assigned to the carbonyl group. Also the intensity of signals related to the OH-group is increased for the IR-spectrum of copolymer with high content of acrylic acid. The content of AA in the copolymer has been calculated using equation 5.1

As already mentioned, there was no opportunity to get pressed thin film from all copolymer samples. Therefore ATR-FT-IR has been applied, as this method requires no sample preparation. An ATR-FT-IR spectra of EAA copolymers produced at high ( $F_{AA}=0.042$ ) and low ( $F_{AA}=0.041$ ) pressures are shown in Figure 5.5.

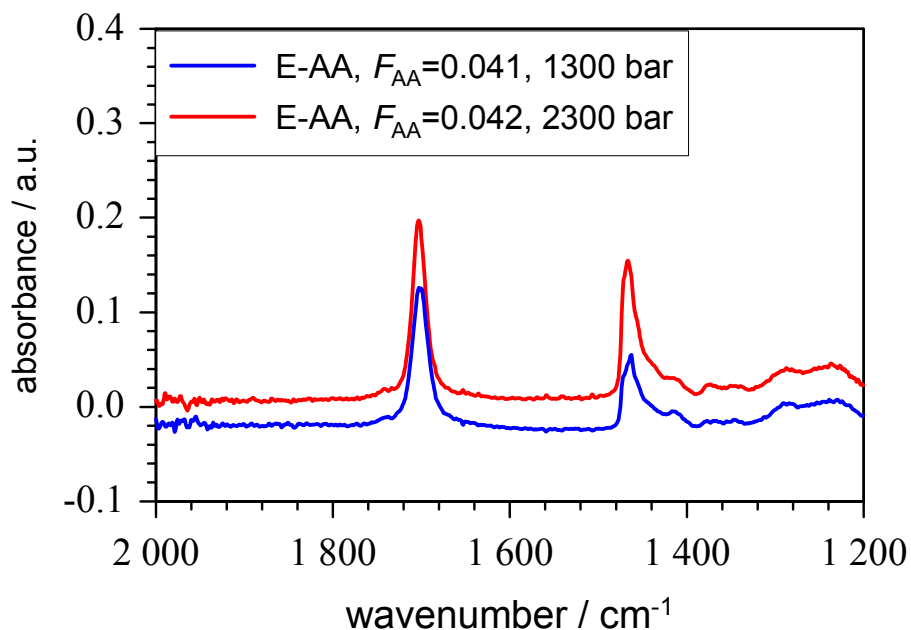


Figure 5.5: ATR-FT-IR Spectra of expected to be random (red) and non-random (blue) copolymers with highest content of AA

The acrylic acid contents of the E-AA copolymers calculated by ATR-FT-IR and FT-IR are very close to each other. The ATR-FT-IR method has been applied for all copolymers to measure acrylic acid content in the copolymer.

$^{13}\text{C}$ -NMR is another method for the determination of AA content in the copolymer and spectra are shown in Figure 5.6. The calculation of AA in the copolymer is based on the ratio of integrated absorption of carboxyl (around 185 ppm) and integration over all of  $^{13}\text{C}$  signals. The disadvantage of this method is the relatively long measuring time compared to FT-IR and ATR-FT-IR spectroscopy.

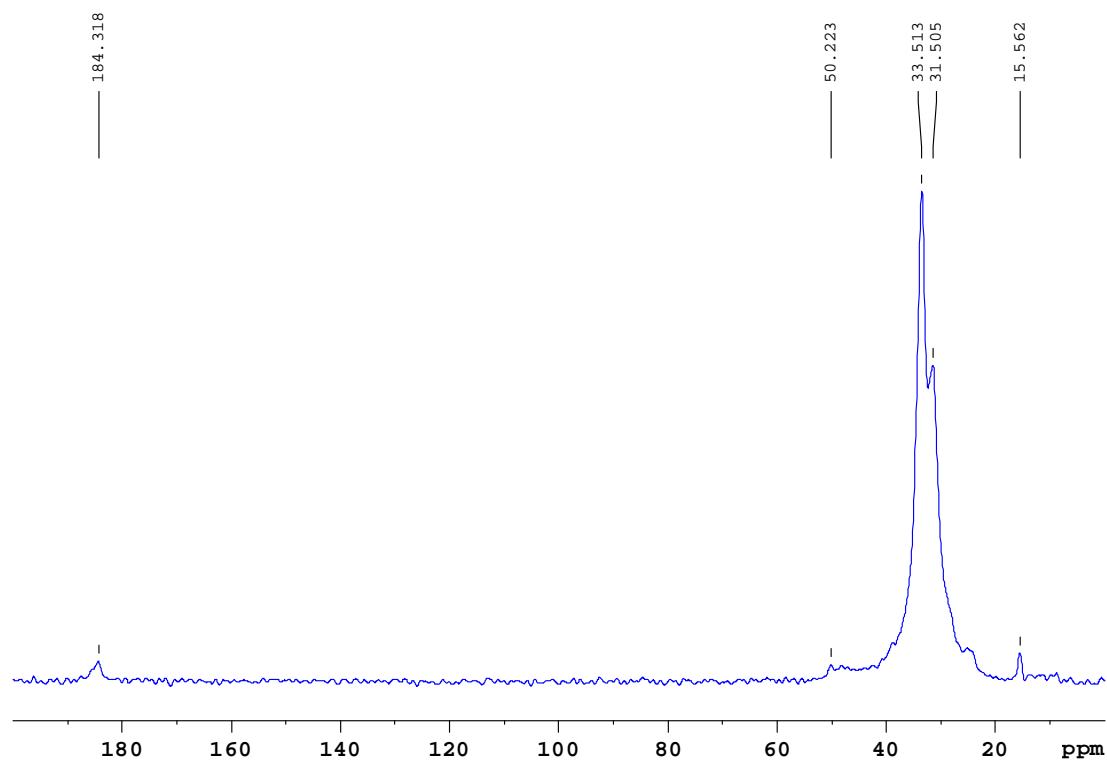
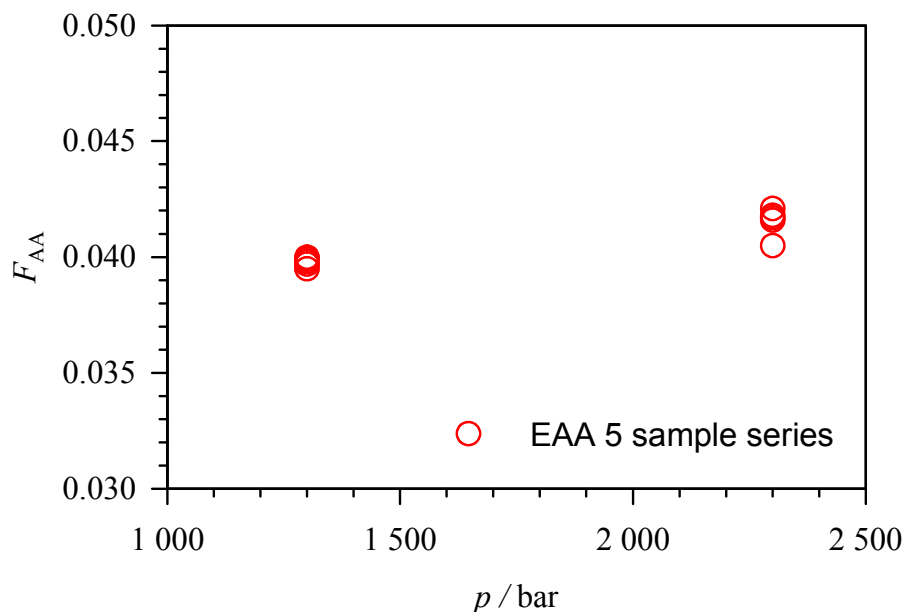


Figure 5.6:  $^{13}\text{C}$ -NMR-Spectrum of low pressure sample with  $F_{\text{AA}}=0.068$

A calculation of AA content from reactivity ratio data may be performed for all synthesized copolymers. This calculation is based on Equation 5.1.

$$F_{\text{A}} = \frac{r_{\text{A}}f_{\text{A}}^2 + f_{\text{A}}(1 - f_{\text{A}})}{r_{\text{A}}f_{\text{A}}^2 + 2f_{\text{A}}(1 - f_{\text{A}}) + r_{\text{E}}(1 - f_{\text{A}})^2} \quad (5.1)$$

To apply this equation, the conversion reached during polymerization is divided 100 equal parts, and the estimated integral  $F_{\text{AA}}$  is performed stepwise. The result is shown in Figure 5.7, for a reaction series (EAA 5), where the flow of acrylic acid was  $42 \text{ g} \cdot \text{h}^{-1}$ .



*Figure 5.7: Calculation from reactivity ratios of AA content in the polymer produced at different pressure*

Four different methods which have been applied in order to calculate the content of acrylic acid in the E-AA copolymers are summarized in Figure 5.8. The result of ATR-FT-IR is in good agreement with the calculated values from equation (5.1). FT-IR and NMR yield values which are somewhat different from the estimated ones (Eq. 5.1) and the ones from ATR-FT-IR. The reason can be that the films prepared for the IR measurements may contain bubbles in the films. The quantitative analysis of the NMR signals may be low due to long relaxation time.

A comparison of the acid contents, which are calculated via equation 5.1 and measured by ATR-FT-IR spectroscopy of copolymers produced at a different flow of acid and different pressure (1300 bar and 2300 bar) are shown in Figure 5.9. At high acid flow the difference between calculated and measured via ATR-FT-IR acrylic acid content increases slightly.

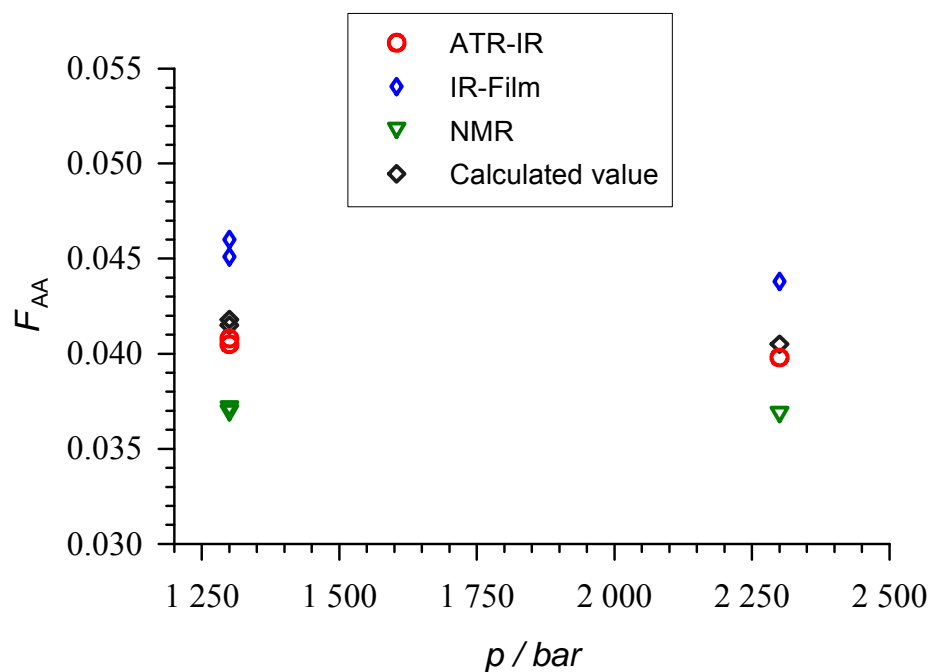


Figure 5.8: Calculated  $F_{AA}$  using 4 different methods

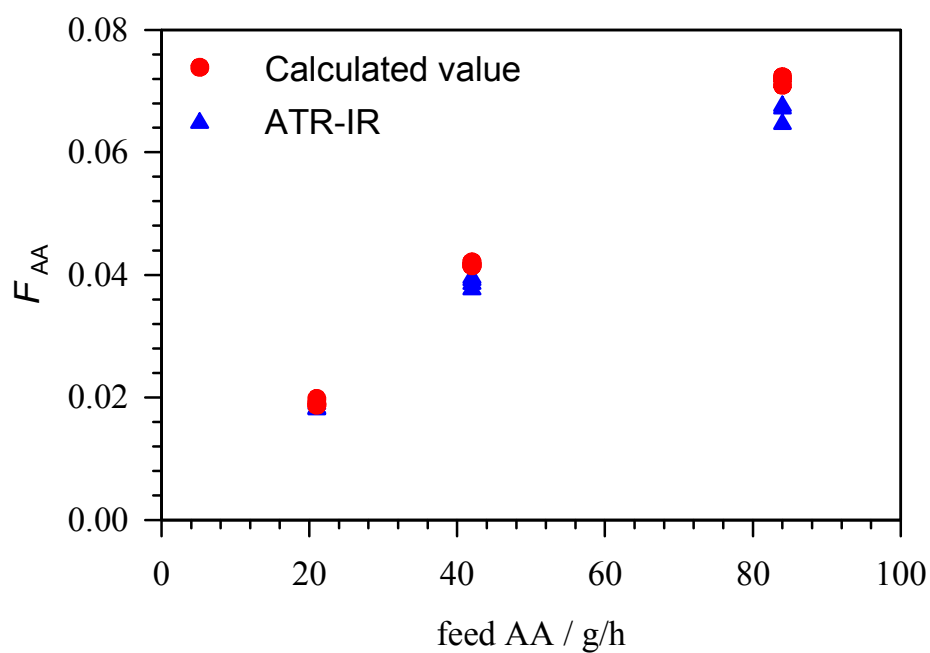


Figure 5.9: Comparison of acrylic acid content calculated by equation 5.1 and measured by mid ATR-FT-IR with different flow of acid

Table 5.1 shows an overview of the evaluations of the acrylic acid content in the E-AA copolymers produced in this work. These synthesized E-AA copolymers can be divided into three categories due to their synthesis conditions. The first group (EAA 1-12) refers to an acrylic acid variation in the dosage. The second group (EAA 13) is copolymers produced under adiabatic conditions, which have nearly the same temperature of reaction mixture and jacket. The advantage of adiabatic series of copolymers is to avoid temperature gradients and facilitate technical simulation. The last group (EAA 2-6) encompasses E-AA copolymers produced at different pressures and temperatures. In this series, random (at 2300 bar) and non-random (at 1300 bar) copolymers have been synthesized depending on cloud-point pressure.

Sample	$p$ / bar	$T_{\text{Jacket}}$ / °C	$T_{\text{Reaction}}$ / °C	AA-Flow / g·h <sup>-1</sup>	$F_{\text{AA ATR}}$ / 10 <sup>-2</sup>	$F_{\text{AA theo}}$ / 10 <sup>-2</sup>
EAA 2.2	2300	220	262-266	42	3.61	3.73
EAA 2.5	1300	220	263-267	42	3.48	3.68
EAA 10.2	2300	220	264-268	21	1.97	2.05
EAA 10.6	1300	220	262-264	21	1.88	2.02
EAA 11.2	2300	220	258-264	84	6.73	7.04
EAA 12.2	1700	220	264-268	84	6.37	6.93
EAA 12.5	1300	220	262-269	84	6.21	6.49
EAA 13.3	2300	240	238-240	42	5.98	6.23
EAA 13.5	1300	240	238-239	42	5.79	6.18
EAA 3.2	2300	250	291-295	42	3.12	3.28
EAA 4.3	1400	250	288-290	42	3.03	3.21
EAA 4.5	1300	250	290-292	42	2.94	3.25
EAA 2.2	2300	220	262-266	42	3.61	3.81
EAA 2.5	1300	220	263-267	42	3.48	3.69
EAA 5.3	2300	190	241-244	42	4.02	4.25
EAA 6.2	1300	190	241-242	42	3.95	4.19

*Table 5.1: Synthesis parameter of copolymer used for next analysis*

From Table 5.1 it may be concluded that the difference between calculated acrylic acid content in the copolymer and measured values via ATR-FT-IR is  $\pm 0.01$  mol %, which demonstrates a good agreement. The acrylic acid contents determined by FT-IR were systematically higher and the values determined by NMR were lower than those from ATR-FT-IR and calculated values. The acrylic acid content in the E-AA copolymers produced at identical temperature depends of synthesis pressure. The acrylic acid content increases with increasing pressure.



### 5.3 Determination of molecular weight distribution of copolymer sample

In this section the molecular weight distributions (MWD) of E-AA copolymers is discussed. The flow of the initiator (amount of initiator injected to the reactor) has influence on the conversion of monomer. In order to get low-pressure samples (pressure near the phase boundary) which have the same reaction temperature as high-pressure samples, a higher amount of initiator is needed in the reactor. Figure 5.10 illustrates the relation of acrylic acid flow and conversion for two synthesis pressures. The average reaction temperatures of these samples were between 260 and 265 °C. The figure shows that low pressure samples require more initiator to keep the reaction temperature constant at about 265 °C. With the increasing acrylic acid in the feed, the amount of injecting initiator also increased.

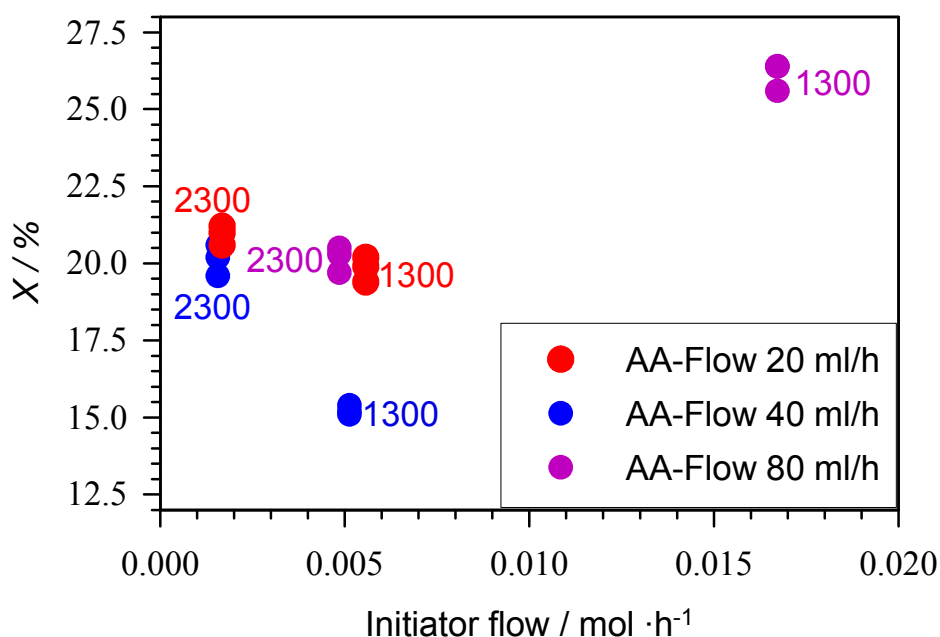
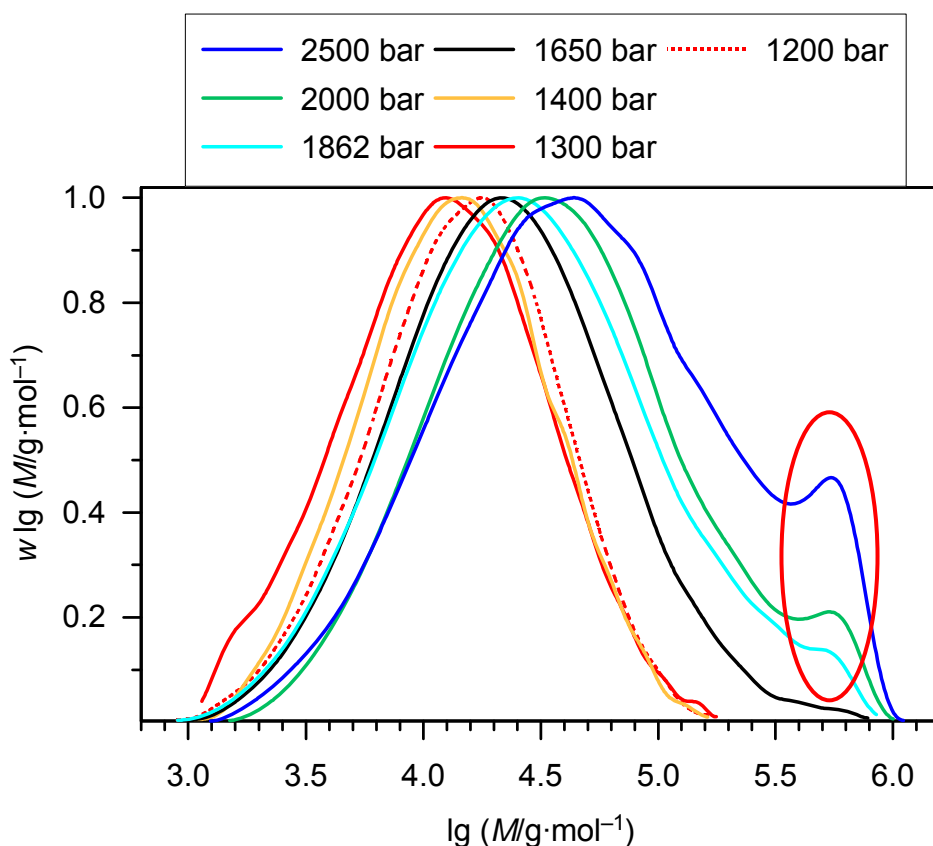


Figure 5.10: Conversion of copolymers produced at the same reaction temperature but at different initiator flows, acrylic acid flows and synthesis pressures

Figure 5.11 shows molecular weight distribution of E-AA copolymer samples synthesized at temperatures from 260 to 280 °C with acrylic acid contents in the copolymers between 0.028 and 0.032 depending on synthesis pressures.



*Figure 5.11: Molecular weight distributions of E-AA copolymers produced at temperature between 260 and 280 °C and at different pressures*

Figure 5.11 shows clearly that the high-pressure samples have a higher molecular weight than the samples produced at low pressure. This increase of molecular weight depends on initiator dosage (see Figure 5.10). Higher amount of initiator produces shorter polymer chains than lower amount of initiator. Therefore copolymers produced at lower pressure have lower molecular weight than copolymers produced at high pressure.

In order to produce samples at low pressure (1200 or 1300) it is very important to know the homogeneity of the reaction system. Phase boundary of E-AA copolymer is different depending on reaction temperature. If low pressure samples are produced at heterogeneous phase then it is not possible to compare them with samples produced at high pressure at homogeneous phase. Homogeneity of the polymerization system could also be monitored via a video recorder through the sapphire window which is installed in the bottom part of the reactor as explained in the methods section.

Another interesting effect is the shoulder on the molecular weight distribution curve of samples which are produced at pressure above 1650 bar (Fig. 5.11). This shoulder increases with increasing synthesis pressure. A similar effect also observed at the other series of high pressure samples. The shoulder may occur because of several reasons: First, it would be possible that column combination of separation process, which is used for high-temperature SEC doesn't work for high molecular weight copolymers. In fact, the E-AA copolymers which have molecular weight above  $10^6 \text{ g}\cdot\text{mol}^{-1}$  could not be seen in the SEC. That means copolymers produced above 1650 bar are at the detection limit of the high temperature SEC device. The polymers can not be separated by their hydrodynamic volume over the full molecular weight region. Polymers with such a high molecular weight pass through the column without separation. There are also samples which show such a shoulder at lower molecular weights around  $10^5 \text{ g}\cdot\text{mol}^{-1}$ . It can thus be concluded that the exclusion limit for high molecular weight polymers can not be the sole effect.

There may be reactor fouling during copolymer production yielding very high molecular weight. Polymers with a very high molecular weight stay longer at the reactor walls and at the stirrer and thus will be rinsed only slowly from the reaction chamber. There is also argument against fouling. On the one hand, the high-pressure samples are produced far-off phase boundary which means in homogeneous phase. On the other hand low pressure samples are produced very close to the phase boundary. Therefore fouling process should not be observed in the case of high-pressure samples, but in case of low-pressure samples. Secondly, the fouling process depends strongly on the reaction time. If the reactor works for long periods then more fouling product should be observed. But the high-pressure samples are always collected at shorter times than the samples synthesized at low pressure.

Therefore this additional maximum (shoulder) may be due to branching reaction. If there is transfer to polymer, there will be branching reaction. Especially, intermolecular transfer leads to increasing molecular weight.<sup>95</sup> These transfer reactions mainly happen at high pressure. Therefore thus appears to be the most reasonable explanation for the additional maximum (shoulder) which is observed with the samples synthesized at high pressure.

Figure 5.12 shows the MWD of copolymers produced at 2300 bar at different synthesis temperatures. Result shows an additional shoulder regardless of polymerization temperature.

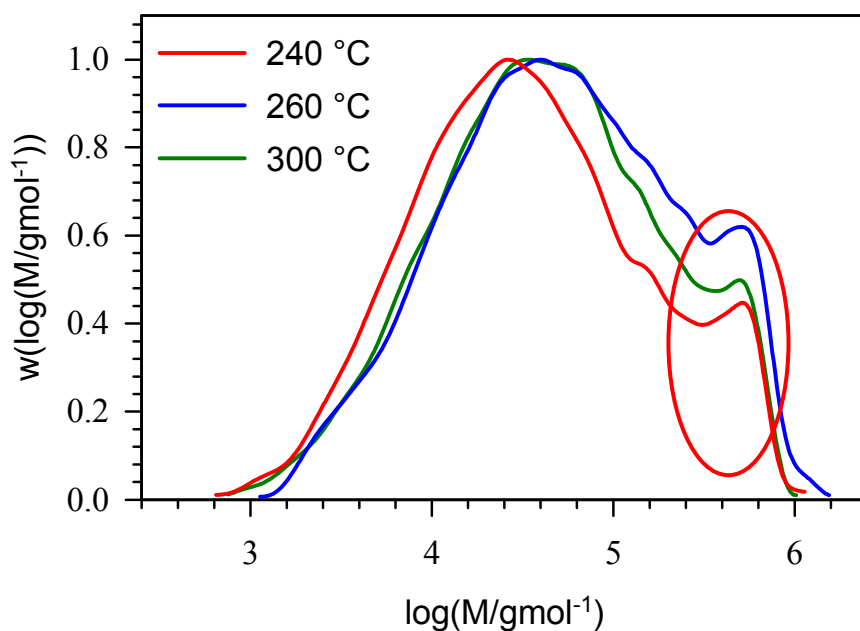


Figure 5.12: Molecular weight distributions of E-AA copolymers produced at 2300 bar at different synthesis temperatures with nearly same content of acrylic acid

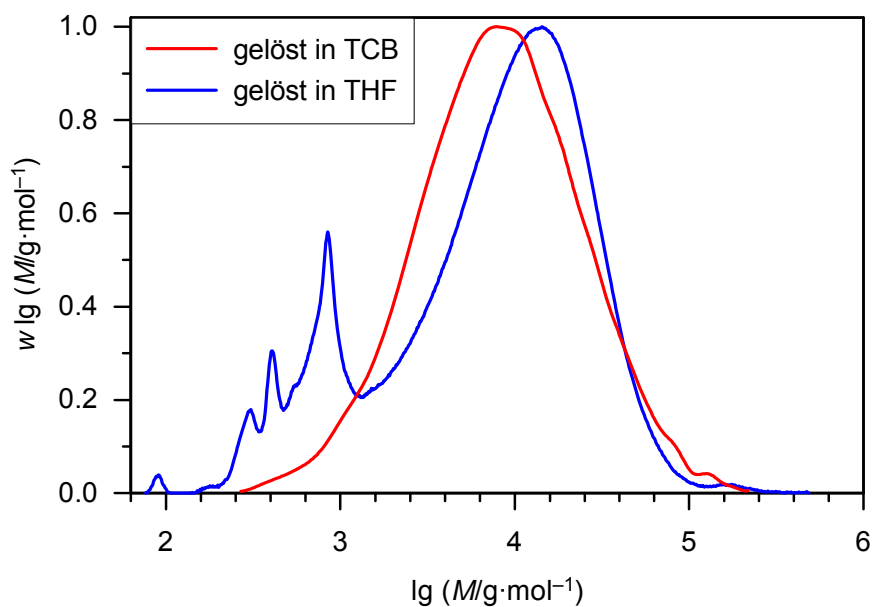


Figure 5.13: MWD of copolymer soluble in two different solvent, copolymers produced at 1300 bar and 300 °C

For some E-AA copolymers with high acrylic acid content, it was possible to obtain a molecular weight distribution at 35 °C with THF as a solvent. The solubility of E-AA copolymer increases with increase of polar moieties in the copolymer. Figure 5.13 shows a high (dissolved in TCB) and a normal (dissolved in THF) temperature SEC of E-AA copolymer samples which both show a high molecular shoulder. The additional peaks have been observed for the molecular weight distribution of polymers dissolved in THF (blue curve). Those peaks are attributed to oligomers.

The weight-average ( $M_w$ ) and number-average ( $M_n$ ) molecular of E-AA copolymers are shown in table 5.2.

Sample	$p$	$T_{\text{Reaction}}$	$F_{\text{AA}}$	X	$M_n$	$M_w$	PDI	Chain length
	/ bar	/ °C	/ $10^{-2}$	/ %	/ $10^4 \text{g} \cdot \text{mol}^{-1}$	/ $10^4 \text{g} \cdot \text{mol}^{-1}$		
EAA 2.2	2300	262-266	3.73	20.6	4.05	23.48	5.8	1350
EAA 2.5	1300	263-267	3.68	15.1	1.85	6.29	3.4	720
EAA 10.2	2300	264-268	2.05	21.2	4.65	30.44	6.5	1560
EAA 10.6	1300	262-264	2.02	20.2	2.14	7.73	3.6	970
EAA 11.2	2300	258-264	7.04	19.7	1.24	3.43	2.8	400
EAA 12.2	1700	264-268	6.93	25.1	0.65	1.62	2.5	209
EAA 12.5	1300	262-269	6.49	25.8	0.43	0.94	2.2	139
EAA 13.3	2300	238-240	6.23	5.9	1.69	3.43	2.0	550
EAA 13.5	1300	238-239	6.18	6.4	0.84	1.49	1.8	394
EAA 3.2	2300	291-295	3.28	27.0	3.17	20.95	6.6	1077
EAA 4.3	1400	288-290	3.21	26.9	0.84	2.83	3.4	285
EAA 4.5	1300	290-292	3.25	24.1	0.81	2.58	3.2	275
EAA 2.2	2300	262-266	3.81	20.6	4.05	23.48	5.8	1350
EAA 2.5	1300	263-267	3.69	15.1	1.85	6.29	3.4	720
EAA 5.3	2300	241-244	4.25	20.5	3.89	23.31	6.0	1302
EAA 6.2	1300	241-242	4.19	18.9	1.91	8.61	4.5	640

Table 5.2: Calculated value of MWD and Polydispersity index (PDI) of E-AA copolymers, produced at different synthesis conditions

All E-AA copolymers synthesized in this work contain more than 100 monomer units in the chain. The chain length has a big influence on the segmental motion of chains which is observed in the dynamic mechanical analysis and differential scanning calorimetry measurements.

To check for an influence of acrylic acid,  $F_{AA}$  as a function of PDI shown is Figure 5.14. The samples shown in Figure 5.14 refer to copolymer produced at different monomer conversion and initiator flow.

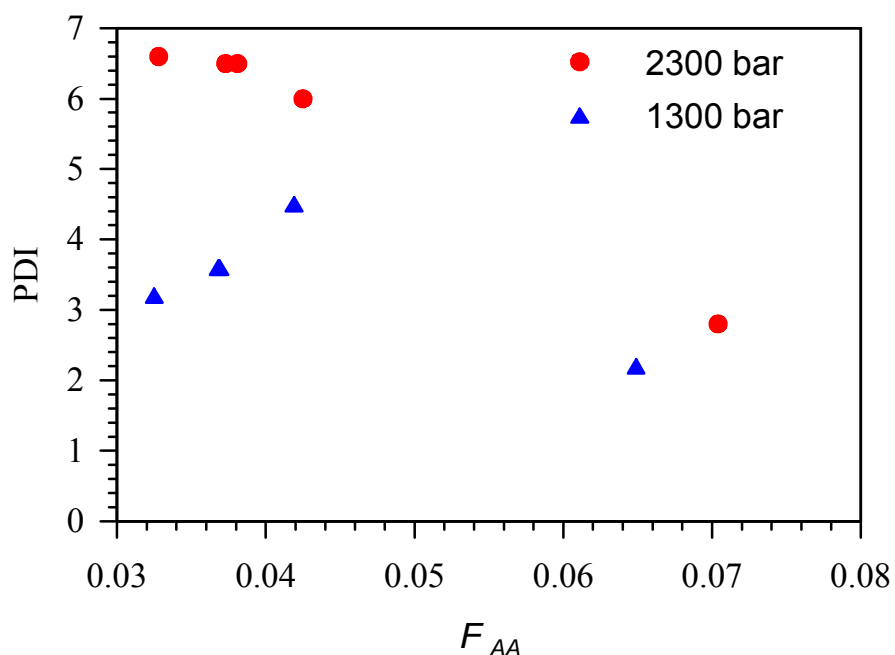


Figure 5.14: Polydispersity index of random and non-random copolymers

Due to shorter chain length, the copolymers produced at low pressure have a smaller PDI compared to high-pressure samples, as can be seen from Figure 5.14. This Figure shows that copolymers with high acrylic acid content have lower PDI compare to copolymer with low acid content.

#### 5.4 ATR-FT-IR spectroscopy investigations

As described in Chapter 5.1, ATR-FT-IR spectroscopy has been applied for the determination of acrylic acid content in the copolymer. From the literature<sup>95-97</sup> it is known that carboxylic acid dimer absorbance occurs in a very broad wavenumber range from 2300 to 3400  $\text{cm}^{-1}$ . The integrated molar absorption of the OH-stretching vibration for the dimer is higher than for the one of the monomeric acid. For example, in the case of acrylic acid the integrated molar absorption coefficient for the O-H stretch of monomeric acid is 65  $\text{km}\cdot\text{mol}^{-1}$  and for the dimer acrylic acid is 580  $\text{km}\cdot\text{mol}^{-1}$ . The samples were measured at a pressure of

250 bar and a temperature of 28°C and tetrachloromethane used as the solvent.<sup>98</sup> If low-pressure samples have non-random structure then there should be more hydrogen bonds (HB) compared to high pressure samples therefore there should be a difference between ATR-FT-IR spectra for high-pressure and low-pressure samples.

#### 5.4.1 Comparison of ATR-FT-IR spectra of high-pressure and low-pressure samples

As expected, the area of OH-stretching vibration for the dimer is found in the wavelength range 2300 to 3400  $\text{cm}^{-1}$ . Due to hydrogen bonds, there will be very strong absorption in this wavelength range. Therefore it could be obtained direct difference between spectrum of high and low pressure samples. A stronger absorption in the region of acid dimer should be obtained for the low-pressure sample. Figure 5.15 shows the ATR-FT-IR spectrum of copolymers EAA 2.2 (random) and EAA 2.6 (non-random), which contain almost the same content of AA unit in the copolymer. The ATR-IR spectrum of PE included as a comparison.

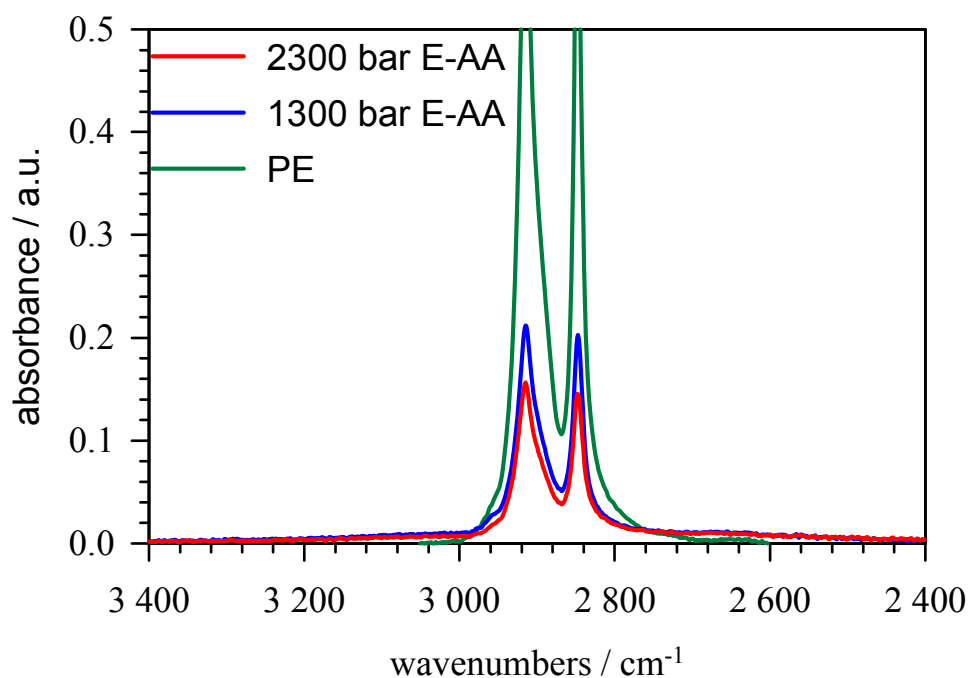


Figure 5.15: ATR-FT-IR spectroscopy of PE, random (red curve) and non-random (blue curve) E-AA copolymers

From Figure 5.15, it is clear that with the E-AA copolymer, some absorbance of OH occur at around  $2960\text{ cm}^{-1}$ . The strong signals at  $2916$  and  $2849\text{ cm}^{-1}$  are assigned to the CH absorbance. The shoulder at  $2960\text{ cm}^{-1}$  for the acid monomer is assigned to hydrogen bonded acrylic acid units (see Figure 5.16).

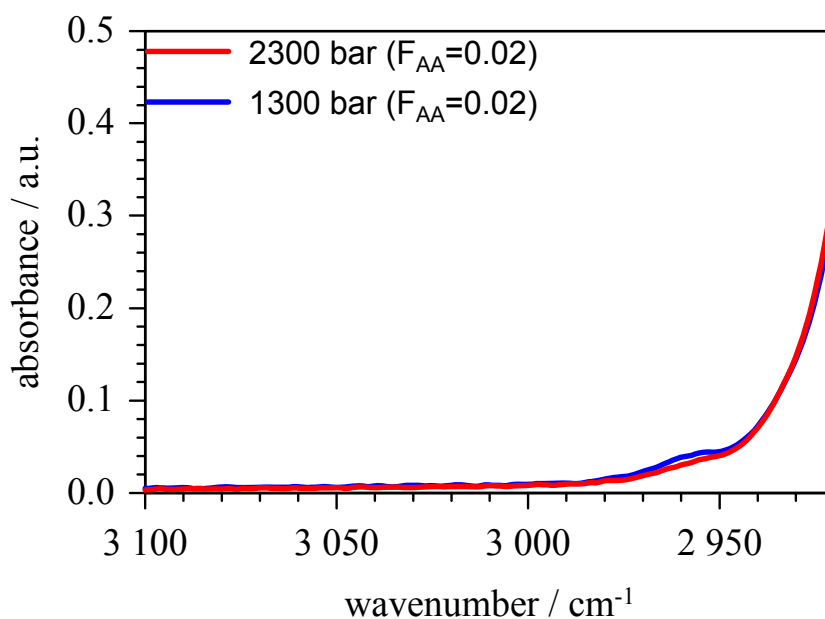


Figure 5.16: Detailed ATR-IR-Spectrum of random and non-random copolymers with low content of acrylic acid, wavenumber region of  $3100$  to  $2920\text{ cm}^{-1}$

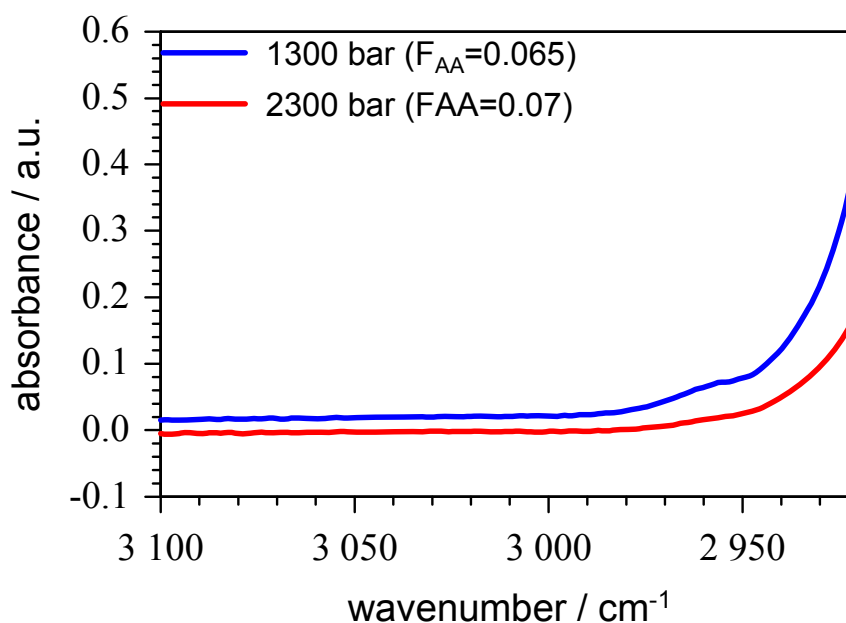


Figure 5.17: Detailed ATR-IR-Spectrum of random and non-random copolymers with relatively high content of acrylic acid, wavenumber region of  $3100$  to  $2920\text{ cm}^{-1}$



Figure 5.17 shows the detailed ATR-IR-spectrum of high-pressure and low-pressure samples both with relatively high content of acrylic acid. Despite the almost identical content of acrylic acid in the copolymer, the samples produced at low pressure have an absorbance component in the wavenumber range around  $2960\text{ cm}^{-1}$ . This is assigned to different extents of hydrogen bonding which thus appears to be stronger at lower pressure.

The integration for the absorbance icntegration region from  $2939$  to  $3000\text{ cm}^{-1}$  has been performed for the quantification. This area depends on the content of acrylic acid in the copolymer. With the absorbance at  $3000\text{ cm}^{-1}$  being chosen as the base line point for the integration.

#### 5.4.2 Effect of AA content on the ratio of the integrated absorbance of Low-/High pressure samples

The relation between the ratio of integrated absorbance of copolymers produced at low and high pressures at different content of acrylic acid in the copolymer is shown in Figure 5.18.

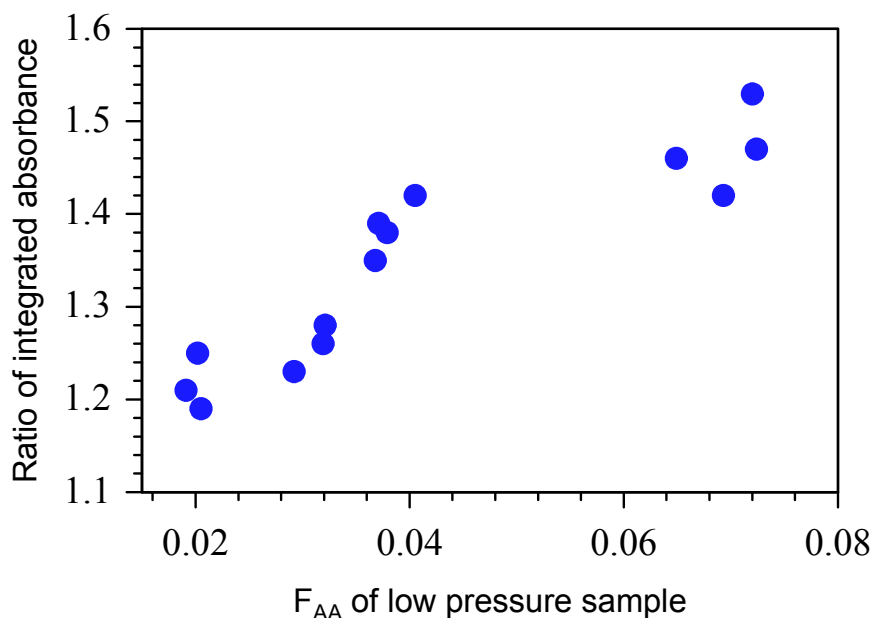


Figure 5.18: The ratio of integrated absorbance of low and high pressure samples vs acrylic acid content in the low pressure EAA copolymers

With increasing acrylic acid content in the E-AA copolymer, this absorbance ratio is increased. The ratio is always above unity, which says that at identical acrylic acid content of

the copolymer, the degree of hydrogen bonding appears to be higher for copolymers produced at the lower pressure.

### 5.5 Density calculation of the reaction mixture in the reactor

In this work copolymers have been synthesized at different reaction pressures. The high-pressure samples were collected at 2300 bar and the low-pressure samples at 1300 bar. In this section, the density of the reaction mixture is calculated assuming that the system behaves like ethene/polyethylene. The contribution of acrylic acid can be neglected at the levels typically used in feed  $f_{AA} = 0.001$ . The calculation of density of the reaction mixture is performed using the following equations.<sup>99</sup>

$$\rho = \frac{1}{\frac{1 - g_p}{\rho_E} + \frac{g_p}{\rho_p}} \quad (5.2)$$

$$\rho_E = 1995.85 - 601.2 \cdot \lg\left(\frac{P}{1000}\right) + 593.3 \cdot \lg\left(\frac{1}{T}\right) - 335.8 \cdot \lg\left(\frac{P}{1000}\right) \cdot \lg\left(\frac{1}{T}\right) \quad (5.3)$$

$$\rho_p = \frac{1}{(9.61 \cdot 10^{-4} + 7.0 \cdot 10^{-7} \cdot T - 5.3 \cdot 10^{-8} \cdot p)} \quad (5.4)$$

here:  $\rho$ : density in reactor  $\text{g} \cdot \text{l}^{-1}$

$g_p$ : weight part of polymer in the reactor

$\rho_E$ : density of ethene under reactions condition  $\text{g} \cdot \text{l}^{-1}$

$\rho_p$ : density of polymer under reactions condition in  $\text{g} \cdot \text{l}^{-1}$

### 5.5.1 Comparison of density in the reactor for high-pressure and low-pressure samples

The density of the polymerizing solution for high (2300 bar) and low (1300 bar) pressure sampling has been estimated using equations 5.2 through 5.4. The obtained values are listed in Table 5.3.

Temperature / °C	Pressure / bar	Conversion / %	Density in the Reaktor / g·l <sup>-1</sup>	Density High-/Low pressure
250	2300	20	539.0	1.17
250	1300	20	462.2	
300	2300	20	519.4	1.18
300	1300	20	439.2	1.18
250	2300	10	516.4	
250	1300	10	439.2	

*Table 5.3: Density and ratio of high to low- pressure density in the reactor*

Table 5.3 shows that the density of the polymerizing system is around 17% higher at 2300 bar than at 1300 bar for 250 °C. When reaction temperature increases from 250 to 300 °C and decrease conversion by factor of 2 then this ratio increases slightly to 18 %.

## 5.6 Calorimetric studies via Differential Scanning Calorimetry (DSC)

Information about phase transitions and structural transformations (topology) of polymer materials can be deduced from differential scanning calorimetry (DSC).<sup>100-105</sup> DSC does not require any special sample preparation. The measuring time depends on the chosen heating rate. The copolymer samples were analyzed at stable conditions with a heating rate of 5 °C per minute in the temperature range from -45 °C to 200 °C. These conditions enable suitable and meaningful DSC measurements for the analysis of structural transformations of the copolymer samples.

### 5.6.1 DSC analyses of PE and PMAA homopolymer systems

In order to investigate the copolymer systems, homopolymers of ethene and acrylic acid have to be studied first. The thermograms of PE (synthesized within the same experimental set-up) and PMAA are shown in Figure 5.19. In the case of PE a clear melting transition can be observed at around 120 °C. Below the melting transition no further transition was observed. The glass transition temperature of PE depends on the chain length and the degree of branching of the polymer and is far below -45 °C, which is the minimum temperature for the DSC assembly available for this work.

The DSC thermogram of PMAA is dissimilar from the one of PE. The broad signal starts at 46 °C and has a minimum at around 112 °C. At 46 °C the material starts to soften. A clear signal for the melting process, as observed in the case of PE, can not be found.

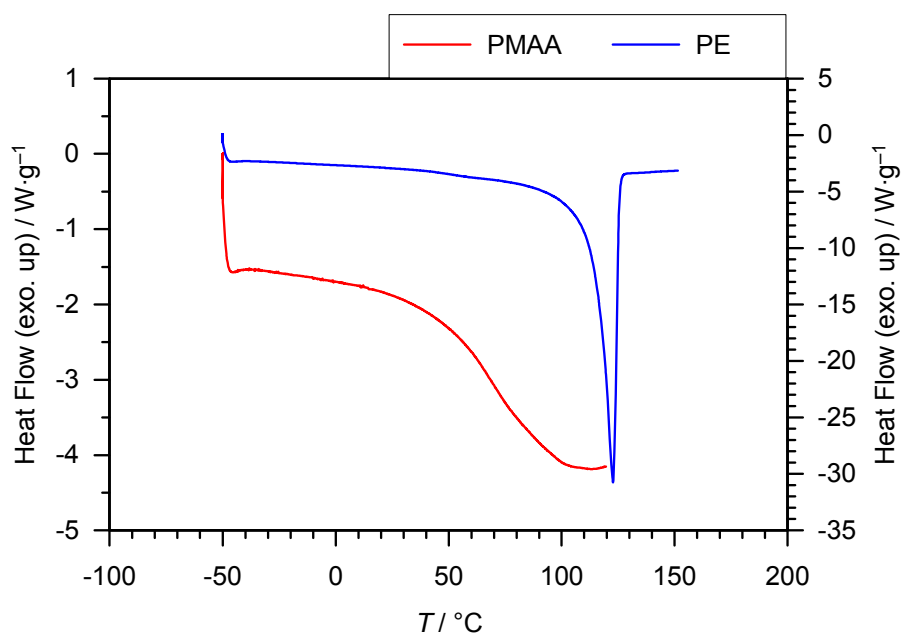


Figure 5.19: DSC-thermogram of PE and PMAA

### 5.6.2 DSC analyses of E-AA copolymers produced at different pressure

The DSC thermograms of EAA copolymers are shown in Figures 5.20 through 5.24. DSC measurements are particularly useful for comparing the heating process of samples which are

produced at high pressure to those that are synthesized at low pressure. Figure 5.20 shows the DSC thermograms of E-AA copolymers produced at low-pressure and high-pressure. The thermogram of the high pressure sample (red curve) shows a transition (signal) in the temperature range 80 to 100 °C, which corresponds to the melting transition ( $T_M$ ) of the copolymer. An additional transition at temperatures between 30 and 50 °C can be observed in the material which corresponds to the glass transition. The temperature at the minimum of this transition, representing the glass transition temperature ( $T_G$ ) of E-AA copolymer is around 38° C. Using acrylic acid as a co-monomer for ethylene therefore leads to a significant increase of the glass transition temperature compared to PE. The DSC thermogram of PE is not show a glass transition in the studied temperature range. The thermogram of the low-pressure sample (blue curve) also shows two transitions at nearly the same temperatures as the high-pressure sample. Furthermore an additional transition below the glass transition can be observed. Since this is another glass transition the corresponding temperature is  $T_{G2}$ . This additional transition shows that there is a difference between E-AA copolymers produced at lower (1300bar) and higher (2300 bar) pressures.

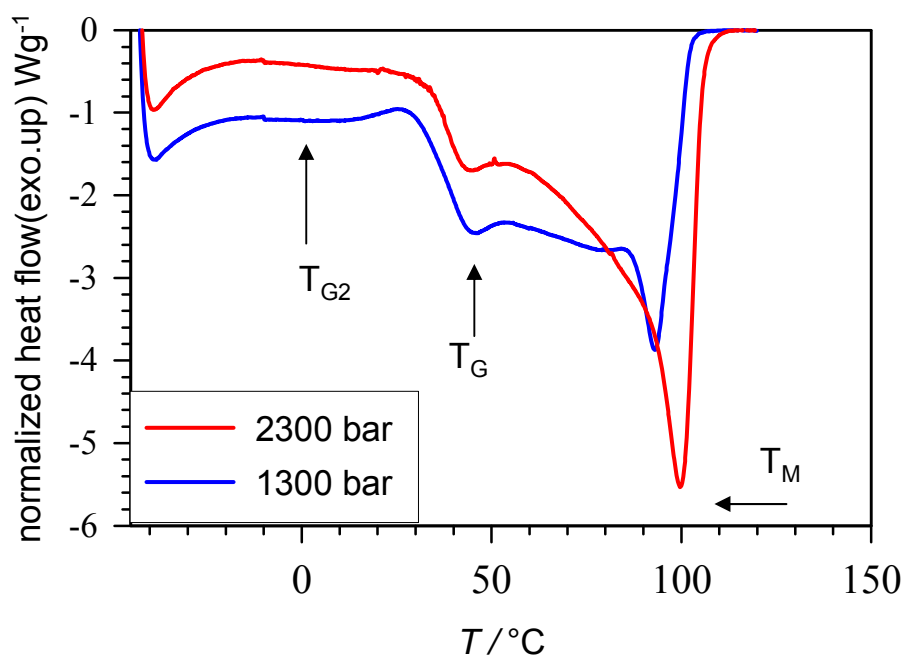


Figure 5.20: DSC diagram of EAA copolymers produced at 2300bar ( $F_{AA}=0.038$ ) and at 1300 bar ( $F_{AA}=0.037$ )

### 5.6.3 DSC measurement of E-AA copolymers with different contents of AA in the copolymer

In order to better understand this additional transition at  $T_{G2}$ , copolymerization experiments at different pressures, different temperatures and flow rates of acrylic acid have been performed. Several E-AA copolymers with different content of acrylic acid in the copolymer have been polymerized at different pressure. Figure 5.21 show the response of this additional relaxation on the acrylic acid content in the copolymer produced at 1300 bar and 260 °C. When the acrylic acid content is increased from 2 mol % to 6.9 mol%, the intensity of the additional  $\beta$ -relaxation increases significantly due to the high content of acrylic acid, which enables the formation of acrylic acid dimer. The reason could be that the high content of acrylic acid makes more acrylic acid dimer than at low acrylic acid content of the copolymer and these more blocks show more strong intensity in the DSC thermogram below the glass transition.

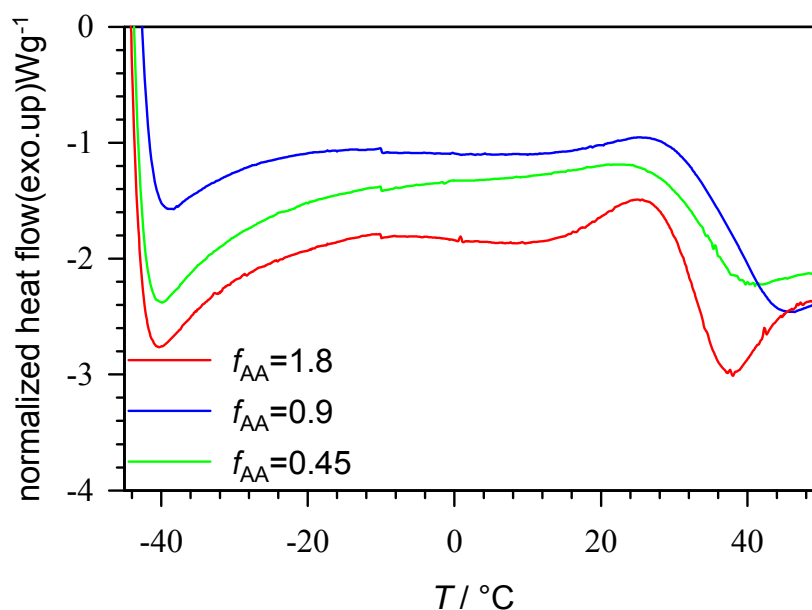


Figure 5.21: DSC-thermogram of E-AA copolymers (temperature range from -45 to 50  $^{\circ}C$ ) produced at 1300 bar and 260  $^{\circ}C$  with different contents of acrylic acid

DSC thermograms of E-AA copolymers produced at 2300 bar and 260  $^{\circ}C$  with the different acrylic acid contents are shown in Figure 5.22. The acrylic acid content in the feed increases 4 times but there is no additional relaxation observed below the glass transition at the thermogram of E-AA copolymers produced at high pressure. If this an additional

relaxation related to the distribution of acrylic acid group in the copolymer, it is clearly shown that E-AA copolymers produced at high pressure have a very low amount of dimer or trimer acrylic acid segments compare to copolymers produced at low pressure. Therefore  $\beta$ -relaxation depends strongly from the synthesis pressure.

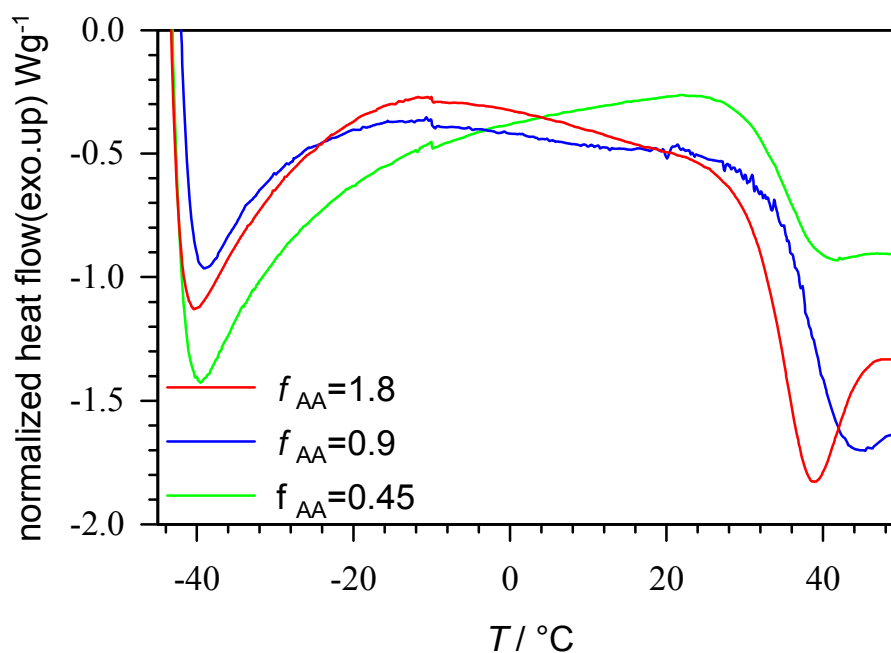


Figure 5.22: DSC-Thermogram of E-AA copolymers (temperature range from -45 to 50°C) produced at 2300 bar and 260 °C with different content of acrylic acid

#### 5.6.4 Variation of the synthesis temperature

A second series of experiment was carried out to produce E-AA copolymer at high and low pressures at different synthesis temperatures but at the same content of acrylic acid. DSC thermograms of E-AA copolymers produced at 2300 bar and 1300 bar at different synthesis temperatures with nearly the same acrylic acid content are shown in Figures 5.23 and 5.24. DSC thermograms of low-pressure samples produced at different temperatures (see Figure 5.23) show that the intensity of the additional  $\beta$ -relaxation increases with increasing synthesis temperature (marked with red arrow). At very high synthesis temperatures (300 °C) the  $\beta$ -relaxation shows its maximum intensity (marked with red arrow).

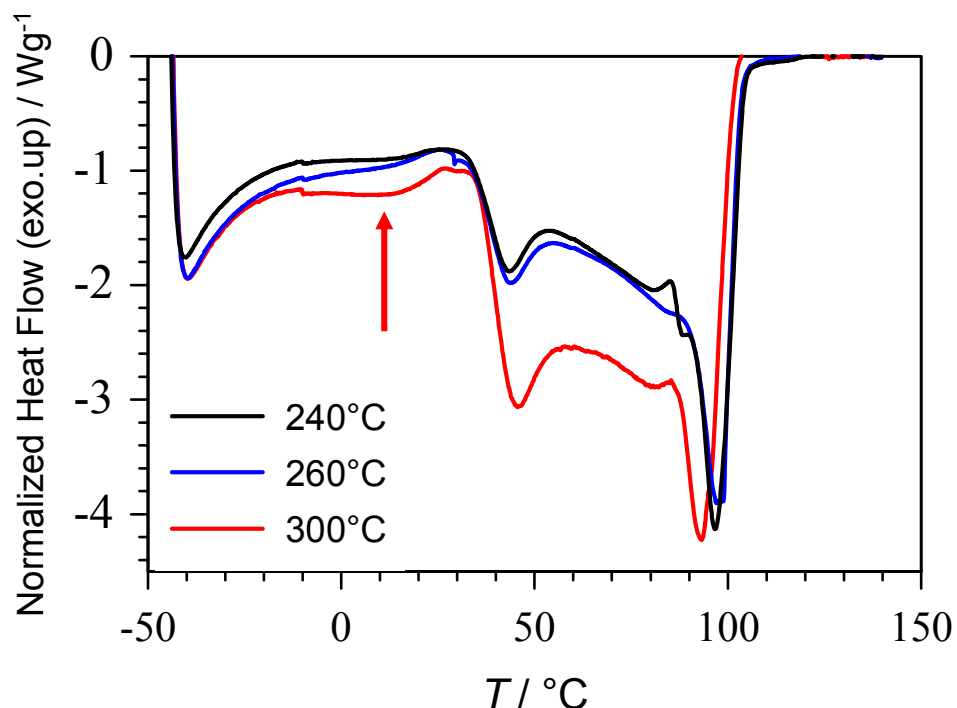


Figure 5.23: DSC-Thermogram of E-AA copolymers produced at 1300 bar at different temperatures,  $F_{AA}$  is nearly same for those samples

The DSC diagram of copolymers produced at high pressure at syntheses temperatures of 240 and 260 °C (see Figure 5.24) show 2 transitions as a mentioned before. However, the DSC thermogram of the copolymer produced at 300 °C shows an interesting effect (marked with green arrow). In this case an additional  $\beta$ -relaxation with a low intensity can be observed, which is not expected due to the random distribution of acrylic acid. The reason for this phenomenon could be backbiting reactions, which may be produced because of the higher synthesis temperature.

Plotted in Figure 5.25 are DSC thermograms of poly (E-co-AA) copolymers produced at 300 °C (highest synthesis temperature which could be applied with this set-up) at different synthesis pressures. The intensity of the additional  $\beta$ -relaxation for the copolymer produced at high pressure is very weak compared to low pressure samples.



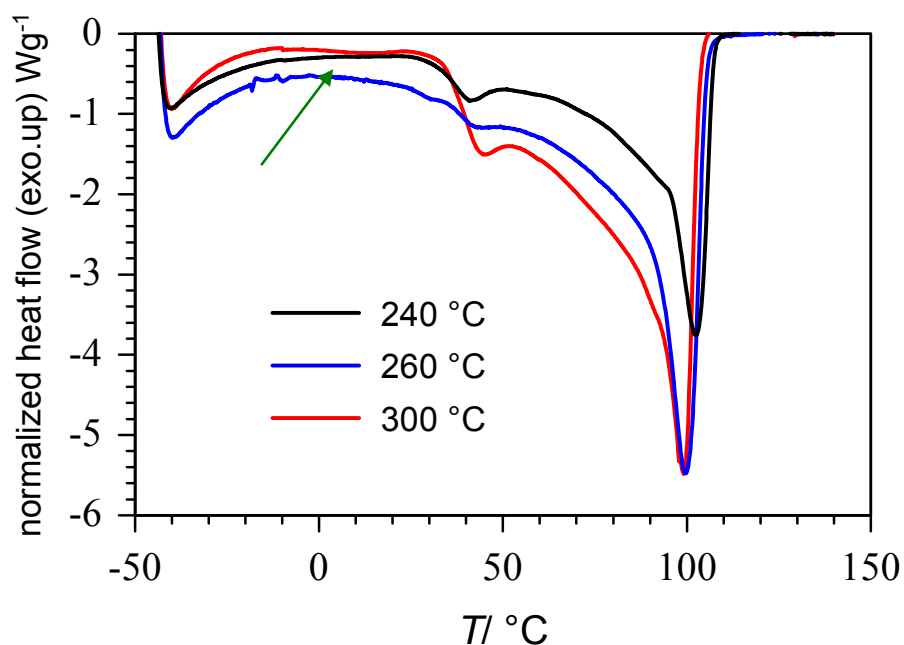


Figure 5.24: DSC thermogram of the E-AA copolymers produced at 2300 bar with different synthesis temperature

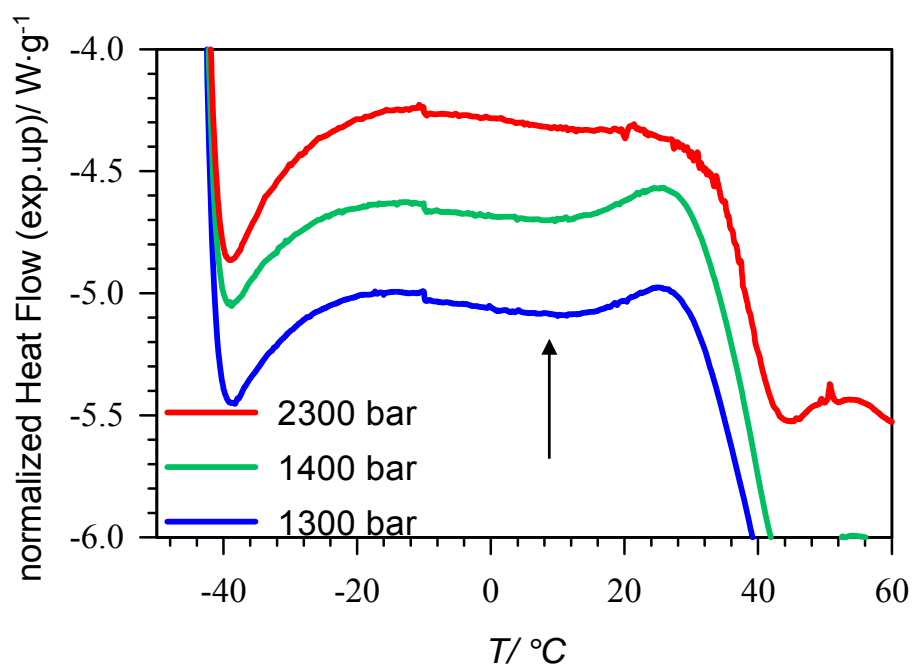


Figure 5.25: DSC thermogram (in the temperature range from -45 °C to 50 °C) of E-AA copolymers produced at 300 °C with different pressure

### 5.6.5 DSC measurement of copolymer samples produced under adiabatic conditions

One series of copolymer samples are produced under adiabatic conditions, which means that the difference between reaction and jacket temperature is negligible ( $\Delta T=0$ ) with constant flow of acrylic acid and at different pressures. Due to the construction of the reactor, the system exchanges heat with the environment. Therefore it is necessary to heat the system in order to hold constant jacket temperature. The temperature of the system is measured only in two positions which are located in the reaction chamber and at the wall of the reactor.

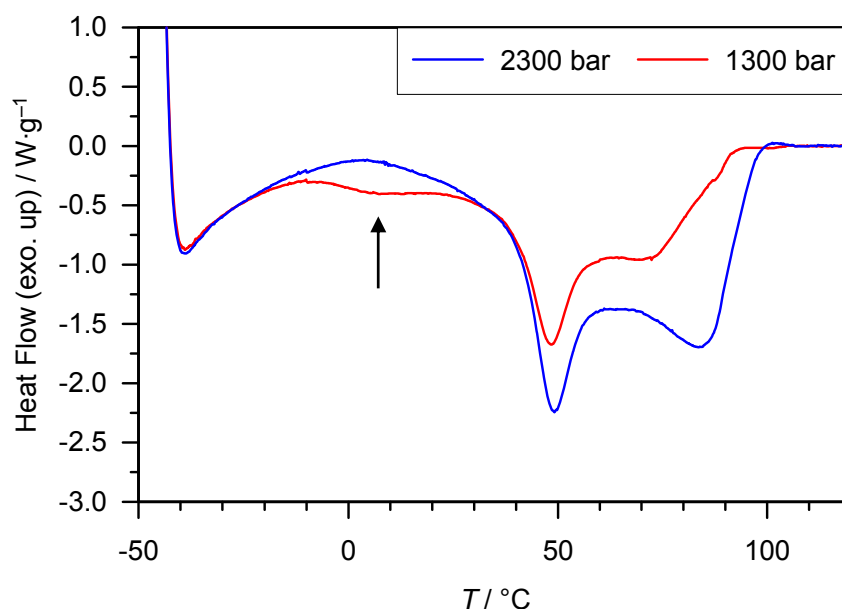


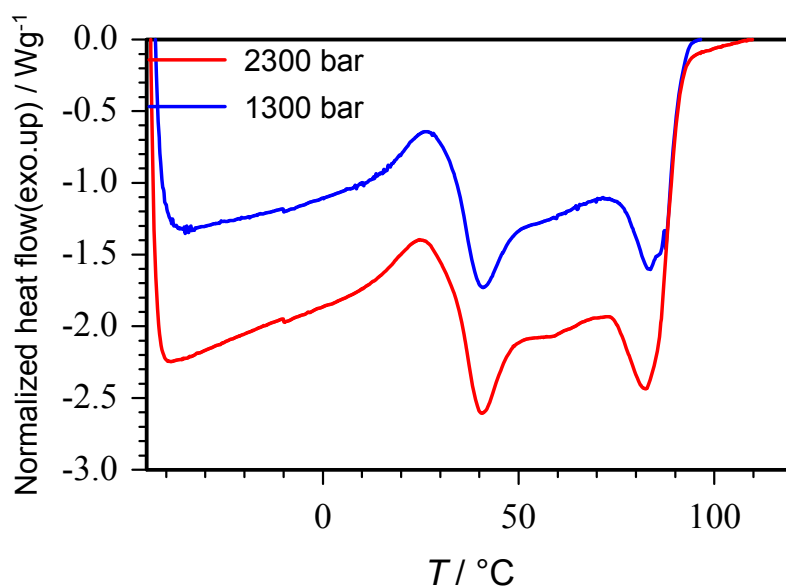
Figure 5.26: DSC thermogram of copolymers produced under adiabatic condition

Figure 5.26 shows the comparison of DSC thermograms between copolymers produced at low and high pressures under adiabatic conditions at a temperature of 240 °C. Even though there is no temperature gradient in the reaction system, the samples produced at low pressure (1300 bar) exhibit an additional  $\beta$ -relaxation at a temperature of 0 °C. One may hence conclude that the synthesis pressure greatly influences the randomness of the distribution of acrylic acid monomer units in the resulting copolymer.

### 5.6.6 DSC measurement of analogous systems

An additional relaxation ( $\beta$ ) appears not only in the thermograms of copolymers produced at low pressure but also in the thermogram of the copolymer produced at high pressure and 300 °C.

a)



b)

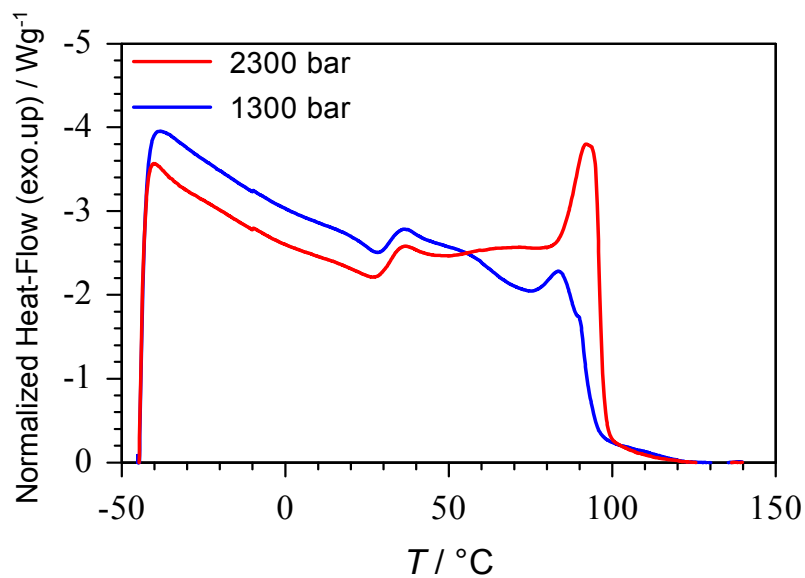


Figure 5.27: DSC thermograms of analogous systems: a ) E-MA copolymer and b )E-MMA copolymers produced at different pressures; all copolymers were produced at 260 °C

In order to find the origin for this relaxation, E-MAA, E-MA and E-MMA copolymers have been synthesized under the same experimental conditions as the E-AA copolymers. If the relaxation is caused by the backbiting reaction than an additional  $\beta$ -relaxation should appear in the case of the E-MA copolymers and if it is caused by hydrogen bonding then it will appear in the case of the E-MAA copolymers.

No differences between the DSC thermograms of E-MA and E-MMA copolymers produced at different pressures can be observed (see Figure 5.27). A glass and melting transition can be observed in almost the same temperature regions as in the case of the E-AA copolymers. In both cases no additional  $\beta$ -relaxation can be observed in the low-temperature region before the glass transition. Therefore it is clear that the additional transition is not due to backbiting reactions but may be caused by hydrogen bonding. Even E-MA copolymers produced at different temperatures shown no effect below the glass transition temperature.

DSC thermograms of E-MAA copolymers which are produced at 260 °C and at different pressures are shown in Figure 5.28. The thermogram of the E-MAA copolymer produced at high pressure (red) also has shown two relaxations which correspond to the glass transition and melting. But the thermogram of the E-MAA copolymers produced at low pressure exhibits an additional relaxation before the glass transition region as in the case of the E-AA system (marked black arrow).<sup>76</sup>

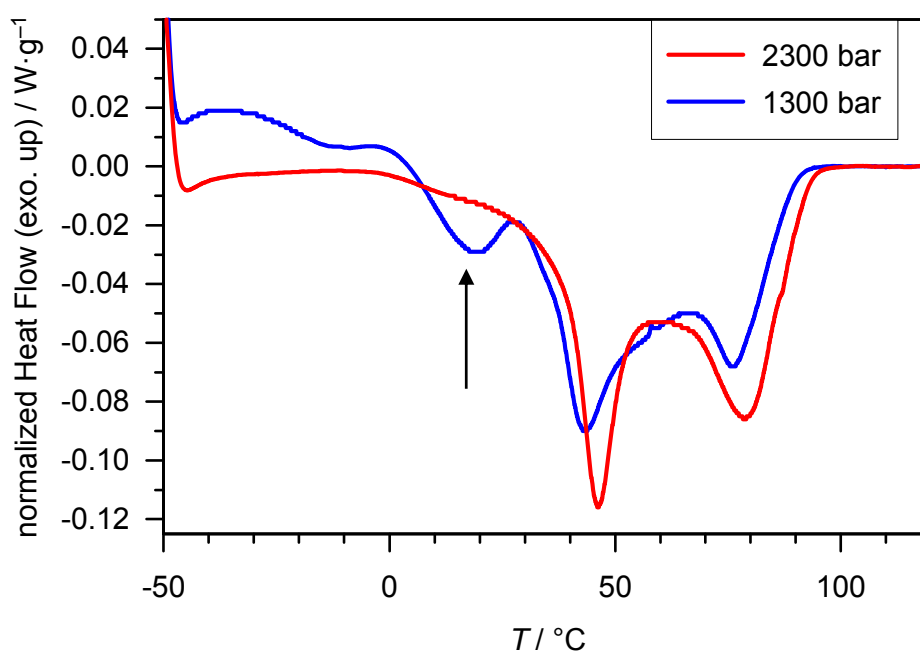


Figure 5.28: DSC curves of E-MAA copolymers produced at 260 °C,  $F_{MAA} = 0.069$

The intensity of this additional relaxation increases with decreasing reaction pressure (see Figure 5.29 marked black arrow). Hence it may be assumed that  $\beta$ -relaxation is caused by hydrogen bonded acid groups in the copolymer.

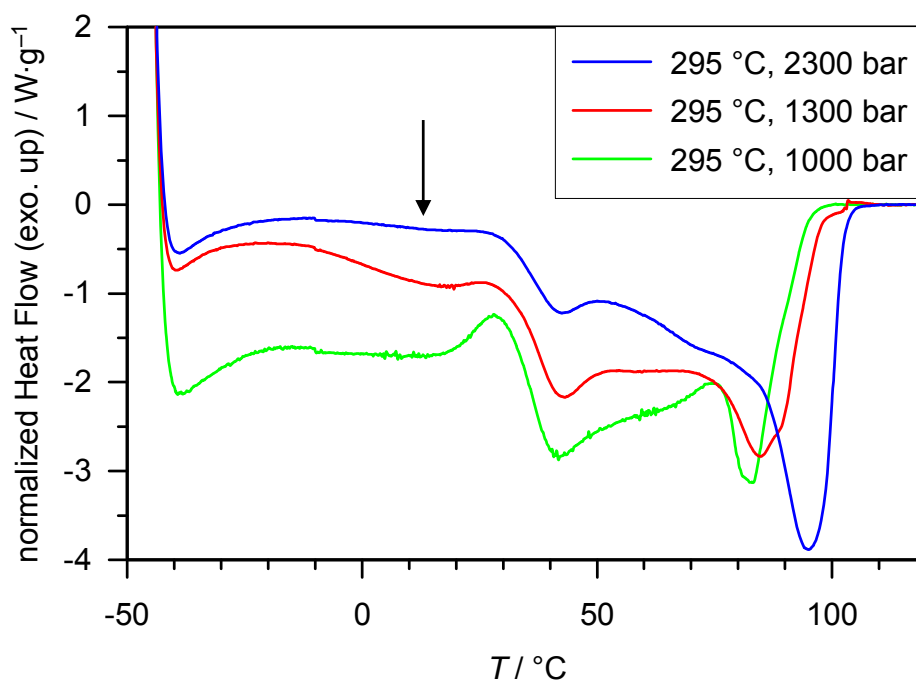


Figure 5.29: DSC-thermograms of E-MAA copolymers produced at constant temperature and different pressures,  $F_{MAA}=0.036$

The DSC thermograms of PE and PMAA homopolymers show a transition in the temperature range of 150 °C. There is a significant difference between the DCS diagrams of E-AA random and non-random copolymers. An additional  $\beta$ -relaxation can be observed in the DSC diagram of non-random copolymer in the temperature range 10 to 30 °C, which can not be found in the DSC diagram of the random copolymer. This additional relaxation is related to a non-random distribution of the acrylic acid moieties. This  $\beta$ -relaxation can also be observed in the DMA measurement of the non-random E-MAA copolymer at low temperature. The intensity of the  $\beta$ -relaxation is rising with increasing acrylic acid content in the copolymer and also with increasing synthesis temperature. The degree of crystallinity of the PE decreases when the content of acrylic acid in the copolymer is increased.

An unexpected additional  $\beta$ -relaxation can be observed in the DSC diagram of the random copolymer produced at 300 °C and at high pressure. In order to find the reason of this effect,

E-MMA and E-MA copolymers were produced in the CSTR. With E-MA copolymers no additional  $\beta$ -relaxation was observed in the temperature region below the glass transition temperature. This indicates that the additional transition is not due to backbiting reactions but may be caused by hydrogen bonding. Even the E-MA copolymers produced at different temperatures show no additional effect below the glass transition temperature. Therefore the  $\beta$ -relaxation is probably not caused by backbiting reactions.

## 5.7 Results of powder X-ray diffraction

### 5.7.1 X-ray diffraction of PE and E-AA copolymers

To extract information about the crystallinity of the copolymer, powder X-ray diffraction was measured first on PE (See Figure 5.30).

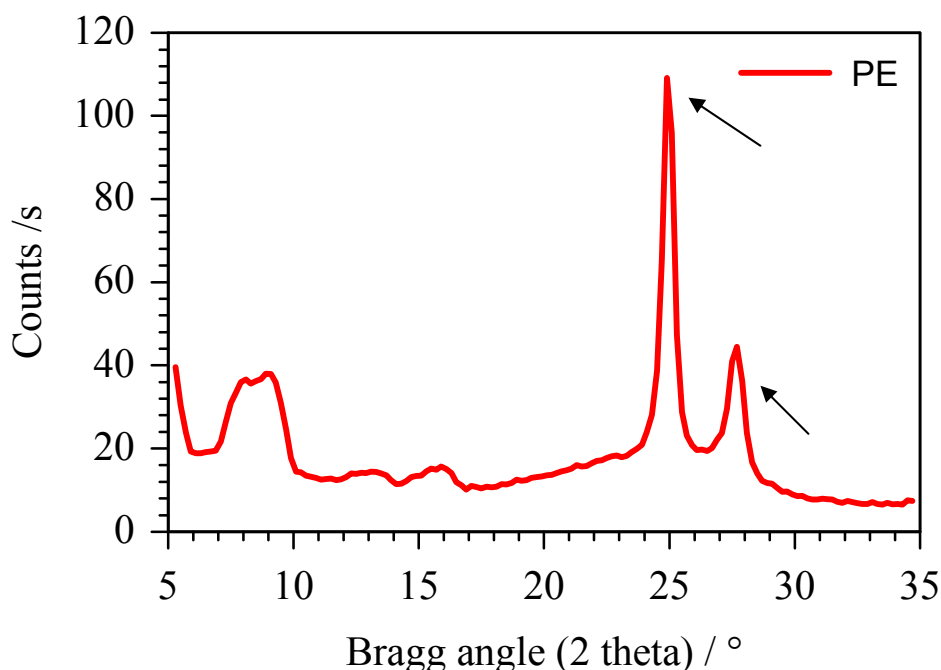
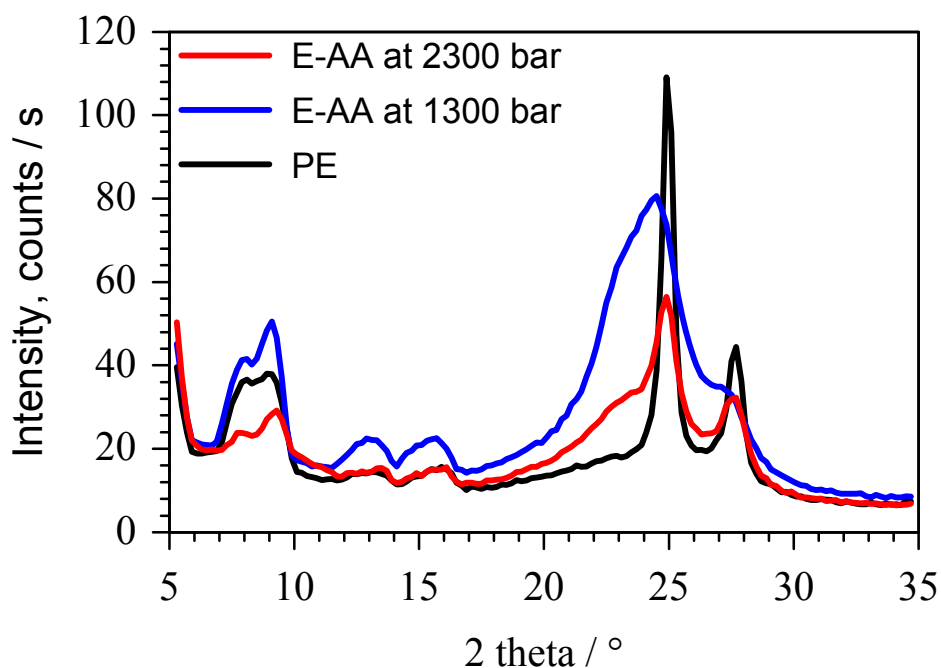


Figure 5.30: Powder X-RAY diffraction diagram analysis of PE

X-ray analysis of PE gives two very strong signals (marked with black arrows) in the region of 23 to 30 Bragg angles, which correlates crystallinity (ordering) and periodicity of the ethylene chain in the PE. The two sharp lines are from the X-ray spectrum of crystalline PE.<sup>107-110</sup>

In case of E-AA copolymers the sharp peaks are decreased and become broader depending on synthesis pressure and content of acrylic acid in the copolymer. X-ray of E-AA copolymers produced at different pressures contains also 2 main peaks in the region of 23 to 30 Bragg angles (see Fig 5.31) however the peaks are broader compared to the PE samples. An X-ray diffraction diagram of random copolymers (copolymers produced at 2300 bar) shows sharper peaks (mixture of amorphous and crystalline structure) in the region of 23 to 30 Bragg angles. But in the case of copolymers produced at low pressure those peaks are broader and show amorphous structure. The reason is that poly-acrylic acid has amorphous (no ordering) and polyethylene has a crystal (very highly ordered) structure. Since non-random copolymers contain more acrylic acid blocks (dimers, trimers) than random copolymers, the ordering is lower. Random copolymers show a mixture of crystalline and amorphous structure and non-random copolymers exhibit a more amorphous structure.



*Figure 5.31: Comparison of X-ray diagrams of random and non-random E-AA copolymers ( $f_{AA}=0.0045$ ) and PE*

Crystallinity decreases with increasing acrylic acid content in the copolymer. Figure 5.32 and 5.33 show X-ray diagrams of E-AA copolymers produced with different acrylic acid contents and at different pressures.

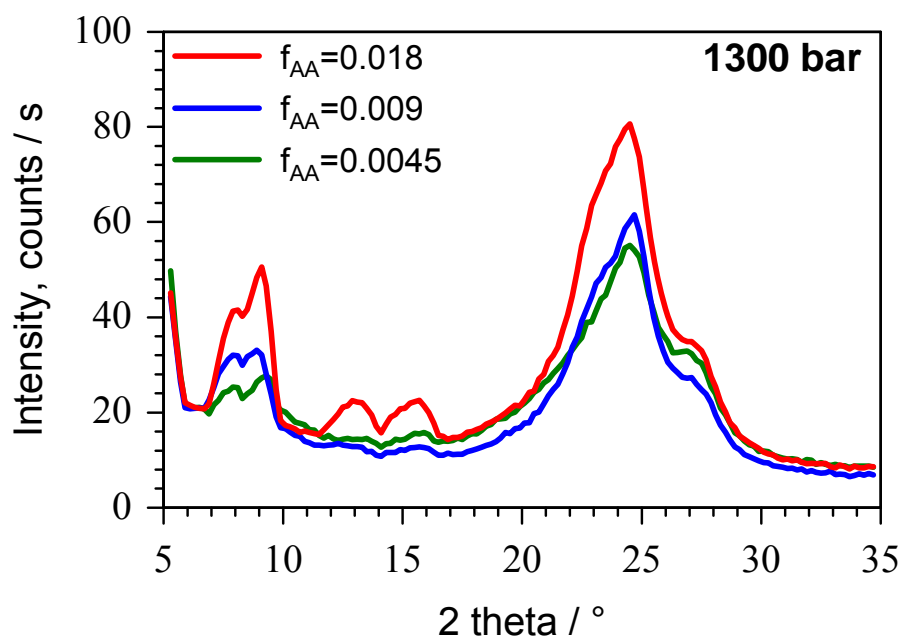


Fig 5.32: X-RAY diagram of E-AA non-random copolymers produced with different acrylic acid contents

The signals in the region of 23 to 30 Bragg become broader in the case of non-random copolymers when the acrylic acid content in the copolymer is increased, which is due to low-pressure samples with higher acrylic acid content contains more acrylic acid dimers compared to low content.

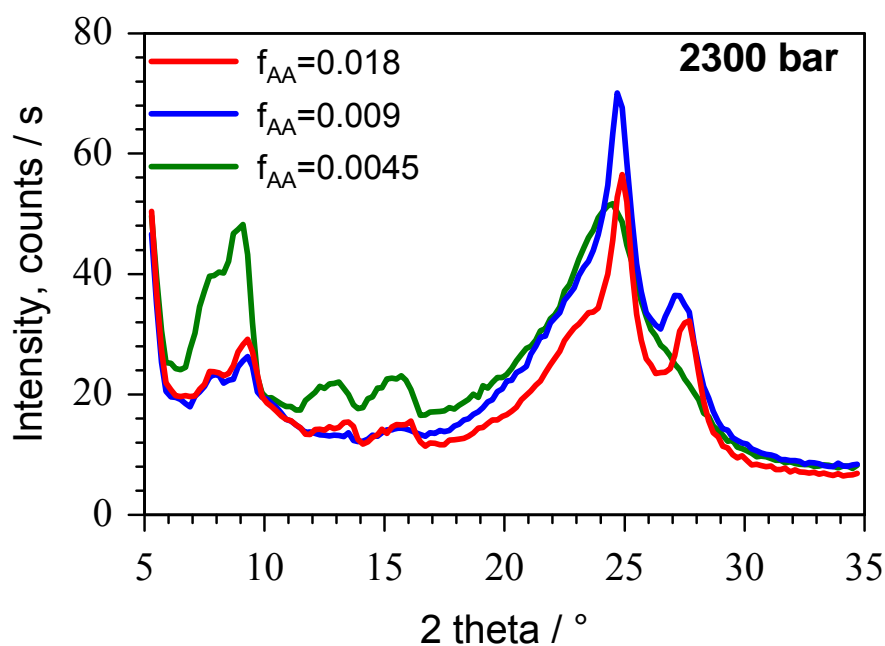


Fig 5.33: X-RAY diagram of E-AA random copolymers produced with different acrylic acid contents



### 5.7.2 Calculation of Full Width at the half maximum (FWHM)

In order to quantify the difference in the distribution of the signals in the region of 23 to 30 Bragg angles, the full width  $w$  at the half maximum (FWHM  $w$ ) of the PE curve was calculated via fitting with two Lorentz functions. (see Figure 5.34)

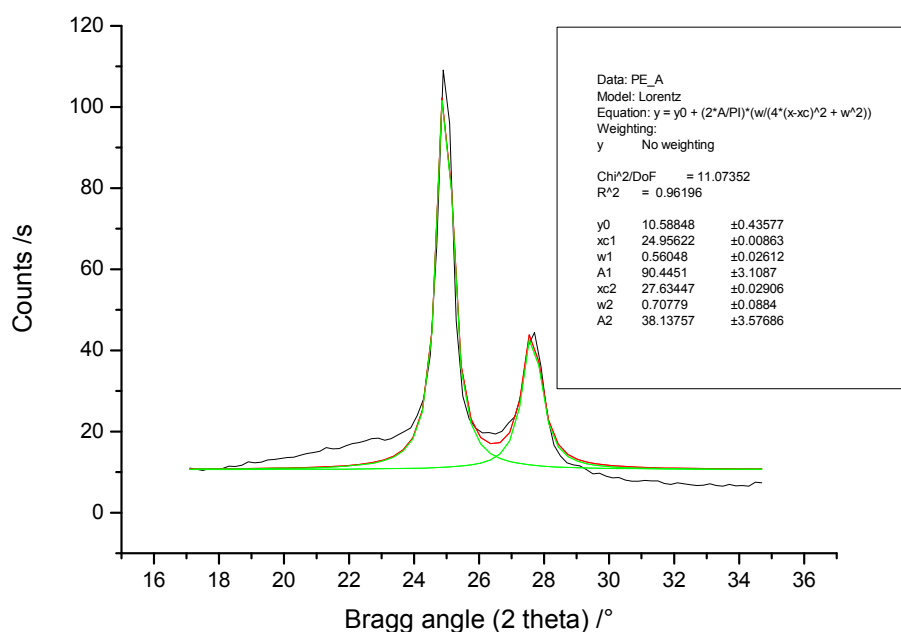


Figure 5.34: The calculation of FWHM for the x-ray diagram of PE in the region of 23 to 30 Bragg angles

The FWHM values  $W_1$  (range of 23 to 26 Bragg angles) and  $W_2$  (range of 27 to 29 Bragg angles) are 0.56 and 0.7 respectively as calculated for the X-ray diagram of PE. But in the case of the copolymers, the value of FWHM is increased compared to PE depending on the content of acrylic acid in the feed, synthesis pressure and temperature. Figure 5.35 shows the calculated FWHM values,  $W_1$  and  $W_2$ , of the E-AA copolymers synthesized at different pressures, which clearly show that the value of  $W_1$  increases with increasing AA content and decreasing of synthesis pressure. The FWHM values of the first curve  $W_1$  for the random E-AA copolymers range from 0.95 to 3.62 and for the non-random copolymers from 4.17 to 5.28 depending on acrylic acid content. The  $W_1$  value for the random copolymer with a low content of acrylic acid (0.95) is very close to the value of PE. However the  $W_1$  value for the

non-random copolymer with low a content of acrylic acid is 4.17, which concludes that the random copolymer with a low content of acrylic acid has a crystal structure more like PE compared to the non-random copolymer, where crystallization is decreased due to the acrylic acid blocks.

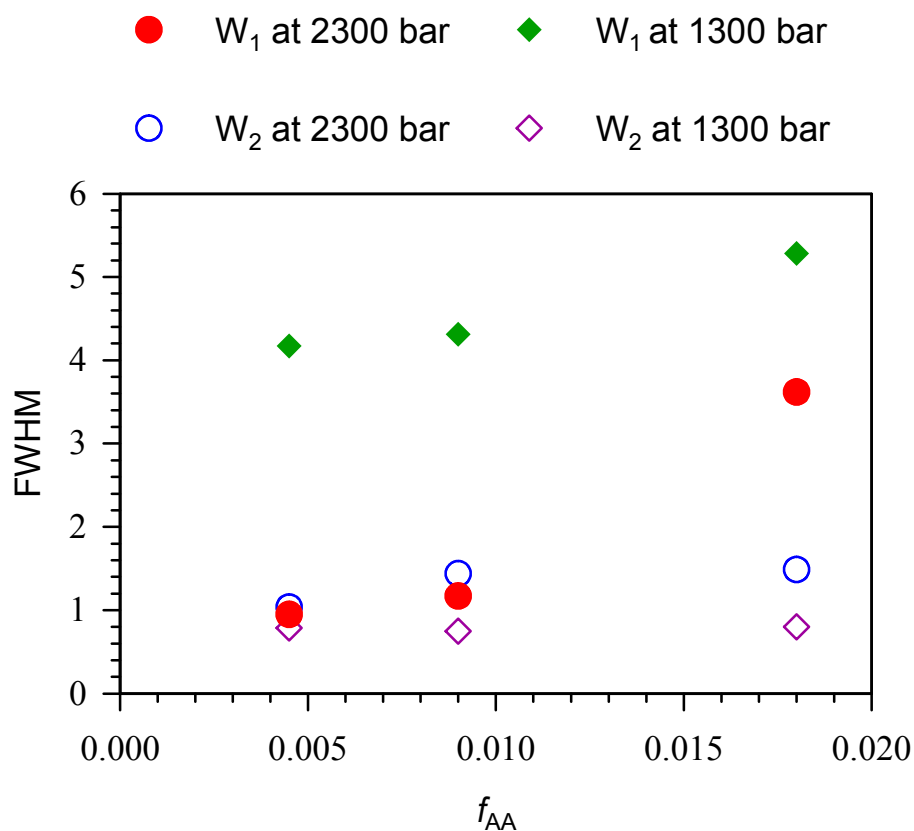


Figure 5.35: Calculated value of FWHM for the E-AA copolymers produced at different pressures and with different AA contents in feed

### 5.7.3 Powder X-ray measurement of reference system

Powder X-ray measurements for E-MMA and E-MA copolymers have been performed in order to obtain reference data. Figures 5.36 and 5.37 show the X-Ray diagrams of the two systems.

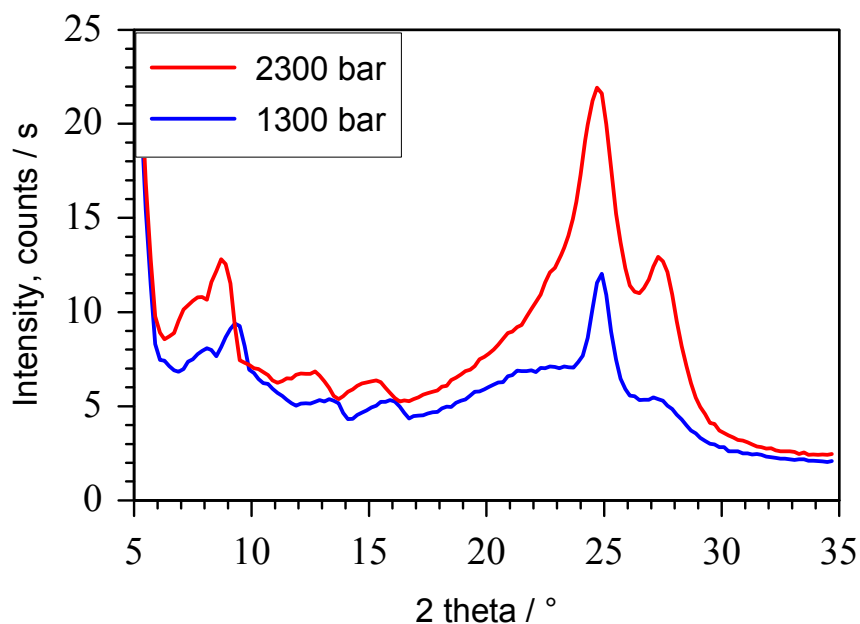


Figure 5.36: X-Ray diagram of E-MMA copolymers produced at different pressures

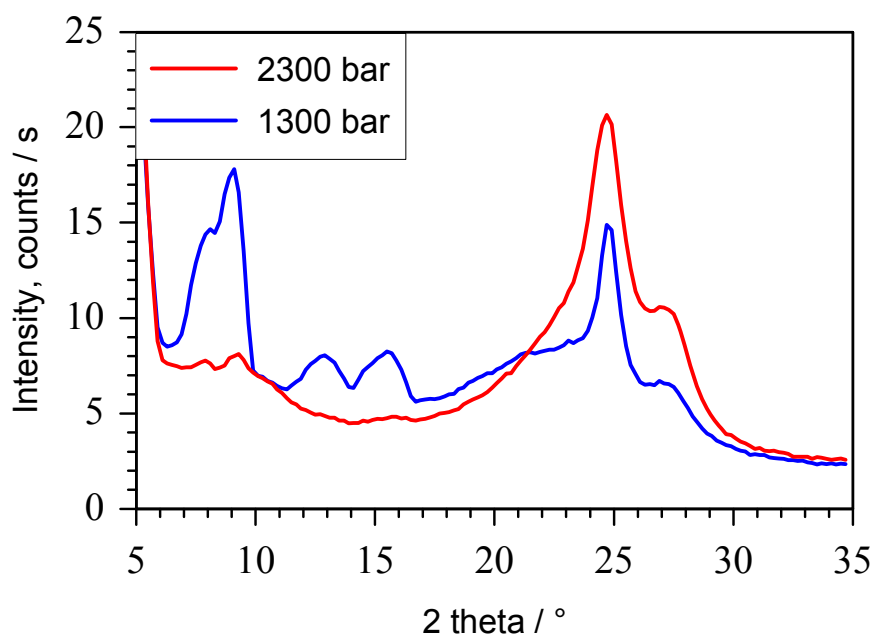


Figure 5.37: Powder X-ray diagram of E-MA copolymers produced at different pressure

The X-ray diagrams of the E-MMA and E-MA copolymers also show 2 significant signals in the region of 23 to 30 Bragg angles. As shown in Figure 5.25, the signals in this region are broader for the non-random copolymers compared to the random copolymers. However for the reference systems (E-MMA and E-MA) the sharpness of these signals doesn't change with decreasing pressure. Therefore it is possible to conclude that E-MMA and E-MA copolymers

have only a random distribution of acrylate moieties even with copolymer produced at low pressure. In addition, the acid group seems to have big influence for the building of random and non-random distribution.

## 5.8 Result of Small Angle X-ray scattering (SAXS)

SAXS diagrams of E-AA, E-MMA and E-MA copolymers are shown in Figures 5.38 and 5.39. In these diagrams two maxima of the scattering vector ( $s$ ) at 0.0085 (red circle) and 0.05 (blue circle)  $\text{\AA}^{-1}$  can be observed.

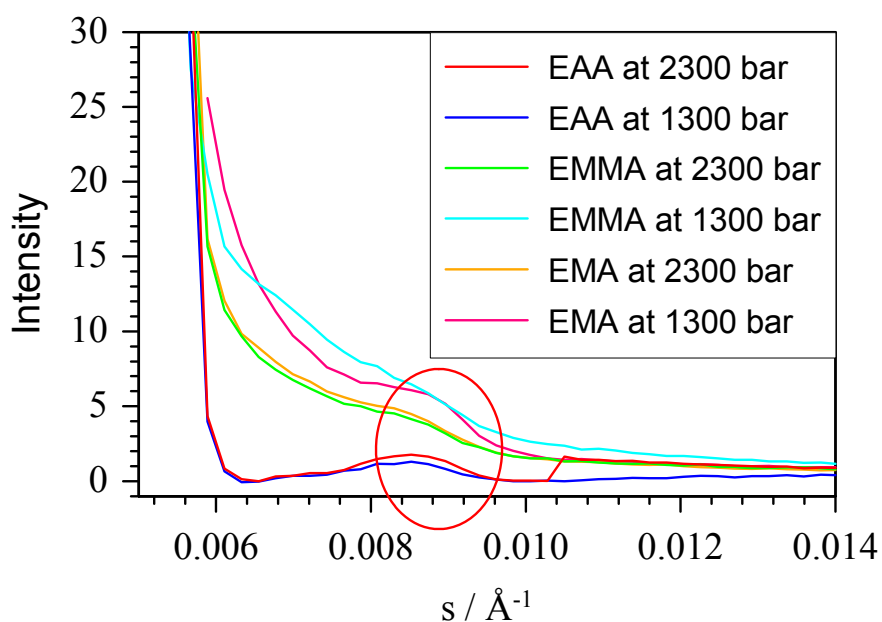


Figure 5.38: SAXS diagram of the first (red circle) maximum of different copolymers produced at 260°C, in the scattering vector range from 0.005 to 0.014  $\text{\AA}^{-1}$

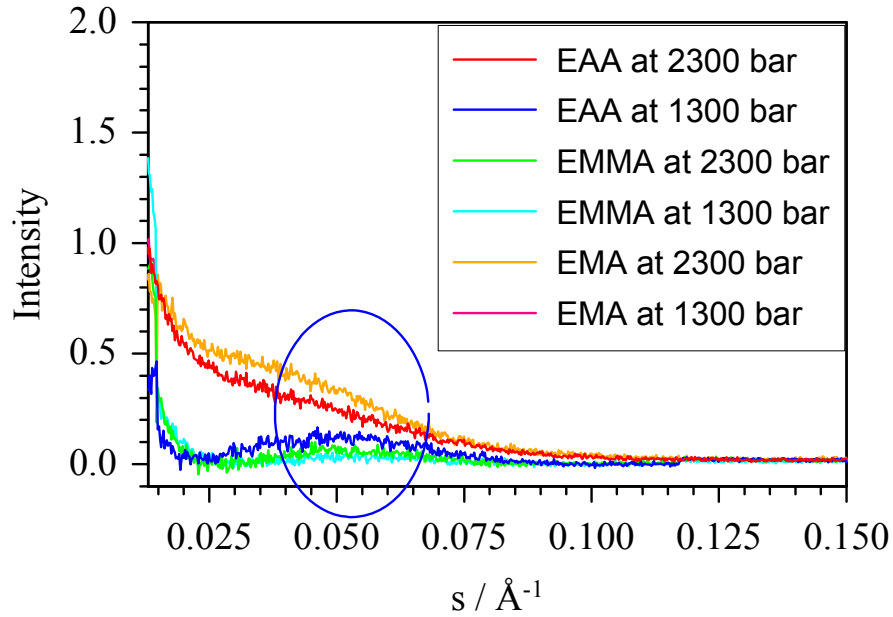


Figure 5.39: SAXS diagram of the second (blue circle) maximum of different copolymers produced at 260°C in the scattering vector range from 0.005 to 0.014 Å<sup>-1</sup>

From those maxima it is possible to calculate distance of two layers by using the following formulas.

$$s = \frac{4\pi \sin \vartheta}{\lambda} \quad (5.5)$$

$$n\lambda = 2d \sin \vartheta \quad n=1 \quad (5.6)$$

$$\lambda = \frac{4\pi \sin \vartheta}{s} \quad (5.7)$$

$$2d \sin \vartheta = \frac{4\pi \sin \vartheta}{s} \quad (5.8)$$

$$d = \frac{2\pi}{s} \quad (5.9)$$

The first maximum has been observed at 0.0085 Å<sup>-1</sup> (s = 0.0085) resulting in a d<sub>1</sub> value of 739 Å (73.9 nm). The second maximum is observed at 0.05 Å<sup>-1</sup> with d<sub>2</sub> value of 125 Å (12.5 nm). As shown in figure 5.40, the d<sub>1</sub> value (marked with red arrows) could represent the

distance between the crystalline regions and  $d_2$  (marked with blue arrows) the distance between two main chains.

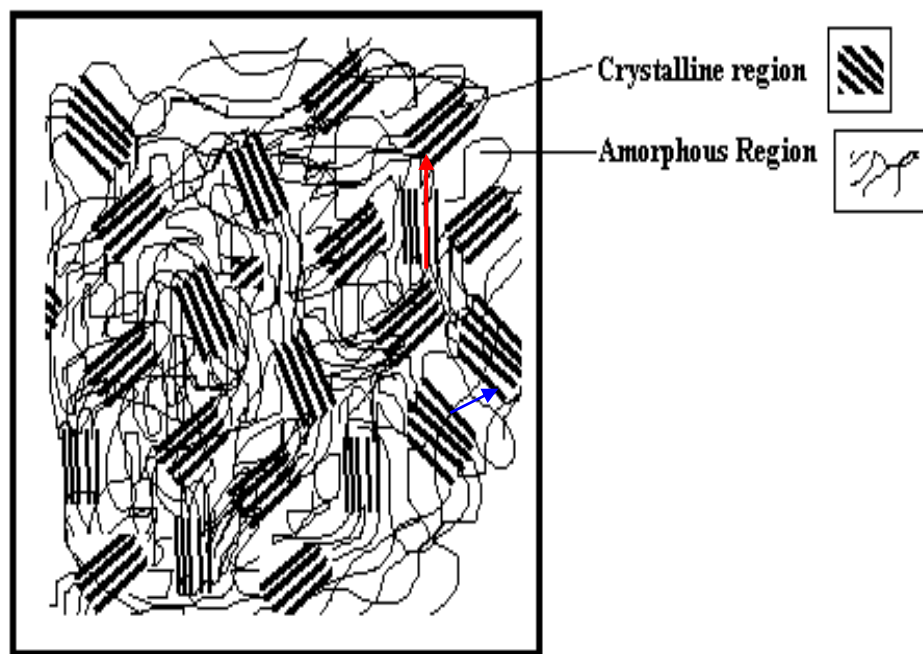


*Figure 5.33: Mixed amorphous and crystalline macromolecular polymer structure*

No impact on the SAXS spectrum is seen from neither comonomer content nor from synthesis at low or high pressure.

## 5.9 Structure analysis of solid state NMR- spectroscopy

As described in chapter 5.1, ss-NMR analysis of copolymer samples has been measured for the E-AA and E-MAA copolymers. This measurement may help to learn about the structure of copolymer especially it may helps to quantitatively identify a difference between random and non-random copolymers.

First series of ss-NMR measurements have been done at room temperature for the E-MAA copolymers but signal intensity was poor. Therefore temperature was increased from room temperature to 50 °C (see Figure 5.34). With increasing temperature signal to noise ratio decreases. This is probably due to high mobility of the polymer chain at high temperature has

negative effect to the transfer efficiency during “Cross Polarization (CP)”. The polarization transfer is based on dipole coupling, which depends from the orientation of dipole vector towards the magnetic field. The movement can occur at higher temperatures therefore dipole coupling may disappear in the effect.

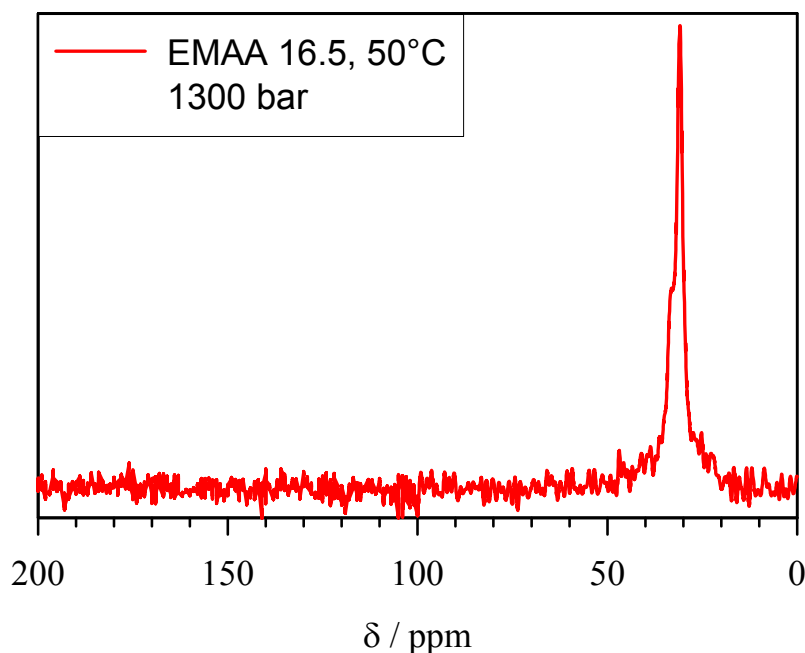


*Figure 5.34:  $^{13}\text{C}$ -CP/MAS-NMR spectra of E-MAA copolymer synthesized at temperature of 260 °C and pressure of 1300 bar under adiabatic conditions.*

For this reason, another spectrum recorded at 5 °C was taken. Figures 5.35 and 5.36 show  $^{13}\text{C}$ -CP/MAS-NMR spectra of E-AA copolymer produced at high and low pressure. The C-atoms of the CH groups of acrylic acid appear at 49 ppm, C-atoms of the CH group of acrylic acid units linked to each other occur at 43 ppm and C-atoms of the CH group of an ethylene monomer at 31 and 33 ppm. The fraction of linked acrylic acid as compared to the over all acrylic acid content was calculated by the Equation 5.10.

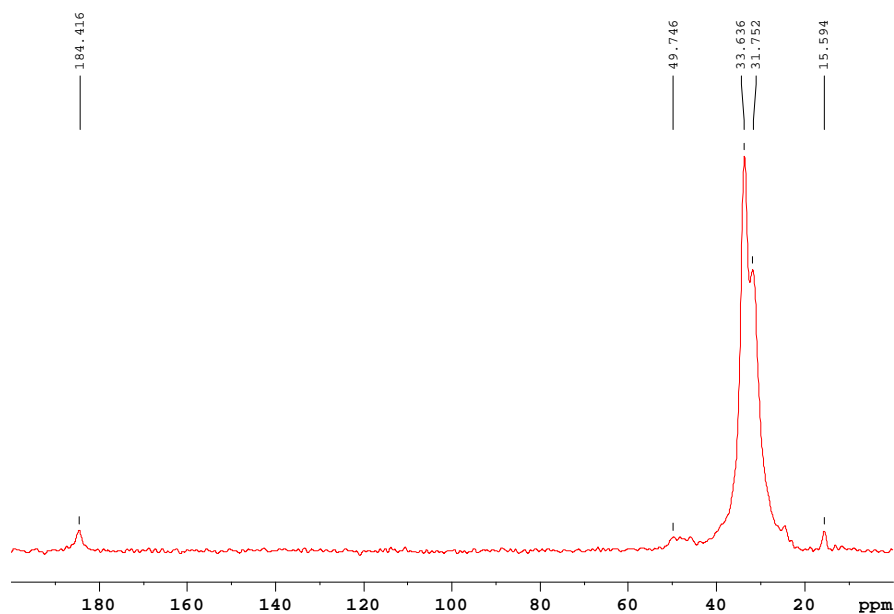


Figure 5.35:  $^{13}\text{C}$ -CP/MAS-NMR-Spectra of EAA copolymer produced at 260 °C

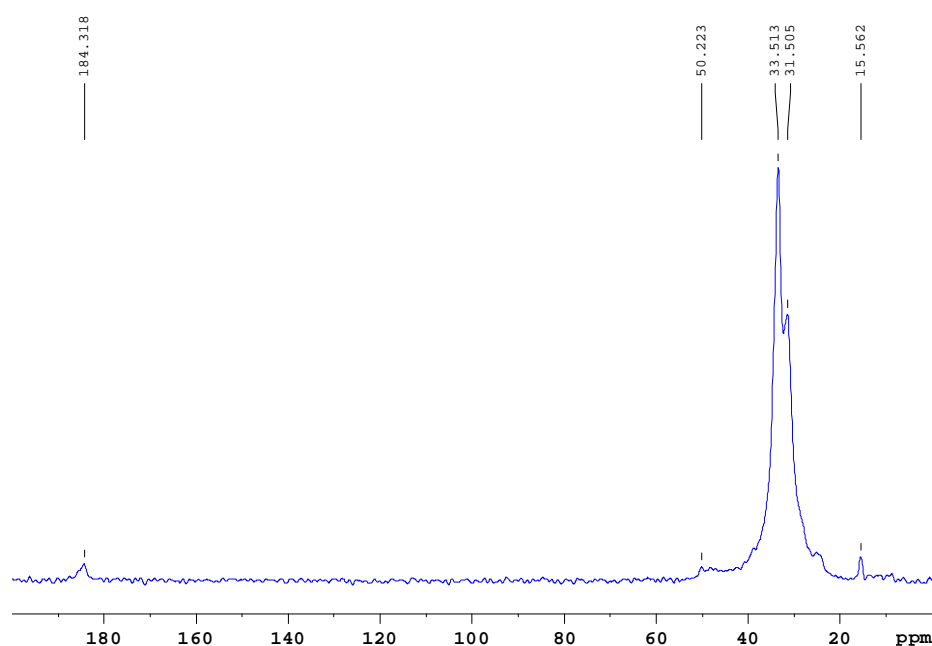


Figure 5.36:  $^{13}\text{C}$ -CP/MAS-NMR-Spectra of EAA copolymer produced in the low-pressure at 260 °C

The linked acrylic acid may be calculated from the ratio of integrated intensities between 40 and 45 ppm which is the absorbance of C-H of linked carbon atoms of the acrylic acid moieties and the integrated intensities from 40 to 52 ppm which refers to the absorbance of the total acid C-H content of the copolymer chain.



$$\text{Clustered AA, \%} = \frac{\int (40-45) \text{ ppm}}{\int (40-52) \text{ ppm}} \times 100 \quad (5.10)$$

The acrylic acid content in the copolymer can be calculated by the ratio of integrated intensities between 40 to 52 ppm and between 20 to 52 ppm which is the total carbon atom content in the copolymer.

$$\text{Content AA, \%} = \frac{\int (40-52) \text{ ppm}}{\int (20-52) \text{ ppm}} \times 100 \quad (5.11)$$

The percentage of linked acrylic acid increases with the content of acrylic acid in the feed both in the case of low-pressure and high-pressure samples (see Figure 5.37). However, the increase of linked acrylic acid and acrylic acid content is more pronounced at low pressure compared to high pressure. At fixed acrylic acid content in the feed, the amount of linked acrylic acid units in the low-pressure sample is higher than in the high pressure sample. This is due to the non-random copolymers containing more dimer species interacting via hydrogen bonding in the high-pressure copolymers.

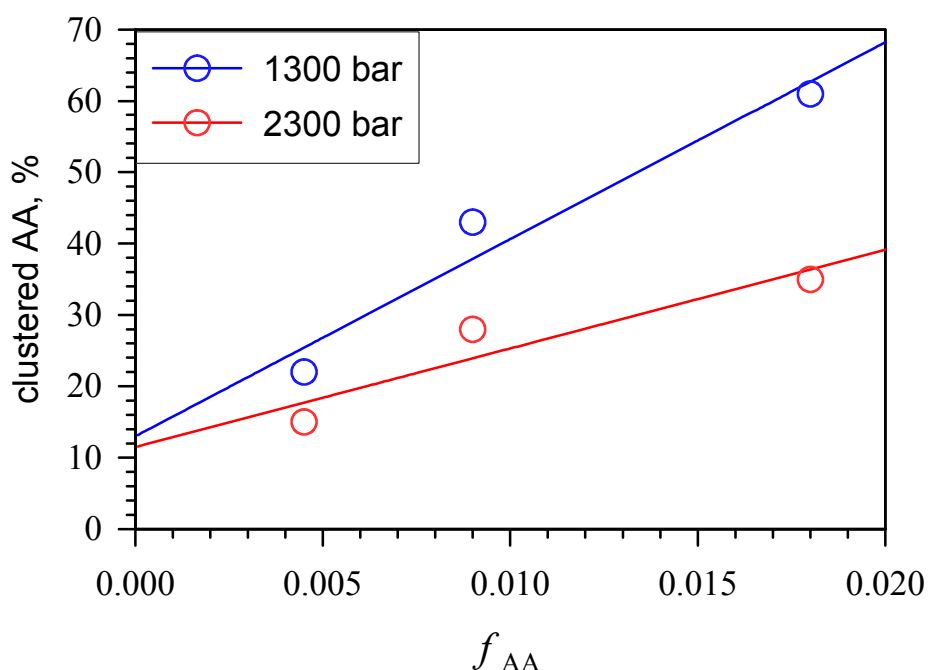


Figure 5.37: The fraction of linked AA in the copolymer as a function of total AA content in the copolymer for different synthesis pressure

## 5.10 Results of the pulsed laser deposition

The pulsed laser deposition (pulsed laser deposition PLD) is a suitable method for the production of thin layers of different materials.<sup>112</sup> The PLD method is often applied for the deposition of metals. This chapter addresses deposition processes of different polymers. There is a possibility to produce thin layers from high-pressure and low-pressure samples using by PLD method and to study their surface structure.

### 5.10.1 PLD of polymers produced from polar monomer

PLD studies of some polymers are already available.<sup>113</sup> Mainly homopolymer of poly(methylmethacrylate) (PMMA) has been used as an example of polymers produced from polar monomer.

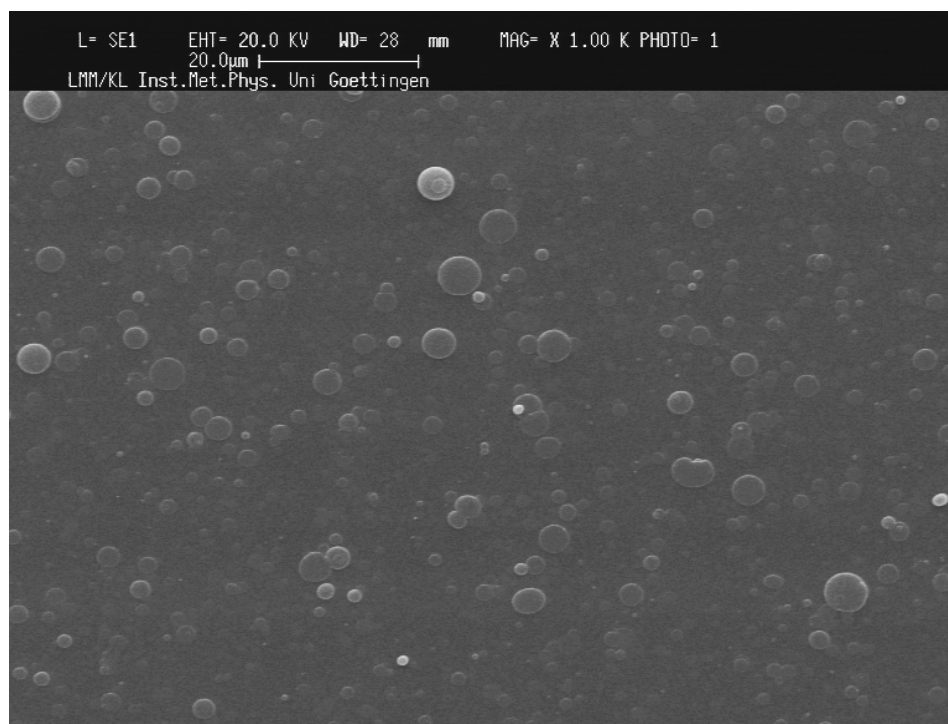


*Figure 5.38: SEM image of deposited PMMA, benchmark 10 microns (magnified approximately 1000 times).*

The deposition process is not yet fully resolved. Particularly interesting is the establishment of a model and information about the nature of the deposited chains. There are several question not yet fully answered such as:<sup>114-117</sup>

-Are the polymers degraded by the laser to the level of monomers and do they reorganize themselves after contact with the substrate or are the polymers transferred as an individual chains?

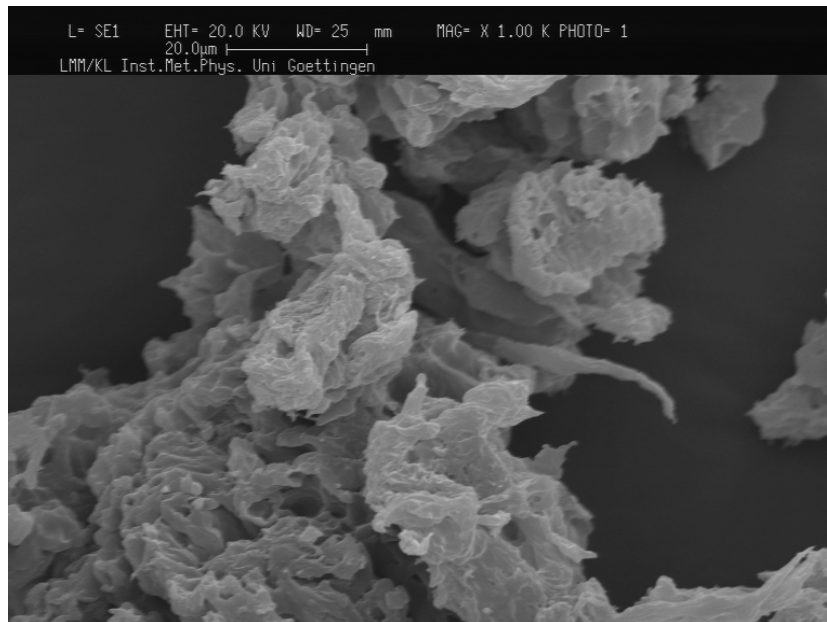
-Is the emergence of droplets an indication that polymer chains are transferred?

Figure 5.38 shows a typical surface structure of PMMA deposited on silicon and it shows a clear homogeneous surface with a high number of droplets, which are called superimposed droplets. Results of PLD of the PMMA layers show that the molecular weight distribution of polymer (PMMA) changes to smaller molecular weight [].

It would be interesting to study the deposition process of E-AA copolymers, which contain a polar part from acrylic acid moieties and non-polar part from PE chain. In order to obtain full information about the deposition process of E-AA, it is necessary to study deposition process of PE first.

### 5.10.2 Surface structure of polyethylene

Polyethylene used for characterization of surface structure has been produced at 230 °C in the same high-pressure set-up and it has a number average molecular weight ( $M_n$ ) of 2940  $\text{g}\cdot\text{mol}^{-1}$  and weight average molecular weight ( $M_w$ ) of 11061  $\text{g}\cdot\text{mol}^{-1}$ . The SEM image of PE directly after depressurizing the polymerization mixture is shown in Figure 5.39. In this image a lot of small polymer particles have been obtained. In order to get detailed information about these particles some image with a10000 times higher magnification has been observed (see Figure 5.40). The surface is pervaded by furrows and soft edges. When separation has occurred by releasing pressure from 2000 bar to atmospheric pressure, changes in the structure take place. After separation process, PE was obtained as a powder. Therefore SEM images for PE sample after melting and defined cooling (with heating and cooling rate of 5  $^{\circ}\text{C}\cdot\text{min}^{-1}$ ) in the DSC apparatus have been recorded and are shown in Figure 5.41.



*Figure 5.39: SEM image of PE after direct separation process, scale 20  $\mu\text{m}$  (magnified approximately 1000 times)*

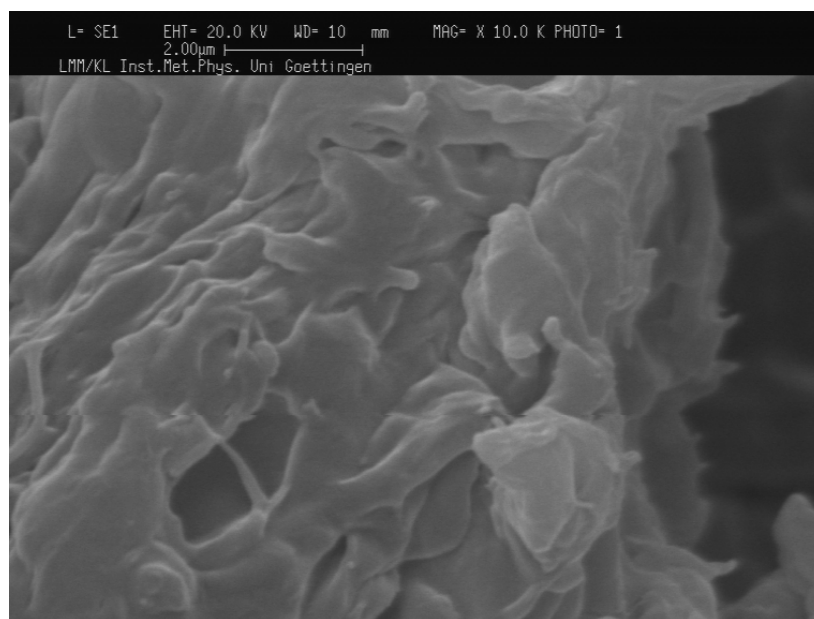


*Figure 5.40: SEM image of PE after direct separation process, benchmark 50  $\mu\text{m}$  (magnified approximately 10000 times)*

PE shows a different surface structure after melting and defined cooling compared to PE after the separation process. The surface is getting sharper, as during the defined cooling process more crystalline areas have been produced. There are also soft parts as is indicate amorphous (non-periodic) structure.

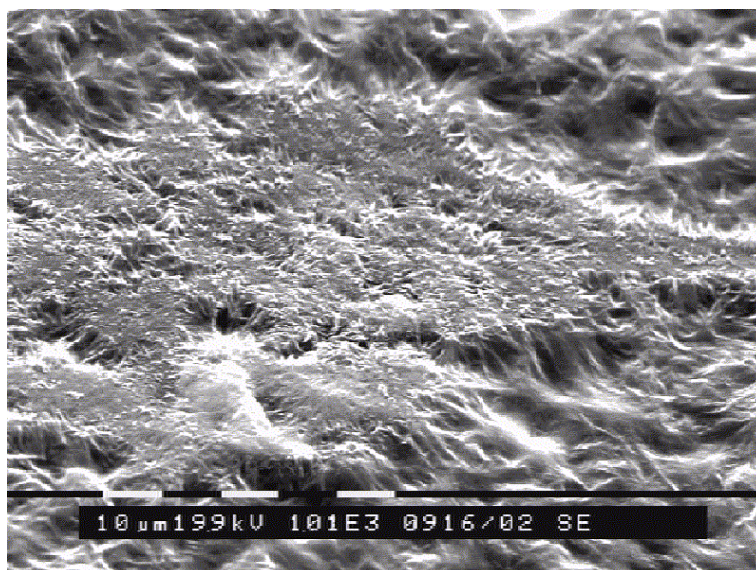


*Figure 5.41: SEM image of defined cooled PE (DSC  $5^{\circ}\text{C} \cdot \text{min}^{-1}$ , scale 10 microns (magnified approximately 1000 times)).*

SEM image with even higher magnification have been observed (see Figure 5.42). The SEM image 10000 times magnification shows a sharper surface compared to the 1000 times magnified images.

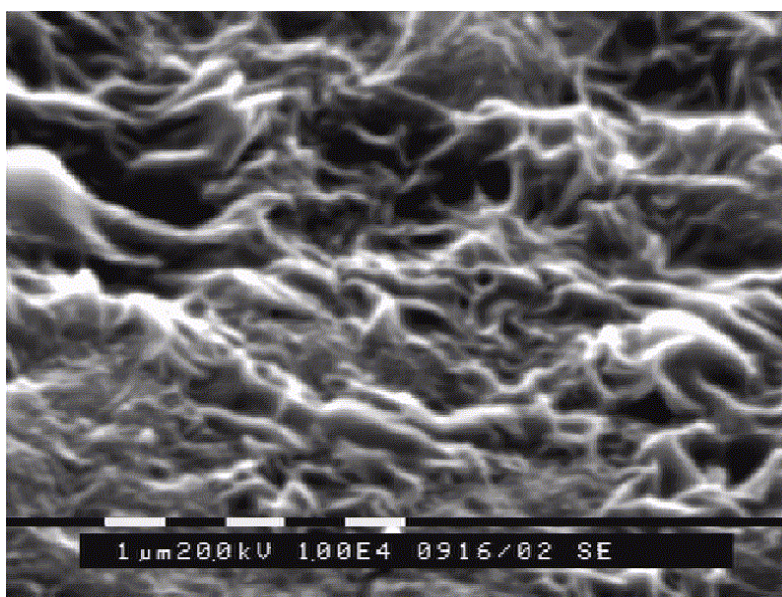


*Figure 5.42: SEM image of defined cooled PE (DSC  $5^{\circ}\text{C} \cdot \text{min}^{-1}$ , scale 10 microns (magnified approximately 10000 times)).*



### 5.10.3 Surface structure analysis of PE prepared by PLD

A PE tablet has been prepared with a diameter of 2.5 cm. In order to make this PE tablet, PE has been pressed with 40 kN force and heated up to 100 °C (for the preparation of a homogeneous tablet it is necessary to heat). After this process water cooling with a heating rate range of 5 to 10 °C ·min<sup>-1</sup> has been applied. The homogeneous PE tablet was used as a target for the PLD. 2000 pulses have been applied for the PLD process of PE.

The SEM surface image of the PE after pulsed laser deposition is given in figure 5.43. Two different structures were observed. One is droplets which are shown in the SEM of deposited PMMA and the other is string structure. This structure has not been observed in the SEM of deposited PMMA therefore it is special for PE. There are two differences between PE and PMMA. The first difference is that PMMA consists of polar monomer units and PE of non-polar units. And secondly, PE chains have crystalline whereas PMMA has amorphous structure. From the SEM images of PE after PLD, it is possible to say that after the deposition process the structure of PE is destroyed and deposited PE shows a mixture of amorphous and crystalline parts. The crystalline part shows a string structure and the amorphous part exhibits droplet structure.

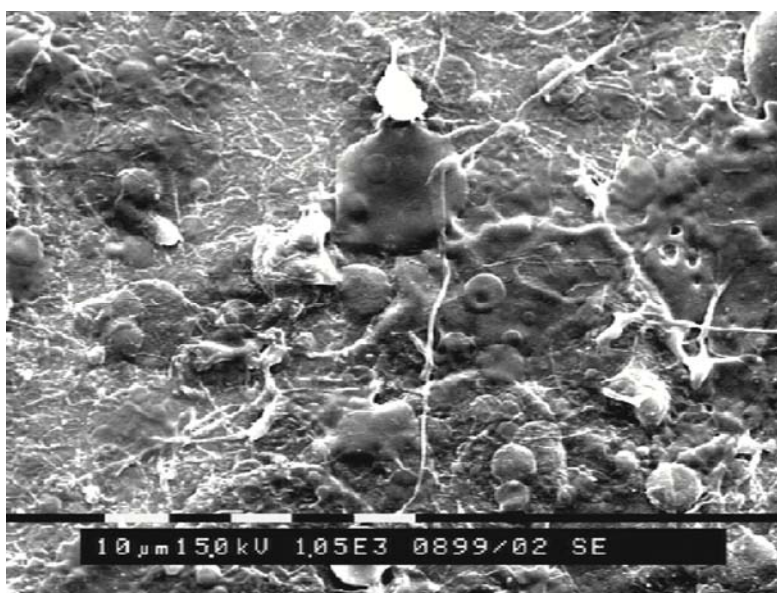


*Figure 5.43: SEM image of the deposited PE, benchmark 10 microns (magnified approximately 1000 times).*

#### 5.10.4 Surface structure of produced EAA copolymer layers using by PLD

EAA copolymers might be good material for the more detailed study of deposition process. It is interesting to see whether EAA copolymer film deposits rather like PMMA or like PE or whether a mixture of those two forms is deposited. The E-AA copolymer thin layers are deposited as a mixture of those two previously described types (PE and PMMA), SEM images of deposited E-AA copolymer with different magnification are shown in Figure 5.44 and 5.45. About 1000 pulses were applied for making the deposited E-AA thin layer. SEM image of deposited E-AA copolymer has significantly different surface structure compare to PE surface. It shows mixture of droplets and strings but the film is very smooth.

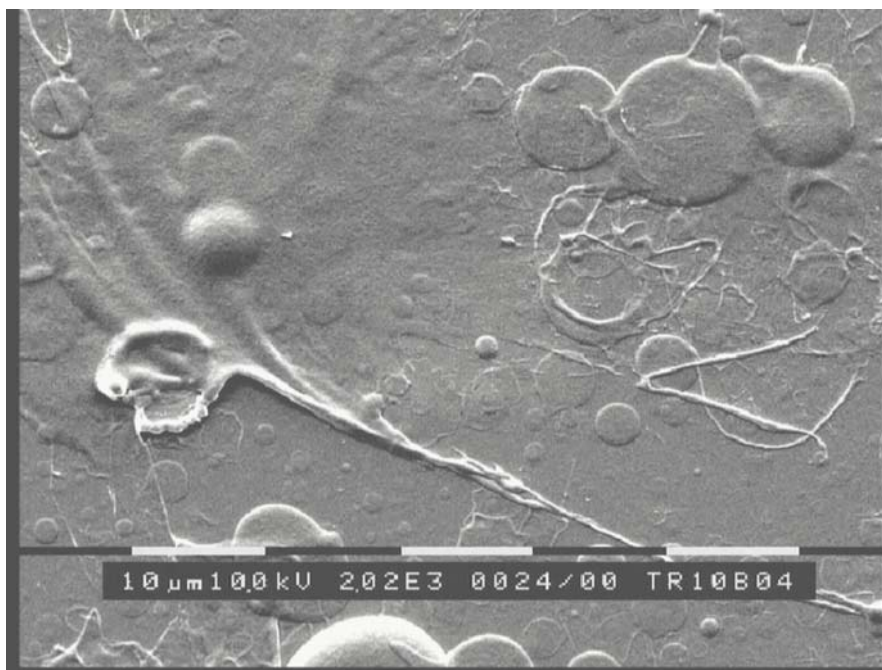


*Figure 5.45: SEM image of deposited EAA copolymer synthesized at 1300 bar, benchmark 10 μm microns (magnified approximately 1000 times).*

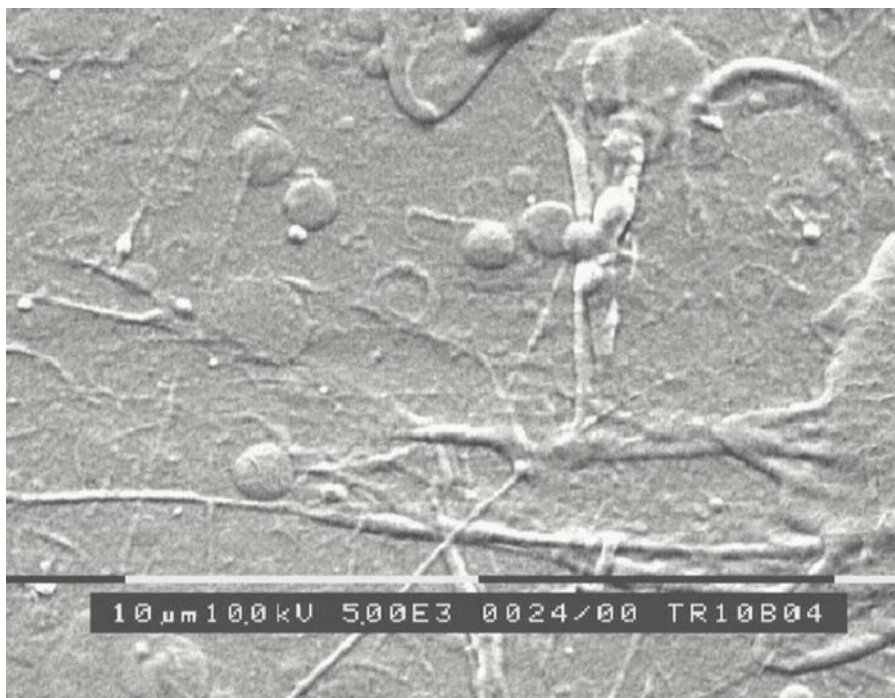


*Figure 5.46: SEM image of deposited EAA copolymer synthesized at 1300 bar, benchmark 10  $\mu\text{m}$  microns (magnified approximately 5000 times).*

The PLD experiment of E-AA (non-random copolymer) shows, that the EAA copolymer deposits like as PMMA. And it can be concluded that E-AA copolymer has amorphous structure. Acrylic acid units destroy the periodicity of the ethylene chain, as is also indicated by the results of powder x-ray measurement.

### **5.11 Results of measuring the hardness of random and non-random E-AA copolymers.**

The hardness of the copolymer samples as obtained from force vs. thickness measurements is shown in Figures 5.47 and 5.48. Random and non-random copolymers behave differently. From these curves, it is possible to calculate<sup>119</sup> the hardness of the copolymer. The calculated values are listed in Table 5.2.



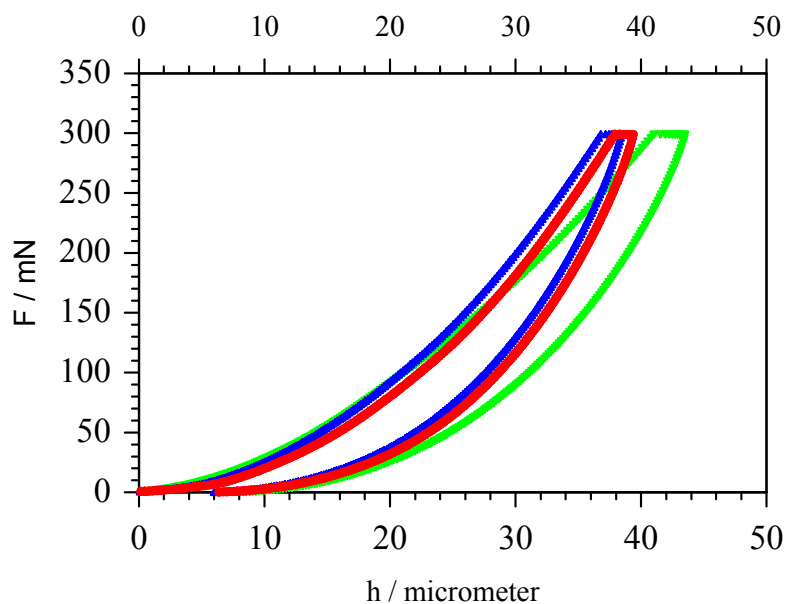


Figure 5.47: Hardness curve for Random copolymer

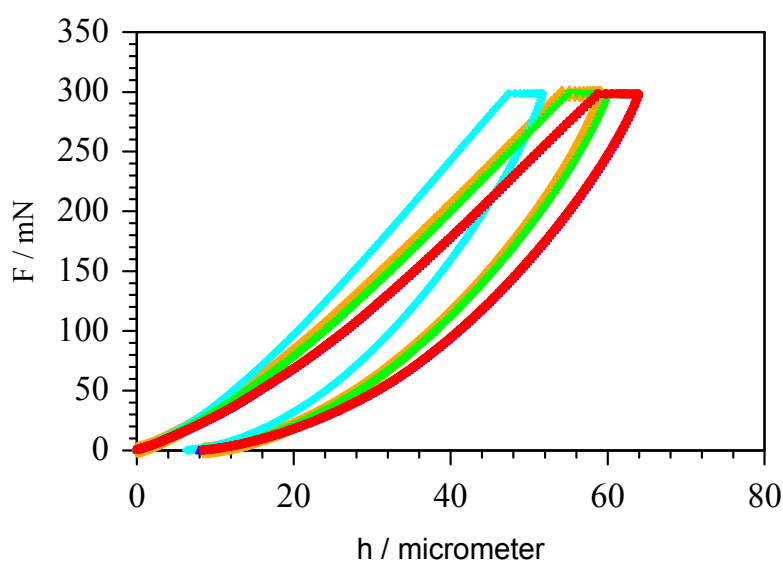


Figure 5.48: Hardness curve for Non-random copolymer

The interesting observation from the data in Table 5.2 is that the “non-random” samples from copolymerization at lower pressure are distinctly harder than the samples from high-pressure polymerization. This may be another indication of a larger extent of association via hydrogen bonds in the “non-random” samples.

Random	Non-random
Hardness N/ mm2	
3.2	5.7
3.2	5.6
3.6	5.8
3.4	5.6
3.5	6.0
3.4±0.2	5.6±0.2

*Table 5.2: Hardness data which is observed via nanoindentor*



## Chapter 6

### Summary

Free-radical copolymerizations of ethene (E) with acrylic acid were carried out in a continuously operated stirred tank reactor at pressures up to 2300 bar and temperatures up to 300 °C. The copolymer samples have been analysed via different several physical methods. Synthesis carried out at higher pressure and temperature, well above the cloud-point curve which separates single-phase and two-phase regions, favors production of random copolymers. Non-random copolymers, on the other hand, may occur in syntheses close to this phase boundary. The aspect of randomness is particularly important in the case of copolymers where one monomer unit is non-polar and the other highly polar and may even form hydrogen bonds.

The molecular weight of the copolymers increases with increasing synthesis pressure. E-AA copolymers produced at higher pressure exhibit a shoulder on the MWD which is also seen in the case of samples produced at high temperature and are thus assigned to the backbiting reaction.

The results of the DSC measurements show clear differences for samples prepared either close to or far off the cloud-point pressure curve. An additional  $\beta$ -relaxation below the glass transition temperature is observed with the lower-pressure copolymer samples which suggest that these samples are non-random. The intensity of this additional relaxation increases with increasing acrylic acid content in the copolymer, which is assigned to the formation of dimeric acrylic acid segments reducing segmental motion. Such differences have not been seen in DSC thermograms of E-MA and E-MMA copolymers produced at low and high pressure. As the DSC thermogram of E-methacrylic acid copolymers produced at conditions close to the phase boundary also show this additional  $\beta$ -relaxation, it may be assumed that this effect is caused by hydrogen bonding of acid units in the copolymer.

X-ray measurements show different structures for random and non-random copolymers. Since non-random copolymers contain more acrylic acid dimers blocks than random

copolymers, the ordering is lower. Random copolymers show a mixture of crystalline and amorphous structure whereas non-random copolymers exhibit an amorphous structure. For the reference systems of E-MMA and E-MA copolymers it may be concluded that they primarily show a random distribution of acrylate moieties even when they are produced at lower pressure. The fraction of linked dimeric acrylic acid and methacrylic acid is more pronounced in lower pressure synthesis. No significant difference between high-pressure and low-pressure E-AA copolymer samples is seen in PLD and SAXS measurements.

**List of abbreviations**

AA acrylic acid

ATR attenuated total reflection

$c$  concentration

$c_{CTA}$  concentration of chain transfer agent

$c_I$  initial initiator concentration

$c_M$  initial monomer concentraion

$d$  dynamic force

DMA dynamic mechanical analysis

DSC differential scanning calorimetry

E ethene

EAA poly(ethene-co-acrylic acid)

EMAA poly(ethene-co-methacrylic acid)

EMA poly(ethene-co-methacrylate)

EMMA poly(ethene-co-methyl methacrylate)

$f$  monomer content in the feed

$F$  monomer content in the copolymer

FT fourier transformation

HPLC High performance liquid chromatography

Ini flow rate of initiator

IR infra red

lg  $\log_{10}(\text{Number})$

MA methacrylate

MMA methyl methacrylate

$M_n$  number average molecular weight

MW molecular weight

$M_w$  weight average molecular weight

NIR near infra red

NMR nuclear magnetic resonance

$p$  pressure

PDI polydispersity  
PE polyethylene  
PLD pulsed laser deposition  
PMMA poly(methyl methacrylate)  
ppm parts per million  
 $r$  copolymerization parameter  
SEC size exclusion chromatography  
SEM scanning electron microscopy  
SAXS small angle x-ray scattering  
T temperature  
TCB 1,2,4-trichlore benzene  
 $T_G$  glass transition temperature  
 $T_{jack}$  jacket temperature of reactor  
theo theoretically calculated value  
THF tetra hydro furan  
 $T_{reac}$  reaction temperature of reactor  
TxB di-*tert*-butyl peroxide  
TxF *tert*-butyl peroxyacetate  
 $X$  monomer conversion

## References

1. H. Staudinger, *Helv. Chim. Acta* **1922**, 4, 785.
2. Verband Kunststoffherzeugende Industrie (VKE), [www.vke.de](http://www.vke.de)
3. [http://www.seilnacht.com/Lexikon/k\\_gesch.html](http://www.seilnacht.com/Lexikon/k_gesch.html)
4. Stevens, Malcolm (1990). *Polymer Chemistry An Introduction*. Oxford University Press. ISBN 019505759.
5. P. Barghoorn, *Nachr. Chem. Lab.* **46**, 2, (1998) 221
6. H.F. Mark, N. M. B., C. G. Overberger, G. Menges, *Encyclopedia of Polymer Science and Engineering* Wiley-Interscience: New York, 1988.
7. S. Bonotto, C. L. Purcell, *Mod. Plastics* **42** (1965) 135
8. *A Guide to IUPAC Nomenclature of Organic Compounds*, Blackwell Scientific Publications, Oxford (1993)
9. R. Kahovec, R. B. Fox, K. Hatada; "Nomenclature of regular single-strand organic polymers (IUPAC Recommendations 2002);" *Pure and Applied Chemistry*; IUPAC; 2002; 74 (10): pp. 1921–1956.
10. Doroudiani S, Kortschot MT (2004) "Expanded Wood Fiber Polystyrene Composites: Processing-Structure-Mechanical Properties Relationships" *Journal of Thermoplastic Composite Materials* **17**:13-30.
11. B. S. Furnell et al., *Vogel's Textbook of Practical Organic Chemistry*, 5th edition Longman/Wiley, New York, 1989.
12. Edwards, S.F. (1965), "The statistical mechanics of polymers with excluded volume" *Proc. Phys. Soc.* **85**: 613.
13. United States Patent 4,248,990
14. European Patent 0146620B1
15. N. Kang, Y. -Z. Xu, J. -G. Wu, S. -F. Weng, D. -F. Xu, *Phys. Chem. Chem. Phys.* 2000, 2, 3627-3630.
16. G. A. Mun, Z. S. Nukeeva, V. V. Khutorvanskiy, A. D. Sergaziyev, *Colloid. Polym. Sci.* 2002, **280**, 282-9.
17. *Handbook of Metathesis*; R. H. Grubbs., Ed.; Wiley-VCH: New York, 2003; Vol. 3.



18. “*Macromolecular Engineering. Precise Synthesis, Materials, Properties, Applications*”, Matyjaszewski, K.; Gnanou, Y.; Leibter, L. (Eds), Wiley-VCH, Weinheim, 2007
19. H. Kaczmarek, A. Szalla, A. Kaminska, *Polymer*. 2001, **42**, 6057-69
20. T. Baughman, K. Wagener. *Adv. Polym. Sci.* 2005, **176**, 1-42.
21. P. Beyer, E. Nordmeier, *Eur. Polym. J.* 1999, **35**, 1351-65
22. M.Buback, R. G. Gilbert, G.T. Russell, D.Hill, G. Moad, K. F. O’Dristol, J.Shen, M. A. Winnik, *J.Polym.Sci., Polym. Chem. Ed.* **1992**, 30, 851.
23. S. Beuermann, M. Buback, T. P. Davis, R. G. Gilbert, R.A. Hutchinson, O.F. Olaj, G.T. Russell, J. Schweer, A. M. van Herk, *Macromol. Chem. Phys.* **1997**, 198, 1545-1560
24. M.Buback, M. Egorov, R. G. Gilbert, V. Kaminsky, O. F. Olaj, G. T. Russell, P. Vana, G. Zifferer, *Macromol. Chem. Phys.* **2002**, 203, 2570-2582
25. K. Matyjaszewski, T. P. Davis, in *Handbook of Radical Polymerization*, Willey-Interscience, Hoboken, **2002**
26. S. Fiorentino, A. Ghielmi, G. Storti, M. Morbidelli. *Ind. Eng. Chem. Res.* **1997**, 36, 1283-1301
27. M. Buback, *Macromol. Chem.* **1990**, 191, 1575.
28. B. Friedman, B. O’Shaughnessy, *Macromolecules* **1993**, 26, 5726
29. G. B. Smith, G. T. Russel, J. P. A. Heuts, *Macromol. Theory Simul.* **2003**, 12, 299.
30. M. Buback, *Macromol.Chem-Macromol.Chem.Phys* **1990**, 1575-1587
31. M.Buback, L.H. Garcia-Rubio, R. G. Gilbert, D. H. Napper, J.Guillot, A.Hamielec, D.Hill, K. F. O’Dristol, O.F. Olaj, J.Shen, D.Solomon, G. Moad, M. Stickler, M. Tirrel, M. A. Winnik, *J.Polym.Sci., Polym., Lett. Ed.* **1988**, 26, 293.
32. S. Beuermann, M. Buback, *M. Prog. Polym. Sci.* **2002**, 27, 191-254
33. A. N. Nikitin, R. A. Hutchinson, *Macromolecules*, **2005**, 38, 1581-1590
34. Moad, G.; Solomon, D. H. *The chemistry of Free radical polymerization*; Pergamon: Oxford, **1995**
35. Mayo, F. R. *J. Am. Chem. Soc.* **1943**, 65, 2324
36. M. Buback, M. Busch, K. Lovis, F.-O. Mähling, *Chem. Ing. Tech.* **67** (1995) 1652
37. M. Busch, *Ph.D Thesis*, Göttingen (1993)
38. M.Buback, T. Dröge, *Macromol. Chem. Phys.* **1997**, 198, 3627
39. M. Buback, T. Dröge, A. van Herk, F. –O. Mähling, *Macromol. Chem. Phys.* 1996, 197, 4119.

40. M. Buback, T. Dröge, *Macromol. Chem. Phys.* 1999, 200, 256.
41. L. Wittkowski, *Ph.D Thesis*, Göttingen (1998)
42. M. Buback, M. Busch, K. Lovis, F.-O. Mähling, *Macromol. Chem. Phys.* **197** (1996)
43. K. Lovis, *Ph.D Thesis*, Göttingen (1995)
44. M. Buback, B. Fischer, S. Hinrichs, S. Jauer, J. Meijer, J. Sandmann, *Macromol. Chem. Phys.*, 2007, 208, 772-783
45. F.-O. Mähling, *Ph.D Thesis*, Göttingen (1995)
46. M. Buback, H. Lendle, *Z. Naturforsch.* **34 a** (1979) 1482
47. M. Müller, *Ph.D Thesis*, Göttingen (2005)
48. M. Busch, *Habilitation*, Göttingen (2003)
49. M. Buback, M. Busch, T. Dröge, F. -O. Mähling, C. Prellberg, *Eur. Polym. J.* 3 (1997) 375-379
50. M. Buback, C. Hinton, *High-pressure Techniques in Chemistry and Physics – A practical approach*, B. W. Holzappel and N. S. Isaacs, Oxford University Press **1997**.
51. M. Buback, H. Latz, *Macromol. Chem. Phys.* **204** (2003) 638-645
52. H. Latz, *Ph.D Thesis*, Göttingen (2004)
53. F. Becker, M. Buback, H. Latz, G. Sadovskii, F. Tumakaka, *Fluid Phase Equilibria*, **215** (2004), 263-282
54. B. M. Hasch, M. A. Meilchen, S.-H. Lee, M. A. McHugh, *J. Polym. Sci. Part B: Polym. Phys.* **30** (1992) 1365-1373
55. C. F. Kirby, M. A. McHugh, *Chem. Rev.* 99(1999) 565-602
56. H. S. Byun, B. M. Hasch, M. A. McHugh, F.-O. Mähling, M. Busch, M. Buback, *Macromolecules* 29 (1996) 1625-1632
57. C. Müller, L. R. Oellrich, *Acta Polym.* 47 (1996) 404-406
58. R. W. Wind, *Ph.D Thesis*, Darmstadt (1992)
59. T. Junkers, *Ph.D Thesis*, Göttingen (2006)
60. E.S. Watson, J. Justin, N. Brenner, M. J. O'Neil, *Analytical Chemistry* **36** (7) (1964)
61. M. D. Lechner, E. H. Nordmeier, *Nachr. Chem. Tech. Lab.* **42** (1994) 6
62. L. G. Weyer, *Appl. Spectroscopy Rev.* **21** (1985) 1
63. R. M. Bly, P. E. Kiener, A. B. Fries, *Anal. Chem.* 1966, **38**(2), 217.
64. H. D. Siesler, *Macromol. Chem. Symp.* **52** (1991) 113

65. B. Stuart, "Infrared spectroscopy: Fundamentals and applications", John Wiley&Sons (2004)
66. M. Buback, L. Wittkowski, S. A. Lehmann, F.-O. Mähling, *Macromol. Chem. Phys.* **200** (1999) 1935
67. M. Buback, L. Wittkowski, *Macromol. Chem. Phys.* **201** (2000) 419-426
68. Y. Fuji, H. Yamada, M. Mizuta, *J. Phys. Chem.* **1988**, 92, 6768
69. C. Josefiäk, G. M. Schneider, *J. Phys Chem.* **1979**, 83, 2126
70. F. Becker, *Ph.D Thesis*, Göttingen (2006)
71. B. Steisel, *Ph.D Thesis*, Göttingen (2007)
72. O. V. Mazurin, Yu. V. Gankin: "Glass transition temperature: problems of measurement and analysis of the existing data"; *Proceed. Int. Cong on Glass*, 2007, Strasbourg, France
73. J. Hachenberg, *Ph.D Thesis*, Göttingen (2006)
74. Perkin-Elmer, "User Manual 7 Series / Unix DMA 7 / DMA 7e", manual version F, Perkin-Elmer (1994)
75. K. P. Menard, "Dynamic mechanical analysis: a practical introduction", CRC Press (1999)
76. J. Hachenberg, B. Steisel, Undrakh Nergui, D. Bedorf, M. Buback, K. Samwer, *Int. J. Mat. Res.* **99** (2008) 5, 502-505
77. Chrisey, D. B.; Piqué, A. ; McGill, R. A.; Horwitz, J. S.; Ringeisen, B. R.; Bubb, D. M. ; Wu, P. K., *Chem. Rev.* **103** (2003) 553
78. D. B. Chrisey and G. K Hubler: Pulsed laser deposition of thin films, Wiley, New York, 1994
79. C. Scarfone, M. G. Norton, C. B. Carter, J. Li and H. W. Mayar, *Mat. Res. Soc. Symp. Proc.* **191**, 183 (1991)
80. T. Scharf, *Ph.D Thesis*, Göttingen (2006)
81. H. P. Myers (2002) *Introductory Solid State Physics*, ISBN0-784-00660-3
82. Carl. R. Nave, *Hyper Physics*, Georgia State University, retrieved on **2008**
- 83.** Glatter. O, Kratky. O, *Small Angle X-ray Scattering*, Academic Press, **1982**
84. D. I. Svergun, M. H. J. Koch, *Small-angle scattering studies of biological macromolecules in solution. Rep. Prog. Phys.* **2003** 66, 1735-1782
85. L. A. Feigin, D.I. Svergun: *Structure Analysis by Small-Angle X-ray and Neutron Scattering*. New Yourk: Plenum Press, **1987**

86. E. R. Andrew, A. Bradbury, R. G. Eades, *Nature* **182** (1958) 1659
87. B. M. Fung, A. K. Khitrin, K. Ermolaev, *J. Magn. Reson.* **142** (2000) 97-101
88. M. Etzkorn, S. Martell, O. C. Andronesi, K. Seidel, M. Englehard, M. Baldus, *Angew. Chem. Int. Ed.* **2007**, 46, 459-462
89. Lucio Frydman, John S. Hardwood. *J. Am. Chem. Soc.* 1995, **117**, 5367-5368
90. D. Massiot, B. Tonzon, D. Trumeau, J. P. Coutures, J. Virlet, P. Florian and P. J. Grandinetti, *Solid-State NMR*, 6, 73 (1996)
91. A. Pines, J. S. Waugh, M. G. Gibby, *J. Chem. Phys.* **56** (1972) 1776
92. Oliver H. Möller, *Ph.D Thesis*, Göttingen (2000)
93. T. Takeuchi, S. Tsuge, Y. Sugimura, *Anal. Chem.* 1969, 41(1), 184.
94. M. Müller, *Ph.D Thesis*, Göttingen (2005)
95. Y. He, B. Zhi, Y. Inoue, *Prog. Poly. Sci.* **2004**, 29, 1021
96. Y. Zheng, Y. Mi, *Polymer* **2004**, 44, 1067-1074
97. E. Meaurio, E. Zuza, J. R. Sarasua, *Macromolecules* **2005**, 38, 1207
98. E.-M. Borschel, *Ph.D Thesis*, Göttingen (1987)
99. G. Luft, R. Steiner, *Chemiker Zeitung*, **95** (1971) 11-15
100. K. Binder, W. Kob, "Glassy materials and disordered solids", World Scientific (2005)
101. H. Teichler, *Phys. Rev. E* **71** (2005) 031505
102. L. H. Sperling, "Introduction to physical polymerscience", second edition, Wiley-Interscience (1992)
103. H. Lüth, "Surfaces and Interfaces of Solid Materials", Springer, Berlin (1995)
104. K. Vollmayr-Lee, A. Zippelius, *Phys. Rev. E* **72** (2005) 041507
105. J. R. MacCallum, *Thermochimica Acta*, **96(2)** (1985) 275
106. I. Low, G. Paglia, C. Shi, *J. Appl. Polym. Sci.* **70** (1998) 2349
107. A. J. Lovinger, in : Development in Crystalline Polymers-1 ; D. C. Bassett, Ed., Applied Science Publishers : London (1982 )
108. M. Doi, S. F. Edwards, "The theory of polymer dynamics", Oxford Science Publications, Clarendon Press (1988)
109. H. Kalakkunnath, D. S. Kalika, H. Lin, B. D. Freeman, *Macromolecules* **38**, (2005) 9679
110. Mark R. Vanlatingham, John S. Villarubia, William F. Guthrie, Greg F. Meyers, *Macromol. Symp.* **167**, (2001) 15-43

111. P. Rösner, J. Hachenberg, K. Samwer, R. Wehn, P. Lunkenheimer, A. Loidl, E. Sueske, T. Scharf, H.-U. Krebs, *New J. Phys.* **8** (2006) 89
112. D. B. Chrisey (Hrsg.), G. K. Hubler (Hrsg.), “Pulsed Laser Deposition Of Thin Films”, New York, Wiley Interscience Publication (1994)
113. T. Scharf, J. Faupel, K. Sturm, H.-U. Krebs, *J. Appl. Phys.* **94** (2003) 4273
114. H.-U. Krebs, M. Weisheit, J. Faupel, E. Süske, T. Scharf, C. Fuhse, M. Störmer, K. Sturm, M. Seibt, H. Kijewski, D. Nelke, E. Panschenko, M. Buback, *Adv. in Solid State Phys.* **43** (2003) 505
115. H.-U. Krebs, S. Fähler, O. Bremert, *Appl. Surf. Sci.* **86** (1995) 86
116. M. Störmer, H.-U. Krebs, *J. Appl. Phys.* **78** (1995) 7080
117. A. Piqué; R. A. McGill, D. B Chrisey, B. J. Spargo, J. H. Callahan, R. W. Vachet, R. Chung, M. A. Bucaro, D. Leonhardt, *Thin Solid Films* **355-356** (1999) 536
118. E. Süske, T. Scharf, T. Junkers, M. Buback, H.-U. Krebs, *J. Appl. Phys.* **100** (2006) 14906
119. N. G. McCrum, B. E. Read, G. Williams, “Anelastic and dielectric effects in polymeric solids”, John Wiley & Sons (1967)

## Acknowledgements

I want to express my profound gratitude to the staffs of scientist and technicians and other persons directly or indirectly involved in the completion of this work. The findings within this dissertation would never have been so fruitful without the help of these people.

First of all, I would like to thank sincerely *Prof. Dr. Michael Buback* for giving me an opportunity to carry out my PhD study under his supervision. Thank you for your input, corrections, discussion and clarification on numerous aspects of this work.

I am grateful to my co-supervisor *Prof. Dr. Hans-Ulrich Krebs* who permitted me work in his research group for the PLD and X-ray studies of E-AA polymers as well as the valuable discussions.

Thanks to the all members of *Prof. Michael Buback* and *Prof. Philipp Vana's* groups for the nice working atmosphere and their guidance and help during my stay in Goettingen. Polymer synthesis in the mini-plant was carried out with my colleague, *Dr. Björn Steisel, H. Rohman* and *S. Lotze*. Besonderer Dank gilt auch allen Mitarbeitern der Institutswerkstätten unter Leitung von Herrn *V. Meyer*.

I am thankful to *Andreas* for the PLD and X-ray measurements, *Dr. Mark Baldus* and *Dr. Robert Schneider* for the NMR measurements, *Britta* for the hardness measurements and *Dr. Davaasambu Jav* for the SAXS measurements.

I thank to DFG-funded Graduate School 782 "Spectroscopy and Dynamics of Molecular Aggregates, Chains and Coils" and Institute for Physical Chemistry, University of Goettingen for the financial support.

I am very thankful to *Prof. Dr. Purevsuren Barnasan* at the ICCT, Mongolian Academy of Science with whom I started my first scientific research.

I am thankful to all my friends in Goettingen as well as in Mongolia (some of who are elsewhere now) for their unconventional support and accompanies.

A special thank you to my wife *Enkhtuul*, who not only supports, encourages and strengthens me in everything but is also completely dedicated to our life goals together – of which this PhD thesis is only a part. My sweet son *Irmuun!* Your smile was the best recreation for daddy. Finally, I am indebted to my parents and grandmother for their understanding, help and encouragement whatever I have carried out in my life. I send my heartfelt thanks to my sisters and brothers in Mongolia.

# Lebenslauf

## Persönlicher Status

Name: Undrakh Nergui  
Geburtsdatum: 7. August 1979  
Geburtsort: Ulaanbaatar, Mongolei  
Staatsangehörigkeit: Mongolisch

## Hochschulausbildung

1996-2000	Bachelor in Chemie und Chemische Technologie an der Universität Ulaanbaatar, Mongolei
2000-2002	Master in Chemie und Chemische Technologie an der Universität Ulaanbaatar, Mongolei
2000-2005	Wissenschaftliche Mitarbeiter am Institut für Chemie und Chemische Technologie, Mongolische Akademie der Wissenschaften
2000-2006	Wissenschaftliche Mitarbeiter an der Fakultät für Zivil und Engineering, Universität Trento, Italien
04/2005-04/2008	Stipendiat der Deutschen Forschungsgemeinschaft
seit 04/2005	Anfertigung einer Dissertation am Institut für Physikalische Chemie im Fachbereich Technische und Makromolekulare Chemie unter der Anteilung von Herrn Prof. Dr. Michael Buback und Herrn Prof. Dr. Hans-Ulrich Krebs
seit 04/2008	Stipendiat der Institut für Physikalische Chemie, Georg-August-Universität Göttingen